

**FUNCTIONAL MAGNETIC RESONANCE
MICROSCOPY OF LONG- AND SHORT-DISTANCE
WATER TRANSPORT IN TREES**

Natalia Homan

Thesis Committee**Thesis supervisor:**

Prof.dr. H. van Amerongen,
Professor of Biophysics
Wageningen University

Thesis co-supervisor:

Dr. H. Van As,
Associate Professor, Laboratory of Biophysics
Wageningen University

Other members:

Prof.dr. O. van Kooten, Wageningen University
Prof.dr.dr.h.c. B. Blümich, RWTH Aachen, Germany
Prof.dr.ir. F. Mohren, Wageningen University
Prof.dr. P. McDonald, University of Surrey, UK

This research was conducted under the auspices of the Graduate School of
Experimental Plant Sciences.

**FUNCTIONAL MAGNETIC RESONANCE
MICROSCOPY OF LONG- AND SHORT-DISTANCE
WATER TRANSPORT IN TREES**

Natalia Homan

Thesis

submitted in partial fulfilment of the requirements for the degree of doctor
at Wageningen University
by the authority of the Rector Magnificus
Prof. dr. M.J. Kropff,
in the presence of the
Thesis Committee appointed by the Doctorate Board
to be defended in public
on Wednesday 4 November 2009
at 1:30 PM in the Aula.

Natalia M. Homan,
Functional magnetic resonance microscopy of long- and short-distance water
transport in trees,
125 pages.

Thesis, Wageningen University, Wageningen, NL (2009)
With references, with summaries in Dutch and English

ISBN 978-90-8585-507-1

Contents

1	General introduction	1
1.1	Introduction	1
1.2	Whole-plant water transport	1
1.3	Cavitation and embolism repair	6
1.4	Radial water transport	8
1.5	Main experimental methods	8
1.6	Outline of the thesis	11
	References	13
2	0.7 and 3 T MRI and sap flow in intact trees: xylem and phloem in action	19
2.1	Introduction	19
2.2	Material and methods	22
2.2.1	Hardware	22
2.2.2	MRI flow imaging	23
2.2.3	Plant material	25
2.3	Results and discussion	25
2.4	Conclusions	31
	References	33
3	Flow characteristics and exchange in complex biological systems as observed by PFG-MRI	37
3.1	Introduction	37
3.2	Theory	39
3.3	Experimental	43
3.4	Results and discussion	44
3.5	Conclusions	51
	References	55

4	Dynamics of water transport and water content in storage pools in diffuse-porous trees	57
4.1	Introduction	58
4.2	Materials and methods	59
4.2.1	Plant material	59
4.2.2	The NMR imaging setup	59
4.2.3	MRI flow measurements	60
4.2.4	Water content imaging	62
4.3	Results	62
4.3.1	Variation in axial flow	62
4.3.2	Water content in sapwood and cambial zone	63
4.3.3	Radial variation in sap flow	64
4.3.4	Diurnal variation of water content in sapwood and cambial zone	65
4.4	Discussion	66
4.4.1	Variations in axial flow	66
4.4.2	Water content in sapwood and cambial zone during drought stress and recovery	67
4.4.3	Radial variation in sap flow	68
4.4.4	Diurnal variation of water content in sapwood and cambial zone	69
4.5	Conclusion	70
	Appendix	71
	References	79
5	Cavitation in ring-porous xylem	83
5.1	Introduction	84
5.2	Materials and methods	85
5.2.1	Plant Material	85
5.2.2	Single-pressure protocol	86
5.2.3	Drydown protocol	86
5.2.4	MRI procedures	86
5.2.5	Water content imaging and analysis	87
5.2.6	Imaging and analysis of xylem flow	88
5.2.7	Water potential (Ψ) measurements	89
5.2.8	Dye perfusions	89
5.2.9	Centrifuge and air-injection tests	90
5.2.10	Anatomical measurements	90
5.2.11	Experiments on <i>Quercus gambelii</i>	91
5.3	Results	92
5.3.1	Water content imaging	92
5.3.2	Flow conducting area and volume flow rate imaging	94
5.3.3	Dye perfusions	97
5.3.4	Centrifuge and air-injection of <i>Q. robur</i> trunk segments	97
5.3.5	<i>Quercus gambelii</i> experiments	97

CONTENTS III

5.4 Discussion	98
Appendix	105
References	107
6 Summarizing discussion	111
7 Samenvatting	115
Acknowledgements	119
Curriculum Vitae	121
Publications	123

Chapter 1

General introduction

1.1 Introduction

Water transport in plants is one of the processes in the global water cycle that has a direct effect on climate and weather and supports plant growth. Water is absorbed by roots from the soil and is transported via the xylem to the leaves where it evaporates, the vapour diffuses to the atmosphere via the stomata. This flux of water vapour out of the leaf is accompanied by the diffusion of CO_2 into the leaf, a process driven by the photosynthetic fixation of CO_2 in the leaf (Sperry, 2004). From 100 up to 1000 water molecules are lost per fixed CO_2 molecule (Maseda *et al.*, 2006). Of all the water absorbed by plants, less than 5% remains in the plant for growth and storage following growth. Transpiration by higher plants accounts for about one eighth of all the water evaporated to the atmosphere, or about three quarters of all water that evaporates from land. Therefore, water transport in plants plays a significant role in the global water cycle (Sellers *et al.*, 1997). The mechanisms of water uptake and transport within the plant to the leaves and growing tissues and the means by which these fluxes are determined and regulated are still incompletely understood despite their evident importance to photosynthesis and growth and global water cycle.

1.2 Whole-plant water transport

The major path by which water enters plants is via the roots from the soil. Water enters via the tips of growing roots and is then transported to the root's xylem, passing in route through various morphological structures, such as the epidermis, the endodermis, the cortical cells and the walls of xylem vessels (Steudle *et al.*, 1998). Three different transport pathways have been identified within the root (Fig. 1.1). The first pathway corresponds to the apoplast where water moves via cell walls and intercellular space. In the symplastic pathway water flows in a continuum of cytoplasm, passing from one cell to another via the plasmodesmata and remaining outside the vacuoles. The third pathway is the cell-to-cell one in which water crosses

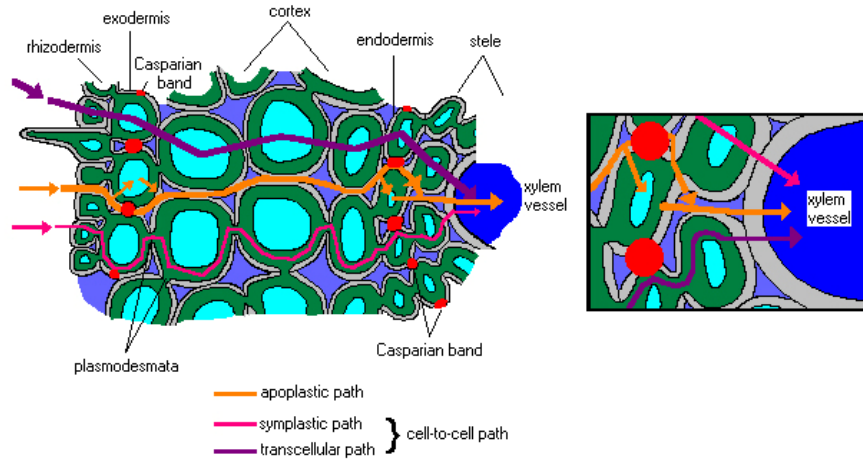


Figure 1.1 : *The symplast, apoplasts and cell-to-cell pathways of water in roots (Steudle, 2000).*

membranes to go from one cell to the next one. Regardless of the pathway, a water molecule has to cross the endodermis, which contains a layer of cells, called the Casparian strip, whose walls are enriched with hydrophobic wax and therefore is impermeable for water. Water is then forced to pass membranes. This creates a sieving effect.

Two different forces drive the water flow in the roots. The first one is a hydrostatic pressure gradient between the soil and the root xylem. The second driving force is an osmotic gradient. In parallel with water uptake, solutes enter the root from the soil water. Moving with water in the cell-to-cell pathway they (partly) cross semi-permeable membranes by passive or active permeation and create an osmotic gradient across the membranes. The driving force for the apoplastic pathway is a hydrostatic pressure gradient. The driving force for the symplastic and cell-to-cell fluxes has both hydrostatic and osmotic components. The complex anatomical structure of the root and anatomical features like the Casparian strip require that water flow in the root follows all three pathways. The hydraulic and osmotic flows interact with each other, and the proportion of water following the various pathways may therefore vary depending on the prevailing driving forces and the relative conductivity of the pathways, which themselves are subject to modulation by environmental conditions. Under the condition of active transpiration a higher hydraulic gradient between soil and xylem is created and the passive water transport dominants. The transport of solutes into the roots simultaneously with water will, on the other hand, increase the osmotic pressure gradient across semi-permeable membranes, thus providing a driving force for the osmotic components of the symplast and cell-to-cell pathways.

The water conductivity of roots changes mainly as a function of their age and

stage of development. It is also sensitive to water and salt stress and temperature changes. Water and nutrients loaded from the soil are transported from roots to leaves, growing cells and other tissues via the xylem. The driving force in the xylem is a pressure gradient (negative with respect to the atmospheric pressure) that is generated by the water evaporation in leaves. That means that xylem elements should satisfy the following conditions. They should have relatively low resistance to the flow of water. The walls of water conducting cells have to withstand the compressive forces that develop in actively transpiring plants. To provide the long distance mass flow of water and solutes the cell walls must be waterproof. At the same time the cell walls should not be entirely isolated in order to be able to allow the exchange of water and nutrients between different types of cells in xylem and other tissues.

The water conducting elements of xylem are vessels and tracheids (Fig. 1.2). The

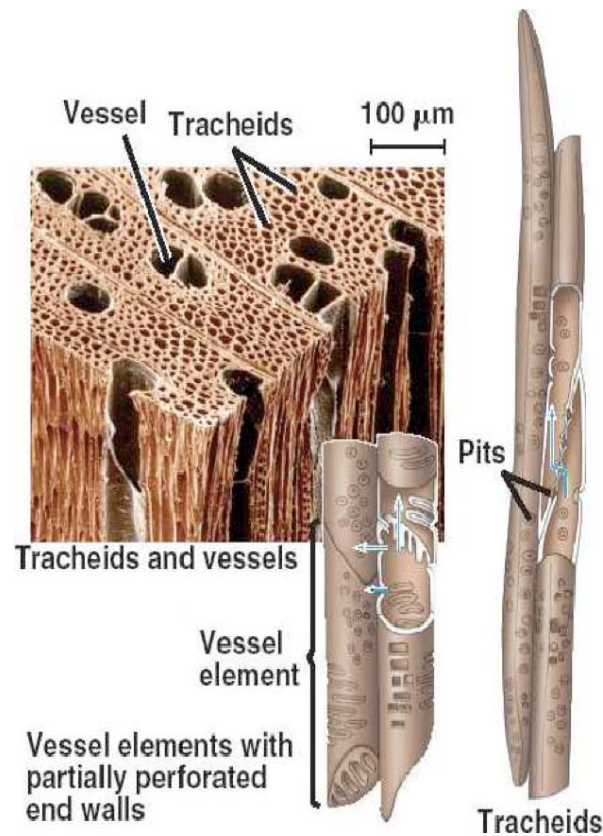


Figure 1.2 : The structure of xylem system in plants (<https://eapbiofield.wikispaces.com>).

mature xylem vessels are formed from long cells that lack a protoplast, and the axial walls of these cells are perforated or removed. Such structural features of vessels keep their hydraulic conductivity high. Water moves from vessel to vessel via pits that are water permeable membranes. Mature tracheids also lack protoplast and their walls contain pits. The hydraulic conductivity of xylem is determined by the permeability of the perforation plates and pit membranes and the diameter of the xylem vessels or tracheids. According to Poiseuille's law the hydraulic conductivity of water flow is proportional to the fourth power of the vessel radius. Thus, even a small change in the radius of water conducting cells will cause a significant change in resistance.

To withstand the large negative pressure vessels and tracheids have a lignified secondary cell wall that covers the primary wall entirely except for the pit membranes. The secondary cell wall provides the strength and prevents leakage from the water transporting xylem elements. The pits contain a membrane structure that is formed from a modified primary cell wall. They are highly permeable and form the path for water movement between the xylem conduits themselves, and between the water transporting elements and the adjacent xylem parenchyma cells. Bordered pits are characterized by an arched shape. Such a shape makes pits an important element of the system protecting plants against cavitation and embolism (Zwieniecki and Holbrook, 2000). Since the water permeability of lignified secondary cell walls of xylem vessels is low water enters the vessels via pits that cover about 10-20% of the surface. Calculations of water flow in roots showed that the xylem parenchyma/xylem vessel interface should be a "bottle-neck" in the path of water transport from the soil to the xylem. To resolve this problem the presence of low resistance water channels or aquaporins was proposed and subsequently confirmed (for reviews see Maurel, 1997, Johansson *et al.*, 2000, Maurel and Chrispeels, 2001).

Once delivered to the leaves water evaporates from the surface of the mesophyll cells into the air-filled substomatal cavity of the leaf. From there, water vapour diffuses via the stomata to the atmosphere surrounding the leaf, a process driven by the water vapour pressure difference between the interior air space of the leaf and the adjacent atmosphere. A consequence of water evaporation from the surface of the mesophyll cells is a decrease in the water potential (mostly via a decrease in osmotic potential) of these cells, which results in a driving force for the movement of water from the xylem network of the leaf (for a review see Buckley, 2005). The conductance of stomata for the diffusion of water vapour (and CO₂) is under physiological control; each stomate is comprised of two guard cells and the adjustments of the turgor pressure results in changes to the degree of stomatal opening and thus their diffusive conductance. Stomata therefore play a critical role in the rapid regulation of water loss and appear to respond to any change in the soil-plant-atmosphere hydraulic continuum (Schulze and Küppers, 1979, Jones, 1998, Giorio *et al.*, 1999).

The second long-distance transport system in plants is phloem (Fig. 1.3). It transports photosynthates or stored carbohydrates, commonly in the form of sucrose both up and down the stem, depending on which organs are currently sinks (have deficit of sucrose) and which are sources (have an excess of photosynthates or are breaking down storage carbohydrates, such as starch). Phloem mainly consists of two types of cells: sieve tube elements and companion cells. Sieve elements are living cells

with elastic un lignified cellulose walls. Their cytoplasm is relatively empty and are interconnected by porous sieve plates, which allows the carbohydrate solution to move from element to element. As they mature, sieve cells lose their nuclei and retain only few organelles so they are dependent upon the companion cells surrounding them. These have both cytoplasm and nuclei and are connected to sieve elements by plasmodesmata and function as life support units for sap transporting elements. According to the pressure flow hypothesis proposed by E. Münch phloem flow is the result of an osmotically-generated pressure gradient. Active loading of sucrose into the phloem in source tissues generates low osmotic potential in sieve elements and water then enters the phloem down this potential gradient. Active unloading of sucrose in sinks generates a higher osmotic potential in sieve elements, so water flows out of the phloem, generating a hydrostatic pressure gradient. This pressure gradient pushes the phloem sap along the stem from source to sink (Thompson, 2006).

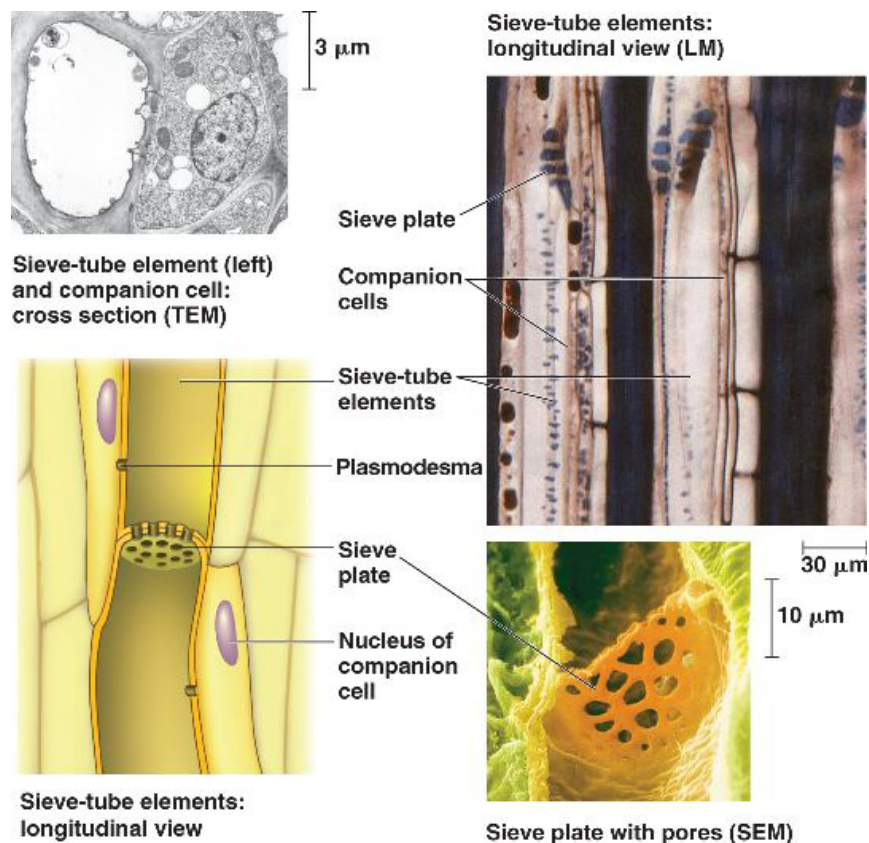


Figure 1.3 : The structure of phloem in plants (<https://eapbiofield.wikispaces.com>).

1.3 Cavitation and embolism repair

Water is transported in the xylem conduits under tension. That makes the vessels vulnerable to cavitation (rupture of the water column) resulting in an embolism (filling the vessels with air) (Zimmermann, 1983). The vulnerability of xylem to cavitation increases with conduit diameter both across and within species (Salleo and Lo Gullo, 1989, Lo Gullo and Salleo, 1993), and root xylem is usually more vulnerable than that of the stem (Sperry and Ikeda, 1997).

An air bubble can be removed from the conduit only by forcing the gas to dissolve in water. The water in an embolized conduit is at atmospheric pressure and is in equilibrium with atmospheric gases, so according to Henry's law, the pressure of the gas inside an air bubble is:

$$P_g = P_x + \frac{2T}{r}, \quad (1.1)$$

where P_x is the pressure inside the xylem element, T is the surface tension of water and r is the radius of the curvature of the air-water interface (the maximum r is the radius of the conduit) (Sperry, 2004). Therefore, when the pressure in the embolized conduit exceeds $-2T/r$, the pressure in the air bubble is greater than atmospheric and the gas in the bubble starts to dissolve.

Numerous measurements show that during the repair of the embolized vessel other xylem elements are under tension. That means that damaged conduits must be sealed hydraulically from the rest of the xylem, but at the same time water has to enter to refill the conduit. An explanation for this puzzle was proposed by Tyree *et al.* and Holbrook and Zwieniecki (Tyree *et al.*, 1999, Holbrook and Zwieniecki, 1999). The water permeability of the lignified secondary cell walls is low. The remaining path for water flux is then through the pits. According to their theory, the non-zero contact angle of water and the bordered pit membrane forms a convex gas-water interface in the pit channel. The surface tension of this convex interface withstands a positive pressure that is high enough to dissolve gas within the lumen, but not high enough to force the gas-water interface across the bordered pit channel. Thus, the embolized conduit remains hydraulically isolated from the neighboring active xylem elements until all air has been dissolved.

The next question is how a plant generates an above atmospheric pressure in the embolized vessel. The first proposed mechanism is root pressure, which is generated during the night when transpiration is low. Measurements in a range of plants have confirmed the presence of root pressure under certain conditions (Sperry *et al.*, 1987, Tyree and Yang, 1992, Cochard *et al.*, 1994, Stiller *et al.*, 2003). However, it seems that several plants never develop root pressure (Fisher *et al.*, 1997). Moreover, pressure decreases by gravity at a rate of 10 kPa/m and it is unlikely that in a tall tree roots are able to generate the required positive pressure in their upper shoots. It then follows that positive pressure should be generated locally in the embolized conduit. Many hypotheses for embolism-refilling mechanisms have been proposed (Salleo *et al.*, 2004, Hölttä *et al.*, 2006), but no one can explain the process entirely. There are three main hypotheses for embolism repair.

The osmotic hypothesis assumes that the xylem parenchyma cells surrounding an

embolized vessel inject osmotically active ions such as K^+ and Cl^- into the vessel via the pit membranes (Grace, 1993). Water then loads into the conduit due to osmosis. This hypothesis is supported by observations of an increase in the concentration of inorganic ions in the xylem sap during refilling of embolized conduits (Tyree *et al.*, 1999). According to calculations, however, the osmotic potential that develops in refilling conduits due to the increased concentration of inorganic ions is too small to create a large water flux and refilling would require about 10 h (Vesala *et al.*, 2003, Hacke and Sperry, 2003). Experimentally, however, relatively fast embolism repair has been shown in petioles of sunflower (Canny, 1997a), the primary root of squash plants (Berndt *et al.*, 1999), young stems of laurel (Tyree *et al.*, 1999, Salleo *et al.*, 2004) and the roots of maize plants (Facette *et al.*, 2001), which is a major problem for this hypothesis.

The second hypothesis is the reverse osmotic one. Reverse osmosis occurs when surrounding parenchyma cells increase their osmotic potential by conversion of starch to sugars. The increase of the osmotic potential results in an increase of turgor pressure in the parenchyma cells, and the water from these cells is squeezed into the embolized vessel (Canny, 1997a, b; McCully, 1999, Tyree *et al.*, 1999). The problem with this theory is that the water flow from the over-pressured parenchyma cell will not be directed only towards the ruptured conduit (Tyree *et al.*, 1999). In the previous mechanism the flow is directed by specific loading of ions into an embolized element. However microscopic investigation of root xylem reveals an uneven distribution of aquaporins in the cell membranes (Siefritz *et al.*, 2001). This could indicate that aquaporins are concentrated near to the contact pits between xylem parenchyma cells and xylem vessels ensuring a polarity in the hydraulic resistance of cells adjacent to the conduits and which would channel the water flow from the parenchyma cell towards the xylem.

The phloem-driven xylem refilling mechanism is based on the observation that recovery from embolism was reduced in laurel (Salleo *et al.*, 1996), red maple, the tulip tree and northern foxglove (Zwieniecki *et al.*, 2000) when the plants were girdled (where secondary phloem was removed). This led to the proposal that that phloem participates in the repair of embolized conduits. It has been proposed that a proton pump is activated and a radial flow of solutes is induced from phloem to a cavitated xylem element in response to hormonal signaling. In this case, radial flow would assist osmotic flow into the embolized conduit.

The correlation between the xylem pressure and the loss of hydraulic conductivity suggests that cavitation is part of a feedback mechanism linking the regulation of the stomatal, control of transpiration, and the plant water status. It is known that stomata have a threshold response to a hydraulic signal generated by a perturbation of the hydraulic pathway even if the leaf water potential remains constant (Whitehead *et al.*, 1996). Cavitation causes a temporary release of water that can buffer the leaf water status (Salleo *et al.*, 1992), but at the same time it decreases the hydraulic conductivity, and which of these effects initiates the stomatal response is not exactly known. There may also be a chemical signal involved in the regulation, released by xylem parenchyma at the site of cavitation or somewhere in the leaves, as a response to the change in the water potential gradient (Whitehead *et al.*, 1996). It has been

proposed that cavitation is an adaptive mechanism resulting in a quick reduction of the hydraulic conductance while the stomatal continues to maintain an optimal stomatal conductance (Saliendra *et al.*, 1995).

1.4 Radial water transport

In addition to the long-distance water transport in the xylem (and phloem) tissues in roots and shoots, the stem and shoot connected to the xylem act as water storage capacitors. This capacitor effect has been demonstrated by the simultaneous measurement of the xylem flow near the base of the trunk and in the crown of an intact tree in the morning, when transpiration is increasing. The rise of the basal flow is delayed relative to the branch flow implying the presence of water reservoir or capacitor in the intervening tissues (Goldstein *et al.*, 1998, Meinzer *et al.*, 2003). Also clear delay in changes in water content between the storage tissue down stream and upstream has been observed (Van As *et al.*, 1994). The water potential drop produced by the increase of transpiration from the leaves results in water transport from the storage compartments into the transpiration stream. That helps to compensate for sudden, rapid water loss from the plant and the temporal imbalance between water supply and demand (Holbrook, 1999). The xylem vessels in woody plants are associated with living xylem parenchyma cells, which have a high metabolic activity and are able to perform the energy demanding process of xylem loading. In addition, these parenchyma cells have elastic walls. Therefore they can undergo a significant change in volume with only a relatively small change in turgor. These properties make the parenchyma cells good water storage compartments. Water transport between xylem vessels and parenchyma cells is facilitated by cell wall invaginations that increase the membrane surface area of the parenchyma cells, which is typical for the transport elements. Tissues as pith and bark, whose function appears to serve largely as water storage compartments, are distant from xylem vessels. In order to serve as water buffers in the tree stem they have to have a good hydraulic connection with the xylem conduits. Water stored in the different tissues of the stem can contribute from 6 to 50% of the total daily water loss by transpiration. Even when the contribution of the storage compartments to the daily change of water content in a tree is not considerable, they can still play a significant role in the maintenance of leaf water status and carbon balance (Lo Gullo and Salleo, 1992, Goldstein *et al.*, 1998).

1.5 Main experimental methods

Two main types of NMR measurements are available to investigate water content and water transport in trees. Spin-spin (T_2) and spin-lattice (T_1) relaxation time measurements are used to characterize water content and the physical properties of water in the different tissues. Pulsed field gradient (PFG) NMR techniques can be used to detect displacement (i.e. flow or diffusion) of water.

Most of the T_1 quantification techniques are based on the measurement of the longitudinal magnetization at different time intervals (TI) after inversion of the signal.

When a sample is placed in a static magnetic field and an inversion radio frequency (rf) pulse is applied, the net magnetization of the sample relaxes back to its equilibrium value with the decay time T_1 according to

$$M(TI) = M(0) \left(1 - 2e^{-TI/T_1}\right), \quad (1.2)$$

$M(0)$ is the magnetization at time zero, which is proportional to the proton density. Here it is assumed that the repetition time TR between each TI interval is longer than $5T_1$. If this condition does not hold and $TR < 5T_1$, then saturation takes place. The magnetization measured at time TI is given by

$$M(TI) = M(0) \left(1 - e^{-TR/T_1}\right) \left(1 - 2e^{-TI/T_1}\right) e^{-TE/T_2}. \quad (1.3)$$

Here TE is the echo time (time between the excitation pulse and the detection of the signal). In biological tissues the apparent T_1 (T_{1app}) depends on the actual T_1 and the average residence time of a spin within a compartment (τ) as follows

$$\frac{1}{T_{1app}} = \frac{1}{T_1} + f \left(\frac{1}{\tau}\right). \quad (1.4)$$

In the simplest model, which assumes that the average lifetime is determined by the time to pass the membrane and that all magnetization that passes the membranes is lost for observation, the lifetime of a proton within a compartment is given by the permeability coefficient P of the membrane surrounding the compartment, the surface area S of the membranes and the volume V of the compartment space. Equation (1.4) can then be expressed as

$$\frac{1}{T_{1app}} = \frac{1}{T_1} + P \frac{S}{V}. \quad (1.5)$$

Immediately after excitation with a 90° rf pulse, the signal starts decaying exponentially due to spin-spin interactions. The magnetization, $M(t)$, is therefore determined by the following equation

$$M(t) = M(0) e^{-t/T_2}, \quad (1.6)$$

where the relaxation process is characterized by T_2 . To determine the T_2 relaxation time we make use of the spin echo sequence, where the n th echo amplitude $M(nTE)$ is given by

$$M(nTE) = M(0) \left(1 - e^{-TR/T_1}\right) e^{-nTE/T_2}. \quad (1.7)$$

The T_{2app} observed in biological tissues differs from the bulk T_2 . It is well established that T_{2app} is related to the compartment size (Brownstein and Tarr, 1977, 1979) and reflects the relaxation properties of the membrane and its water permeability (van der Weerd *et al.*, 2001)

$$\frac{1}{T_{2app}} = \frac{1}{T_2} + H \frac{S}{V}. \quad (1.8)$$

H is the net signal loss at the compartment's surface (and reflects the wall relaxation and membrane permeability). We should note that Eq. (1.8) and Eq. (1.5) are very comparable.

Thus, relaxation measurements can provide information on the water content of the tissue; T_1 and T_2 can be used for determination of different proton pools and different types of cells (Glidewell, 2006, Van der Weerd *et al.*, 2001) or cell organelles (Stout and Steponkus, 1978, Sibgatullin *et al.*, 2007), the geometry of cell compartments (Brownstein and Tarr, 1977, 1979, van der Weerd *et al.*, 2001), cell membrane permeability and water exchange (Bacić and Ratković, 1984, van der Weerd *et al.*, 2001).

The displacement of protons can be measured with the pulsed field gradient (PFG) technique. This method uses two gradient pulses of amplitude \mathbf{g} and duration δ separated by the time interval, Δ . If a molecule starting at position \mathbf{r} moves to a position \mathbf{r}' during time Δ , the echo attenuation for an ensemble of molecules can be written as (Callaghan, 1991)

$$E(\mathbf{g}, \Delta) = \int \int d\mathbf{r} d\mathbf{r}' \varrho(\mathbf{r}) e^{-i\gamma\delta\mathbf{g}\mathbf{r}} P(\mathbf{r}|\mathbf{r}', \Delta) e^{i\gamma\delta\mathbf{g}\mathbf{r}'}, \quad (1.9)$$

where $\varrho(\mathbf{r})$ is the spin density and $P(\mathbf{r}|\mathbf{r}', \Delta)$ is the probability that a molecule is displaced from \mathbf{r} to \mathbf{r}' over time Δ .

$P(\mathbf{r}|\mathbf{r}', \Delta)$ describes a process in which the original state at a given time, t_0 , fully determines the final state at time, $t_1 > t_0$, i.e. the final state does not depend on the states of the system at $t < t_0$. That means that the probability $P(\mathbf{r}|\mathbf{r}', \Delta)$ should only depend on the time difference, $\Delta = t_1 - t_0$. Assuming the probability that a molecule moves from \mathbf{r} to \mathbf{r}' , depends only on the displacement $\mathbf{r} - \mathbf{r}'$, Eq. (1.9) may then be rewritten as

$$E(\mathbf{q}, \Delta) = \int d\mathbf{r} \varrho(\mathbf{r}) \int d\mathbf{r}' P(\mathbf{r} - \mathbf{r}', \Delta) e^{-i2\pi\mathbf{q}(\mathbf{r}-\mathbf{r}')}, \quad (1.10)$$

where $\mathbf{q} = \gamma\delta\mathbf{g}/(2\pi)$ is the reciprocal space vector. The diffusional motion with the self-diffusion coefficient, D , results in an incoherent distribution of phase shifts leading to attenuation of signal (Stejskal and Tanner, 1965)

$$E(q, \Delta) = E(0) e^{-4\pi^2 q^2 D(\Delta - \delta/3)}. \quad (1.11)$$

Uniform flow with velocity \mathbf{v} over time Δ along the direction \mathbf{q} causes a net phase shift

$$E(\mathbf{q}, \Delta) = E(0) e^{-i2\pi\mathbf{q}\mathbf{v}\Delta}. \quad (1.12)$$

The combination of PFG and Magnetic Resonance Imaging (MRI) experiments allows one to obtain the dynamic displacement profile for every pixel in an image (Callaghan *et al.*, 1988). The spatial resolution that can be obtained in MRI is limited and in general not sufficient to resolve single xylem vessels (Scheenen, 2001, Windt *et al.*, 2006). A single voxel therefore contains the signal originating from one or more vessels and a significant amount of signal from surrounding cells.

1.6 Outline of the thesis

During their lifetime trees are exposed to multiple environmental stresses, one of the most common of which is drought stress. Since water deficit is an important limiting factor for photosynthesis and the growth of plants, it is expected that they should have developed mechanisms for minimizing both the development of this stress and its consequences. The flow characteristics of plants are very sensitive to variations in plant water status and can give important information about regulation of water transport processes. The analysis of plant water relations indicates that the intrinsic storage capacities in root, stem and leaves are part of a system for regulating water distribution and a mechanism for protection against the formation of embolisms and, if necessary, their repair. Although these principles are now well known, the dynamics of the interrelationship and integration between these processes at the plant level is still lacking. We need to be able to measure phloem and xylem flow in relation to the water content of the surrounding tissues (the storage pools), under both normal and water limiting, or even stress, conditions (e.g. drought) in intact plants. The aim of this thesis is the study (and modeling) of the dynamics of water transport in ring-porous and diffuse-porous trees by non-invasive dedicated plant MRI techniques. The focus is on long-distance xylem transport, the vulnerability of xylem to cavitation, and the repair of embolised vessels during drought and recovery from drought, short distance radial transport, and the behavior of storage pools and their relationship to axial water fluxes.

First we will compare two MRI systems with different field strengths B_0 . Susceptibility effects (local distortions of the magnetic field strength due to differences in magnetic permeability of the tissues) depend on B_0 and result in a dependency of the apparent T_2 values on TE . However this disadvantage of a high B_0 needs to be offset against the higher sensitivity (higher signal-to-noise ratio) that arises from the use of a high B_0 , which allows shorter measurement time or better spatial resolution. In Chapter 2 we compare results of T_2 relaxation measurements and flow parameters obtained for one tree, imaged at a magnetic field strength 0.7 and 3 T. Some evidence was found that at 3 T susceptibility effects can be present. We also demonstrate the possibility of using MRI flow measurements for the physiological mapping of intact trees in different seasons and at different activities of physiological processes in the plant.

For porous systems like a tree stem, (strong) susceptibility effects can be present. These local gradients can result in uncorrected attenuation of the NMR signal of flowing water molecules. In addition, surface relaxation and exchange with stagnant water pools can result in an extra signal loss. In Chapter 3 the results of an investigation of the influence of these mechanisms on measured propagators and apparent flow parameters at increasing observation time are presented. Based on the results, a method for quantification of water exchange between stagnant and flowing fluid with different relaxation behavior is presented.

In Chapter 4 we investigate the contribution of intrinsic water storage capacities in sapwood and the cambial zone to maintain the balance between water supply and demand during a fast increase in transpiration (morning, switching on lamps) as well

as during a period of drought and subsequent recovery in laurel and viburnum trees, which have a diffuse-porous wood architecture. We demonstrate that water storage pools in the sapwood and cambial zone behave differently in relation to the xylem flow. The accuracy with which we are able to distinguish flowing from stationary water is not very high when there is a substantial fraction of fluid flowing with low velocity in the presence of significant signal from stationary water in the cells adjacent to xylem vessels. We propose the use of correlated displacement- T_2 measurements to improve the discrimination between water inside xylem vessels from that in other cell types.

In Chapter 5 we investigate the vulnerability to cavitation of the large earlywood xylem vessels of a ring-porous oak tree (*Q. robur*) during drought. The values of xylem water content and flow conducting area measured with non-invasive MRI methods are for the first time compared to water potential measurements obtained by stem psychrometers. In contrast to the MRI results, results obtained using the standard centrifuge and air-injection methods stem segments indicated complete cavitation at lower xylem pressures than observed *in situ*. An artifact in these destructive methods was revealed. These results demonstrate the power of MRI plant imaging and we suggest improvements to the protocols for measuring vulnerability curves by destructive methods.

References

- Bacić G., Ratković S. (1984) Water exchange in plant tissue studied by proton NMR in the presence of paramagnetic centers. *Biophysical Journal*, **45**, 767-776.
- Berndt M.L., McCully M.E., Canny M.J. (1999) Is xylem embolism and refilling involved in the rapid wilting and recovery of plants following root cooling and re-warming? A cryo-microscope investigation. *Plant Biology*, **1**, 506-515.
- Brownstein K.R., Tarr C.E. (1977) Spin-lattice relaxation in a system governed by diffusion. *Journal of Magnetic Resonance*, **26**, 17-24.
- Brownstein K.R., Tarr C.E. (1979) Importance of classical diffusion in NMR studies of water in biological cells. *Physical Review A*, **19**, 2446-2453.
- Buckley T.N. (2005) The control of stomata by water balance. *New Phytologist*, **168**, 275-292.
- Callaghan P.T., Eccles C.D., Xia Y. (1988) NMR microscopy of dynamic displacements: *k*-space and *q*-space imaging. *Journal of Physics E: Scientific Instruments*, **21**, 820-822.
- Callaghan P.T. (1991) *Principles of nuclear magnetic resonance microscopy*. Oxford: Oxford University Press.
- Canny M.J. (1997a) Vessel contents of leaves after excision - a test of Scholander's assumption. *American Journal of Botany*, **84**, 1217-1222.
- Canny M.J. (1997b) Vessel content during transpiration - embolisms and refilling. *American Journal of Botany*, **84**, 1223-1230.
- Cochard H., Ewers F.W., Tyree M.T. (1994) Water relation of a tropical vine-like bamboo (*Rhipidocadum racemiflorum*): root pressure, vulnerability to cavitation and seasonal changes in embolism. *Journal of Experimental Botany*, **45**, 1085-1089.
- Facette M.R., McCully M.E., Shane M.W., Canny M.J. (2001) Measurements of the

time to refill embolized vessels. *Plant Physiology and Biochemistry*, **39**, 59-66.

Fisher J.B., Angeles G., Ewers F.W., Lopes Portillo J. (1997) Survey of root pressures in tropical vines and woody species. *International Journal of Plant Sciences*, **158**, 44-50.

Giorio P., Sorrentino G., d'Andria (1999) Stomatal behavior, leaf water status and photosynthetic response in field-grown olive trees under water deficit. *Environmental and Experimental Botany*, **42**, 95-104.

Glidewell S.M. (2006) NMR imaging of developing barley grains. *Journal of Cereal Science*, **43**, 70-78.

Goldstein G., Andrade J.L., Meinzer F.C., Holbrook N.M., Cavelier J., Jackdon P. (1998) Stem water storage and diurnal patterns of water use in tropical forest canopy trees. *Plant, Cell and Environment*, **21**, 397-406.

Grace J., (1993) Refilling of embolized xylem. In *Water Transport in Plants Under Climatic Stress*, Cambridge University Press, Cambridge, UK.

Hacke U., Sperry J.S. (2003) Limits of xylem refilling under negative pressure in *Laurus nobilis* and *Acer negundo*. *Plant, Cell and Environment*, **26**, 303-311.

Holbrook N.M. (1999) Stem water storage. In: Gartner B.L. (Ed.), *Plant stems: physiological and functional morphology*. Academic Press, San Diego, 151-174.

Holbrook N.M., Zwieniecki M.A. (1999) Embolism repair and xylem tension: Do we need a miracle? *Plant Physiology*, **120**, 7-10.

Hölttä T., Vesala T., Perämäki M., Nikinmaa E. (2006) Refilling of embolised conduits as a consequence of "Münch water" circulation. *Functional Plant Biology*, **33**, 949-959.

Johansson I., Karlsson M., Johanson U., Larsson C., Kjellbom P. (2000) The role of aquaporines in cellular and whole plant water balance. *Biochimica Biophysica Acta*, **1465**, 324-342.

Jones H.G. (1998) Stomatal control of photosynthesis and transpiration. *Journal of Experimental Botany*, **49**, 387-398.

Lo Gullo M.A., Salleo S. (1993) Different vulnerability of *Quercus ilex* L. to freeze and summer drought-induced xylem embolism: an ecological interpretation. *Plant, Cell and Environment*, **16**, 511-519.

-
- Maseda P.H., Fernandes R.J. (2006) Stay wet or else: three ways in which plants can adjust hydraulically to their environment. *Journal of Experimental Botany*, **57**, 3963-3977.
- Maurel C. (1997) Aquaporins and water permeability of plant membranes of plant membranes. *Annual Review of Plant Physiology and Plant Molecular Biology*, **48**, 399-429.
- Maurel C., Chrispeels M.J. (2001) Aquaporins. A molecular entry into plant water relations. *Plant Physiology*, **125**, 135-138.
- McCully M.E. (1999) Root xylem embolisms and refilling. Relation to water potentials of soil, roots and leaves, and osmotic potential of root xylem sap. *Plant Physiology*, **119**, 1001-1008.
- Meinzer F.C., James S.A., G., Woodruff D. (2003) Whole-tree water transport scales with sapwood capacitance in tropical forest canopy trees. *Plant, Cell and Environment*, **26**, 1147-1155.
- Saliendra N.Z., Sperry J.S., Comstock J.P. (1995) Influence of leaf water status on stomatal response to humidity, hydraulic conductance, and soil drought in *Betula occidentalis*. *Planta*, **196**, 357-366.
- Salleo S., Lo Gullo M.A. (1989) Xylem cavitation in nodes and internodes of *Vitis vinifera* L. plant subjected to water stress: limits of restoration of water conduits. In: Kreeb K.H., Richter H., Hinckley T.M. (Eds.), *Structural and Functional Responses to Environmental Stress: Water Shortage*. SPB Academic Publishing, The Hague, pp. 33-42.
- Salleo S., Hinckley T.M., Kikuta S.B., Lo Gullo M.A., Weilgony P., Yoon T.M., Richter H. (1992) A method for inducing xylem emboli in situ-experiments with a field-grown tree. *Plant, Cell and Environment*, **15**, 491-497.
- Salleo S., Lo Gullo M.A., De Paoli D., Zippo M. (1996) Xylem recovery from cavitation-induced embolism in young plants of *Laurus nobilis*: a possible mechanism. *New Phytologist*, **132**, 47-56.
- Salleo S., Lo Gullo M.A., Trifilo P., Nardini A. (2004) New evidence for a role of vessel-associated cells and phloem in the rapid xylem refilling of cavitated stems of *Laurus nobilis* L. *Plant, Cell and Environment*, **27**, 1065-1076.
- Scheenen T.W.J., van Dusschoten D., de Jager P.A., Van As H. (2000) Quantification of water transport in plants with NMR imaging. *Journal of Experimental Botany*, **51**, 1751-1759.

- Scheenen T.W.J. (2001) *Nuclear Magnetic Resonance imaging of water motion in plants*, PhD thesis, Wageningen Universiteit.
- Schulze E.-D., Küppers M. (1979) Short-term and long-term effects of plant water deficits on stomatal response to humidity in *Corylus avellana* L. *Planta*, **146**, 319-326.
- Sellers P.J., Dickinson R.E., Randall D.A., Betts A.K., Hall F.G., Berry J.A., Collatz G.J., Denning A.S., Mooney H.A., Nobre C.A., Sato N., Field C.B., Henderson A. (1997) Modeling of exchange of energy, water and carbon between continents and the atmosphere. *Science*, **275**, 502-509.
- Sibgatullin T.A., de Jager P.A., Vergeldt F.J., Gerkema E., Anisimov A.V., Van As H. (2007) Combined analysis of diffusion and relaxation behavior of water in apple parenchyma cells. *Biophysics*, **52**, 196-203.
- Siefritz F., Biela A., Eckert M., Otto B., Uhlein N. (2001) The tobacco plasma membrane aquaporin NtAQP1. *Journal of Experimental Botany*, **52**, 1953-1957.
- Sperry J.S., Holbrook N.M., Zimmermann N.H., Tyree M.T. (1987) Spring filling of xylem vessels in wild grapevine. *Plant Physiology*, **83**, 414-417.
- Sperry J.S., Ikeda T. (1997) Xylem cavitation in roots and stems of Douglas fir and white fir. *Tree Physiology*, **17**, 275-280.
- Sperry J.S. (2004) Coordinating stomatal and xylem functioning - an evolutionary perspective. *New Phytologist*, **162**, 568-570.
- Stejskal E.O., Tanner J.E. (1965) Spin diffusion measurements: Spin echoes in the presence of a time-dependent field gradient. *Journal of Chemical Physics*, **42**, 288-292.
- Steudle E., Peterson C.A. (1998) How does water get through roots? *Journal of Experimental Botany*, **49**, 775-788.
- Steudle E. (2000) Water uptake by plant roots: an integration of views. *Plant and Soil*, **226**, 45-56.
- Stiller V., Lafitte H.R., Sperry J.S. (2003) Hydraulic properties of rice and the response of gas exchange to water stress. *Plant Physiology*, **132**, 1698-1706.
- Stout D.G., Steponkus P.L. (1978) Nuclear magnetic resonance relaxation times and plasmalemma water exchange in ivy bark. *Plant Physiology*, **62**, 636-641.
- Thompson M.V. (2006) Phloem: the long and the short of it. *Trends in Plant Science*, **11**, 26-32.

Tyree M.T., Yang S. (1992) Hydraulic conductivity recovery versus water pressure in xylem of *Acer saccharum*. *Plant Physiology*, **100**, 669-676.

Tyree M.T., Salleo S., Nardini A., Lo Gullo M.A., Mosca R. (1999) Refilling of embolized vessels in young stems of laurel. Do we need a new paradigm? *Plant Physiology*, **120**, 11-21.

van der Weerd L., Claessens M.M., Ruttink T., Vergeldt F.J., Van As H. (2001) Quantitative NMR microscopy of osmotic stress responses in maize and pearl millet. *Journal of Experimental Botany*, **52**, 2333-2343.

Vesala T., Hölttä T., Perämäki M., Nikinmaa E. (2003) Refiling of a hydraulically isolated embolized xylem vessel: model calculations. *Annals of Botany*, **91**, 419-428.

Whitehead D., Livingston N.J., Kelliher F.M., Hogan K.P., Pepin S., McSeveny T.M., Byers J.N. (1996) Response of transpiration and photosynthesis to a transient change in illuminated foliage area for a *Pinus radiata* D. Don tree. *Plant, Cell and Environment*, **19**, 949-957.

Windt C.W., Vergeldt F.J., De Jager P.A., Van As H. (2006) MRI of long-distance water transport: a comparison of the phloem and xylem flow characteristics and dynamics in poplar, castor bean, tomato and tobacco. *Plant Cell and Environment*, **29**, 1715-1729.

Zimmermann U. (1983) *Xylem Structure and the Ascent of Sap*. Berlin: Springer-Verlag.

Zwieniecki M.A., Holbrook N.M. (2000) Bordered pit structure and vessel wall surface properties. Implication for embolism repair. *Plant Physiology*, **123**, 1015-1020.

Zwieniecki M.A., Huttyra L., Thompson M.V., Holbrook N.M. (2000) Dynamic changes in petiole specific conductivity in red maple (*Acer rubrum* L.), tulip tree (*Liriodendron tulipifera* L.) and northern fox grape (*Vitis labrusca* L.). *Plant, Cell and Environment*, **23**, 407-414.

Chapter 2

0.7 and 3 T MRI and sap flow in intact trees: xylem and phloem in action

Dedicated MRI hardware is described that allows imaging of sap flow in intact trees with a maximal trunk diameter of 4 cm and height of several meters. This setup is used to investigate xylem and phloem flow in an intact tree quantitatively. Due to the fragile gradients in pressure present in both xylem and phloem, methods to study xylem and phloem transport must be minimal invasive. MRI flow imaging by means of this hardware certainly fulfils this condition. Flow is quantified in terms of (averaged) velocity, volume flow (flux) and flow conducting area, either in imaging mode or as a non-spatially resolved total. Results obtained for one tree, imaged at two different field strengths (0.7 and 3 T), are compared. An overall shortening of observed T_2 values is manifested going from 0.7 to 3 T. Although some susceptibility artefacts may be present at 3 T, the results are still reliable and the gain in sensitivity results in shorter measurement time (or higher signal to noise ratio) with respect to the 0.7 T system. The results demonstrate that by use of dedicated hardware xylem and phloem flow, and its mutual interaction, can be studied in intact trees in relation to the water balance and in response to environmental (stress) conditions.¹

2.1 Introduction

Due to their long life span, changing climatic conditions are of particular importance for trees. Worldwide current forests will be faced with altered environmental conditions during their life time, with likely consequences for species composition and forest management (Saxe *et al.*, 2001). On the other hand forest trees can manage affected parameters, water in transpiration stream and CO₂ after fixation in assimilation transport.

¹This Chapter is based on: Homan N.M., Windt C.W., Vergeldt F. J., Gerkema E., Van As H. (2007) 0.7 and 3 T MRI and sap flow in intact trees: xylem and phloem in action. *Applied Magnetic Resonance*, **32**, p. 157-170.

Long distance water transport processes within trees are directly related to the transpiration stream and provide without doubt key information in relation to understanding responses to changing climatic conditions. These transport processes consist of phloem and xylem, which provide the transport of water, nutrients and signals between the organs of plants. The xylem is responsible for the transport of water and nutrients from the soil to the leaves, whereas the phloem is responsible for the transport of photosynthates, amino acids and electrolytes from source leaves to the rest of the plant. According to the current view the driving forces of long distance transport are hydrostatic pressure, water potential and (sugar) concentration gradients in the transport systems. Gas exchange (water vapour, CO₂, O₂) and associated processes are central factors in regulating long distance xylem transport. It is undisputed that in both, xylem and phloem, complex fragile gradients in pressure and potential exist that are easily disturbed by invasive experimentation (Bancal and Soltani, 2002, Knoblauch and Van Bel, 1998, Van Bel, 2003a, Van Bel, 2003b, Lalonde *et al.*, 2003). Therefore, investigations on xylem and phloem are very difficult, since any manipulation simply leads to artefacts, particularly with respect to quantification. Nevertheless knowledge of transport velocity, fluxes and transported solutes are of major importance for central questions in tree physiology.

For several decades heat tracer methods are used to measure the mass flow in xylem. Up to now they are used in several eco-physiological investigations. This has led to acceptable results if precautions against potential sources of error are taken (Smith and Allen, 1996). A general problem is that heat dissipation probes do not truly integrate velocity along the probe length. Furthermore, the placement of the sensor itself is a source of errors, particularly for the heat-pulse method (Clearwater *et al.*, 1999). Calculations of mass flow rates from sap velocities obtained by heat pulse techniques require a reliable estimate of sap-conducting surface area. Measurement of the active surface in general is very difficult. In addition, it is known that shrinking and swelling of the stem occur periodically (Sevanto *et al.*, 2002), and that day/night rhythm may be accompanied by changes in sap conducting surface area (Windt *et al.*, 2006). All these factors can result in substantial underestimation of the actual sap flow.

The method that has been most successful in providing detailed, non-invasive information on the characteristics of water transport in the xylem as well as in the phloem of intact plants is MRI (for overviews see Refs. MacFall and Van As, 1996, Köckenberger, 2001). Several groups have used different MRI methods. Most of them are based on (modified) Pulsed Field Gradient (PFG) methods, either by using a limited number of PFG steps or by (difference) propagator approaches (Callaghan *et al.*, 1988). Also flow measurements based on uptake and transport of (paramagnetic) tracers have been used (Link and Seelig, 1990, Clearwater and Clark, 2003).

The first (non-imaging) method to measure xylem water transport was presented twenty years ago (Van As and Schaafsma, 1984, Reinders *et al.*, 1988, Schaafsma *et al.*, 1992). In 1988, Jenner *et al.* (Jenner *et al.*, 1988) performed flow imaging and observed *in vivo* water movement on a sub-millimetre scale in developing grains of wheat, by using a PFG spin echo technique combined with micro imaging. With PFG MRI it was possible to measure xylem water flow in single vascular bundles of maize

plants (Kuchenbrot *et al.*, 1998). Using a different version of the PFG method xylem and phloem transport were observed in an intact six day old, nontranspiring seedling of *Ricinus* (Köckenberger *et al.*, 1997). A more rapid method called PFG-FLASH (Rokitta *et al.*, 1999) was shown to be capable of measuring xylem and phloem flow in 40 day old *Ricinus* plants (Peuke *et al.*, 2001) within three to seven minutes. Here image resolution and the ability to record detailed flow profiles (and thus accuracy of the flow data) was traded for the ability to measure quickly.

A full q -space flow imaging method was developed that allowed the flow profile of every pixel in an image to be recorded quantitatively, with a relatively high spatial resolution, while keeping measurement times down to 15 to 30 minutes. This was done by combining flow encoding with a rapid (turbo) spin echo (PFG-TSE) MRI scheme (Scheenen *et al.*, 2000a, Scheenen *et al.*, 2001). Flow is quantified in terms of (averaged) velocity, volume flow (flux) and flow conducting area, without making any assumptions about the flow profile per pixel or the number and diameter of vessels per pixel. This q -space flow imaging approach was used in combination with a low field MRI setup to visualize and quantify xylem flow in tomato (Scheenen *et al.*, 2000a), in stem pieces of chrysanthemum (Scheenen *et al.*, 2000b) and in large cucumber plants (Scheenen *et al.*, 2002).

Phloem transport in plants is particularly difficult to measure quantitatively. The slow flow velocities and the very small flowing volumes in the presence of large amounts of stationary water make it difficult to distinguish the slowly flowing phloem sap from freely diffusing water. Windt *et al* (Windt *et al.*, 2006) further optimized the PFG-TSE method to quantitatively measure for the first time detailed flow profiles (called propagators) of phloem flow, in large and fully developed plants. In this way the dynamics in phloem and xylem flow and flow conducting area was studied. Using that method Peuke *et al* (Peuke *et al.*, 2006) studied the effects of cold girdling on phloem mass flow in the stem of *Ricinus*.

Currently MRI in plant research is still far from being a routine tool. Dedicated hardware is required in order to image intact plants or even trees. MRI systems that are used for plant studies often have been developed for other purposes, such as medical imaging. As a result, many machines consist of horizontal bore superconducting magnets with cylindrical geometry of the magnetic field gradient coils. In such systems plants have to be placed horizontally instead of vertically, and fitting the shoot or roots of a plant through the narrow cylindrical bore of a gradient set can be stressful and damaging for the plant. Better solutions for minimal invasive studies on intact plants, with a (potted) root system and extended shoot (leaves), require special hardware: open access magnets, open access gradient and radio frequency (rf) coil systems, e.g. plan parallel gradient plates or openable gradient coils, and climate control. Here we present some hardware solutions for intact plant MRI and demonstrate the potential of xylem and phloem flow imaging in trees, by comparing results obtained on 0.7 and 3 T MRI systems.

2.2 Material and methods

2.2.1 Hardware

The low field MRI system consists of an Avance console and electromagnet (Bruker, Karlsruhe, Germany) with a 10 cm air gap, generating a magnetic field of 0.7 T (30 MHz proton frequency). The magnetic field is stabilized with an external 19F lock unit. A shielded gradient system with planar geometry accessible from the front and back as well as from above and below is used (Fig. 2.1a). The air gap between gradient plates is 50 mm, and maximum gradient strength that can be generated is 1 T/m. For induction and detection of the NMR signal a custom made solenoid rf coil was used. For that an openable mould with a diameter slightly bigger than the stem diameter was fitted (put) around the plant. The rf coil was constructed by wrapping 9 turns of 0.5 mm copper wire around the mould with a diameter of 1.5 cm. The finished coil was connected to a tuning circuit and electromagnetically shielded with aluminum foil and copper tape. The geometry of magnet and gradient system allows inserting the plant with the coil into the magnet upright and using intact plants with roots and branches and even small trees (Fig. 2.1b). The climate control is supported by a climate control unit. In the NMR setup the plant was subjected to the following environmental conditions: day period 25-27°C, 29-45% RH, 150 μ mol

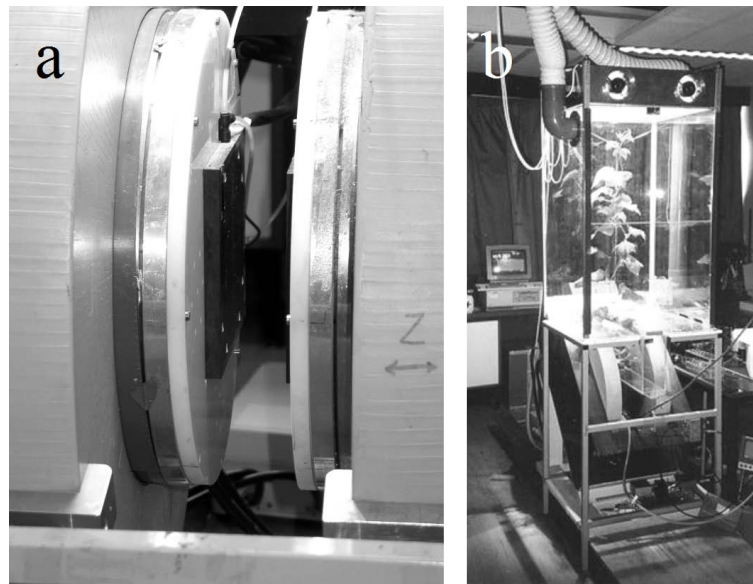


Figure 2.1 : (a) Electromagnet and plan parallel gradient coils plates of the 0.7 T MRI system result in maximum access to the centre of the magnet. (b) Plant in the magnet and climate control unit of the 0.7 T MRI system.

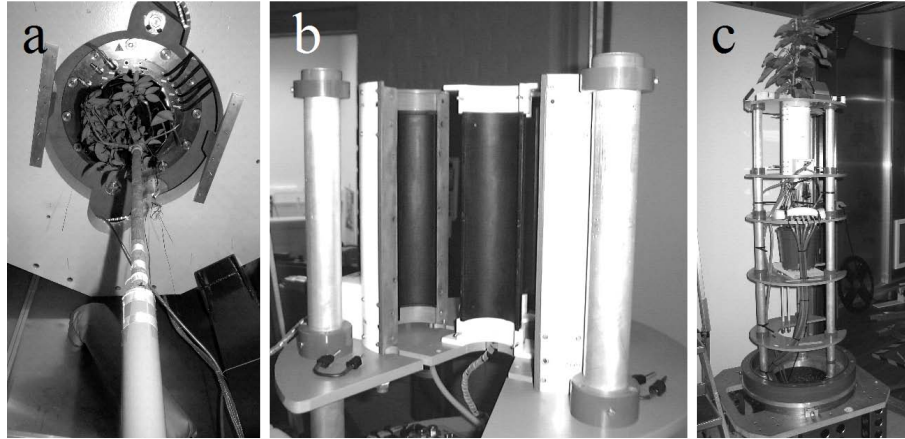


Figure 2.2 : (a) Insertion of a tree in the 50 cm diameter vertical free bore of the cryo-magnet of the 3 T MRI system. Within this bore air temperature, humidity, gas composition and light intensity can be controlled. (b) The demounted openable gradient system. (c) Closed openable gradient system around a small cherry tree.

photons $\text{s}^{-1} \text{m}^{-2}$ PAR; night period 22°C, 24-40% RH.

The 3 T MRI system consists of an Avance console (Bruker, Karlsruhe, Germany) and a superconducting magnet with a 50 cm vertical free bore (Magnex, Oxford, UK) (Fig. 2.2a), generating a magnetic field of 3 T (128 MHz proton frequency). An openable gradient coil (Bruker, Karlsruhe, Germany) consisting of four parts (Fig. 2.2b) can easily be mounted around the stem of a plant (Fig. 2.2c) and generates maximum gradient strengths of 1 T/m. The linearity of the gradients generated by the openable gradient coils system in horizontal and vertical planes is presented in Fig. 2.3. All measurements were performed in the centre of the coil (Fig. 2.3a) where the linearity and calibration of gradients are maximal. For induction and detection of the signal an openable rf coil, consisting of two half cylinders, with inner diameter of 4 cm is used (Fig. 2.2b). The diameters of the superconducting magnet, gradient and rf coils allow the use of this system both for small plants and for measurements of stem or even trunks of (tall) trees, up to a diameter of 4 cm. The open access, vertical bore of magnet and openable gradient and rf coils give the possibility to measure intact plants in the normal, upright orientation. For supporting optimal conditions in the magnet a remote climate control unit is available.

2.2.2 MRI flow imaging

For flow measurements a pulsed field gradient - spin echo - turbo spin echo sequence (PFG-SE-TSE) or pulsed field gradient - stimulated echo - turbo spin echo (PFG-STE-TSE) sequences (Scheenen *et al.*, 2001) have been used. For flow- T_2 measurements a pulsed field gradient - stimulated echo - multi spin echo (PFG-STE-MSE)

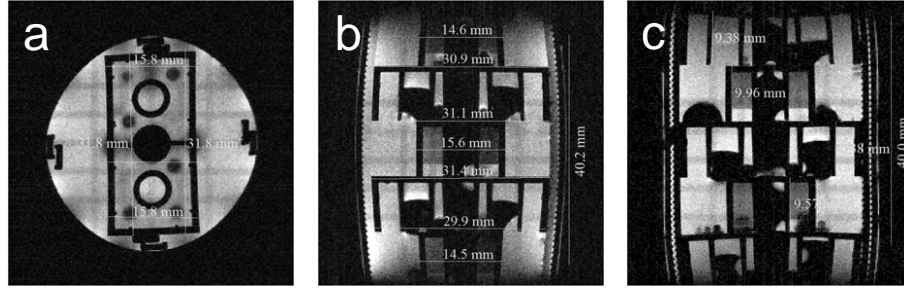


Figure 2.3 : GEFI images of five identical Lego bricks (length 31.7 mm, width 15.7 mm, height 9.3 mm), on top of each other, in doped water (1g/l CuSO_4) in the XY, XZ and YZ planes at the center of the Z, Y and X direction, respectively, of the openable gradient system on the 3 T imager. The effect of the openable construction on the gradient linearity is mainly visible in the Z direction (Fig. 2.3b, 2.3c), the length axis of the system (see also Fig. 2.2b). Gradient linearity is within 10% deviations from the real dimensions. In the centre of the coil (XY plane) hardly any deviations are observed (Fig. 2.3a).

sequence was used. An echo train was acquired for every PFG step, so one can determine the T_2 relaxation time for every displacement step. To conserve the flow induced phase information during the echo train the phase cycling scheme XY-8 (x-y-x-y-x-y-x)n (Windt *et al.*, 2007) was used for the 180° rf pulses generating the echo train. In this way no extra averaging phase cycles are needed. The sequence will be presented in more detail separately by Windt, Vergeldt and Van As (Windt *et al.*, 2007). In all cases linear displacement was measured by stepping the amplitude of PFG's from $-G_{\max}$ to $+G_{\max}$ (q -space imaging). After Fourier transformation the propagator was obtained for every pixel in the image.

A crucial step in quantification of the flow is to discriminate stationary and flowing water. The fact that the propagator for stationary water is symmetrical around zero was used to separate the stationary from the flowing water. The signal in the non-flow direction was mirrored around zero displacement and subtracted from the signal in the flow direction, to produce the displacement distribution of the flowing and the stationary water. Because the signal amplitude is proportional to the density of the mobile protons, the integral of the propagator provides a measure for the amount of water. The average velocity of the flowing water was then calculated by taking the amplitude weighted average of the velocity distribution. The volume flow rate or flux is calculated by taking the integral of amplitude times displacement of the velocity distribution. Using this approach, the following flow characteristics were extracted in a model-free fashion, as described by Scheenen *et al.* (Scheenen *et al.*, 2000b): total amount of water per pixel, amount of stationary water per pixel, amount of flowing water (or flow conducting area) per pixel, average velocity per pixel (including the direction of flow), and volume flow per pixel. The NMR signal

intensity of a reference tube filled with (doped) water was used for calibration of the amplitude to the amount of water.

The T_2 relaxation time for every displacement was calculated by fitting a mono-exponential function to the echo train decay curve.

2.2.3 Plant material

An ornamental cherry tree with a length of about 1 m was grown in a plastic pot. Two weeks before the measurements the tree was placed in a climate chamber with constant temperature (20°C), humidity (60%) and light condition (12 h day-night regime).

2.3 Results and discussion

In Fig. 2.4 the cross-sectional amplitude images of the stem of the cherry tree obtained at field strengths of 3 and 0.7 T are presented. The measurements were performed at almost the same position along the stem of the tree and with the same spatial resolution, and were obtained first at 3 T and the next week at 0.7 T. The amplitude images were obtained from the amplitude at $t = 0$ s of the mono-exponential fit per pixel.

The main parameter, which determines spatial resolution, is the signal to noise ratio (S/N). S/N depends on the magnetic field strength (B_0), the radius of the detecting rf coil (r), pixel volume (V) (which in its turn is defined by the field of view (FOV) and by the number of pixels (N)), the number of averages (N_{aver}), the number of echoes used for the monoexponential fit to obtain the single parameter images of amplitude and T_2 (N_{echo}) and the spectral width (Δf) (Hoult and Richards, 1976, Callaghan, 1993), and can be combined to (Scheenen, 2001)

$$S/N = K B_0^{7/4} r^{-1} V \Delta f^{-1/2} N_{aver}^{1/2} N_{echo}^{1/2}. \quad (2.1)$$

K is a proportionality constant, that includes among others N and the rf coil geometry: a solenoid type coil is about three times more sensitive than a Helmholtz type coil of the same radius. There is enough of literature describing all kinds of ways to establish the best correlation between S/N , the spatial resolution and the measurement time (Callaghan, 1993). Here we will concentrate on the parameters that characterize the used MRI hardware.

One of these parameters is r . From Eq. (2.1) it is clear, that the smaller r , the higher S/N . The best constructive solution is to construct rf coils that fit the part of the object to be imaged as close as possible. This approach can be easily applied for the 0.7 T machine, whereas the radius of the rf coil for the 3 T machine is fixed and equal to 4 cm. Because it is openable we still can get a tree in if we like to study flow in the stem. In this way a good compromise is realized to measure stems up to 4 cm diameter of even tall trees.

Another way to increase S/N is to use higher field strength, B_0 . Increase in the magnetic field strength from 0.7 to 3 T gives significant rise in S/N . However, for

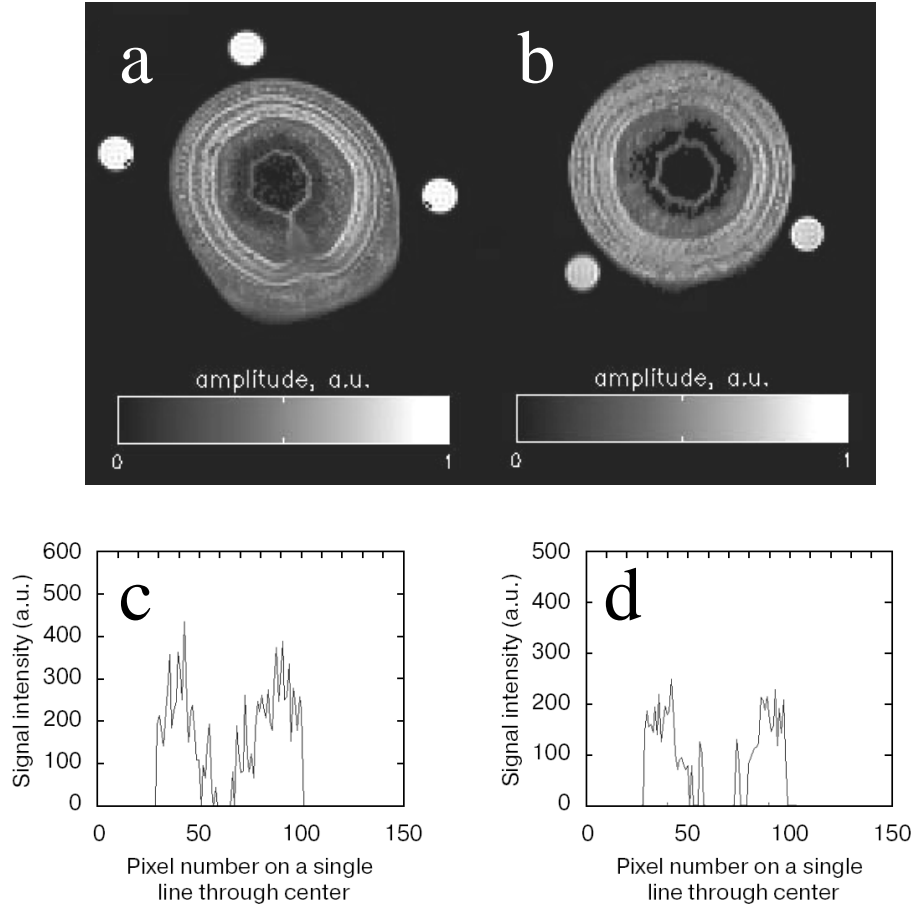


Figure 2.4 : Cross-sectional amplitude images of the stem of the cherry obtained at magnetic field strength of 3 T (a) and 0.7 T (b). The measurements were performed on almost the same height along the stem. Amplitude profiles through the centre of the stem are shown for ease of comparison (c and d, for 3 and 0.7 T, respectively). Parameters of measurement: MSE sequence, resolution $133 \times 133 \times 3000 \mu\text{m}^3$, spectral width 50 kHz, TE 5 ms, TR 3 s, number of echoes 256, number of averages 8.

plant tissues, especially for woody tissue containing a lot of intercellular air spaces, this results in the appearance of magnetic field inhomogeneities (Callaghan, 1993, Scheenen, 2001), which are also proportional to B_0 . The magnetic field inhomogeneity results in increase in susceptibility artefacts.

From Fig. 2.4 we see that a spatial resolution of $133 \times 133 \mu\text{m}^2$ is enough to see anatomical details of the stem structure. The center of the stem consists of heart

wood that does not contain significant amounts of water and is filled with air. So it hardly gives detectable signal and strong susceptibility effects may be expected. It follows from the images that the S/N ratio is better for the 3 T machine, even in the heart wood. For the image obtained at 3 T the signal in the centre is low but still detectable, whereas for the 0.7 T machine the signal in the centre of the stem is not detectable at all. At the same time because of the susceptibility effects (and differences in T_1 and T_2 as well) the image obtained at 3 T has higher contrast between the different tissues that also increases its quality.

Thus, in spite of the advantage of the 0.7 T machine in the rf coil geometry the increase in S/N ratio due to higher magnetic field strength results in the better quality of image for the 3 T machine. Moreover, the higher S/N ratio for magnetic field strength of 3 T allows to make the time of measurement shorter because less number of averages are necessary for the accurate determination of obtained parameters.

The T_2 images obtained at 0.7 T and 3 T are presented in Fig. 2.5. In general, the comparison of T_2 images obtained at 0.7 and 3 T demonstrates that the apparent T_2 values observed at 3 T are shorter than the values obtained at 0.7 T. The T_2 values of identical reference tubes do not differ significantly at 0.7 and 3 T. The T_2 relaxation times obtained for the different tissues are different. Relatively long T_2 values are found in a ring, which, as follows from the amplitude image, consists of the annual rings. These rings contain xylem vessels. The high signal amplitude shows that they are full with water and below we will demonstrate that they take part in active water transport. The outer part of the stem has a short T_2 value, whereas the amplitude image indicates a significant amount of water in this area. There are two mechanisms which can influence the observed T_2 . The first one originates from diffusion motion through the inhomogeneous magnetic field and from chemical exchange. This effect depends on the strength of the magnetic field and echo time (TE). The second mechanism results from diffusion in the presence of the imaging gradients and depends on the spatial resolution (Edzes *et al.*, 1998). At a resolution of 100 μm and echo time of 5 ms T_2 values around 500 ms can still reliably be measured (Edzes *et al.*, 1998). Here we used a pixel size of 133 μm , both for the different tissues and for the measurement at the different magnetic field strengths. The observed T_2 values are below 150 ms, and thus hardly influenced by the imaging gradients. In the outer ring we expect intercellular air spaces that introduce (large) susceptibility inhomogeneities which induce local field gradients. Diffusional motion across regions of variable magnetic susceptibility results in a much more rapid decay of the detected signal. This can be the reason for the very short T_2 values in this ring, especially at 3 T.

The possibility to study plants and trees non-invasively by MRI makes this method especially attractive for the investigation of transport process in alive intact plants. Fig. 2.6 presents results of xylem and phloem flow measurements in the stem of the cherry tree. The flow measurements were processed in a number of ways. Quantitative xylem and phloem flow maps were obtained by analyzing singular flow measurements on a per pixel basis. By analyzing the PFG-SE-TSE measurements as described elsewhere (Scheenen *et al.*, 200b), we were able to construct flow maps of xylem transport (Fig. 2.6c) as well as phloem transport (Fig. 2.3d). Using

the reference tubes for calibration, the flow measurements were processed to yield quantitative flow maps representing the amount of stationary water per pixel (1), the amount of flowing water (2), here presented as the flow conducting area per pixel, the average velocity of the flowing water (3), and the average volume flow per pixel (4), respectively. The position and shape of the phloem and xylem flow maps correspond closely with the phloem and xylem regions that are visible in the anatomical reference provided by the amplitude and T_2 maps (Figs. 2.4 and 2.5). For both xylem and phloem flow measurements "total-propagators" were constructed by summing the propagators of all flow-containing pixels into a one dimensional total-propagator

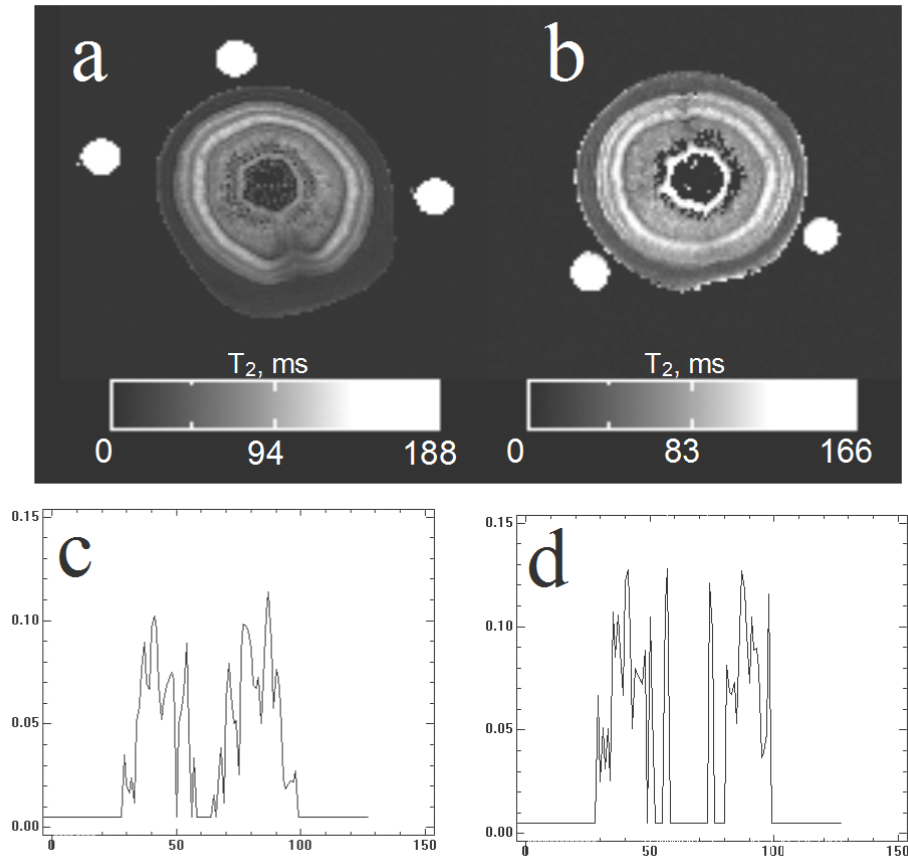


Figure 2.5 : T_2 images of the cross-section of the stem of the cherry tree stem obtained at magnetic field strength 3 T (a) and 0.7 T (b), corresponding to the amplitude images of Fig. 2.4. The T_2 values were calculated per pixel by a mono-exponential fit decay curve of echo train. T_2 profiles through the centre of the stem are shown for ease of comparison (c and d, for 3 and 0.7 T, respectively).

(Fig. 2.6a and b, for xylem and phloem, respectively). Flow containing pixels were identified as such on the basis of previously calculated quantitative flow maps (Figs. 2.6c and d). In this case, the spatial information was not used to calculate flow maps, but to discard pixels that contain stationary water only. In this experiment, performed at the 3 T MRI, low transpiration conditions were created, so that both xylem and phloem flow were in the same range of velocity and could be obtained in one measurement.

The measurements presented in Fig. 2.6 were performed in end of May 2005, when the plant was in the active stage of growth and the velocity of all processes was high, including phloem transport. At normal conditions the phloem flow is characterized by

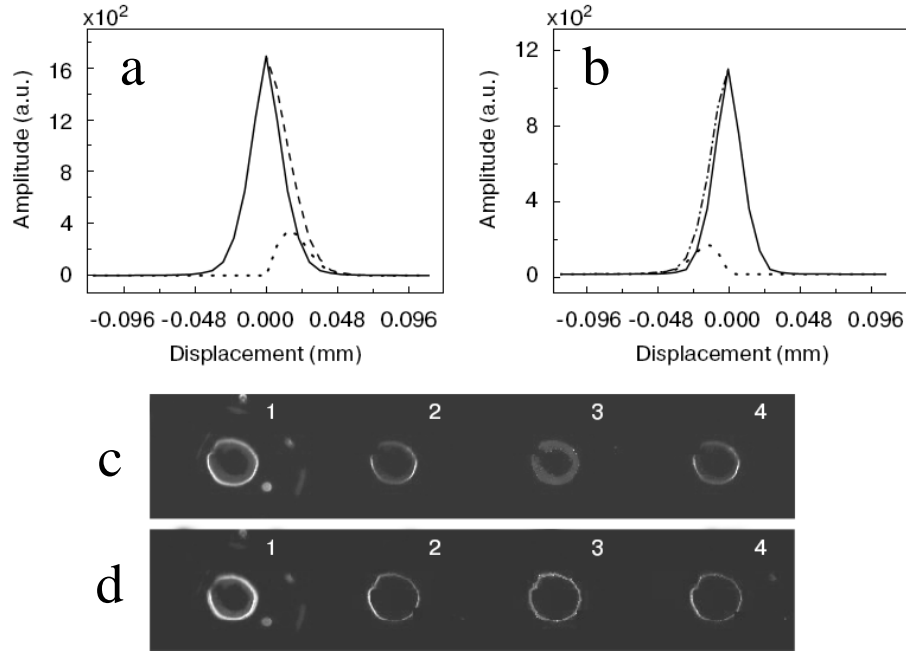


Figure 2.6 : Total propagator (dashed line), the propagators of stationary water (solid line) and flowing water (dotted line) of the flow containing pixels in the xylem (a) and phloem (b) regions. The pixels have been selected from flow containing pixels in the xylem and phloem flow images presented in c and d, respectively. These series of images present proton density (1), flow conducting area (2), average velocity (3), and volume flow (4). The images have been obtained at 3 T. Experimental parameters: PFG-SE-TSE, resolution $200 \times 200 \times 3000 \mu\text{m}^3$, spectral width 50 kHz, first echo time 60.1 ms, TE 6.2 ms, TR 2 s, turbo factor 8, number of averages 2. For flow encoding the following parameters were applied: 32 PFG steps, labeling time $\Delta = 50$ ms, PFG duration $\delta = 4$ ms, $\text{PFG}_{\text{max}} = 0.408$ T/m. Between the two flow encoding gradients 11 180° pulses have been applied.

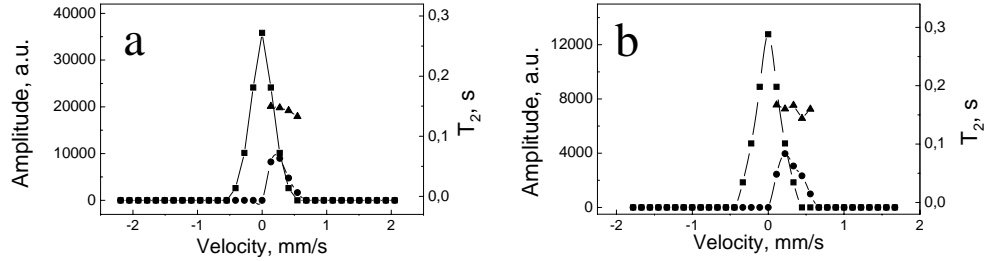


Figure 2.7 : Total propagators of stationary (\blacksquare) water and flowing (\bullet) water from flow conducting pixels in the xylem region of a cherry tree and correlation of T_2 relaxation time (\blacktriangle) with flow velocity obtained at magnetic field strength 3 T (a) and 0.7 T (b). Experimental parameters: PFG-STE-MSE, resolution $323 \times 323 \times 3000 \mu\text{m}^3$ (Fig. 2.7a) and $313 \times 313 \times 3000 \mu\text{m}^3$ (Fig. 2.7b) spectral width 50 kHz, TE 7 ms, TR 2 s, number of averages 2, 32 PFG steps, labeling time $\Delta = 80$ ms, PFG duration $\delta = 3$ ms, $\text{PFG}_{\text{max}} = 0.357$ (at 3 T) or 0.440 T/m (at 0.7 T).

lower amount of flowing water, smaller cross-sectional area and lower velocity. Then a long flow labeling time is required for the measurement of slow phloem transport (averaged velocities in the order of 0.2 - 0.4 mm/s (Windt *et al.*, 2006)). Sometimes we need flow labeling times as long as a few hundreds of milliseconds. Within this time T_2 relaxation is active and if the T_2 of the flowing fluid is short PFG-SE-TSE is hardly possible. That is why for phloem flow measurements the PFG-STE-TSE is usually applied instead of the PFG-SE-TSE, which is usually used for xylem flows (Windt *et al.*, 2006, Peuke *et al.*, 2006).

In view of these arguments and the general observation that T_2 decreases at increasing B_0 , knowledge about the T_2 values of the flowing fluid as a function of B_0 is very valuable, because it determines the detection limit and the correctness of the calibration procedure for fluxes. We therefore measured the correlation between T_2 relaxation time and the flow velocity at 0.7 and 3 T.

In Fig. 2.7 total propagators of stationary and flowing water in all pixels in the xylem region measured at magnetic field strength 3 T (Fig. 2.7a) and 0.7 T (Fig. 2.7b) and the correlation between T_2 relaxation time and flow velocity are presented. The propagator of stationary water is a symmetrical peak centered at zero displacement. The propagator of flowing water is asymmetric. The measurements have been done during one week and at similar environment conditions. The propagators measured at 0.7 T and 3T have similar shape and comparable values of the maximum flow velocity. The T_2 values measured at 3 T are slightly shorter than those at 0.7 T (around 0.14 and 0.16 s, respectively), in agreement with the above presented overall results of T_2 imaging (Fig. 2.5). At 0.7 T the relation between flow and T_2 at higher light intensity ($150 \mu\text{mol photons s}^{-1} \text{ m}^{-2}$ PAR) is different: the T_2 values tend to increase at increasing velocities (data not shown). These higher light conditions could not be created in the 3T magnet and, unfortunately, these results can therefore

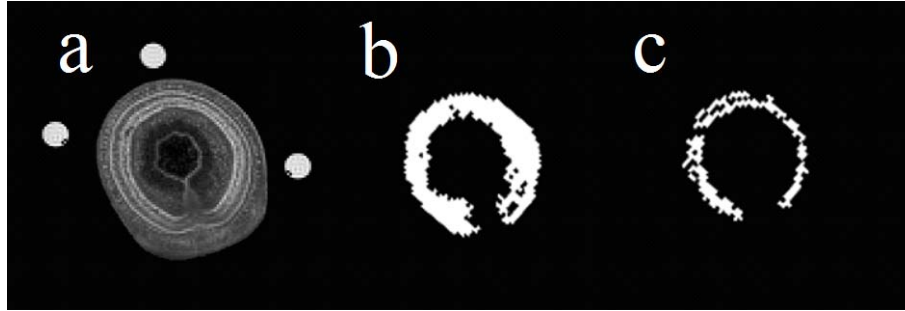


Figure 2.8 : Amplitude image (a) and xylem flow containing area in the stem of the cherry tree observed in May 2005 (b) and in March 2006 (c). The amplitude image is given for reference of positions, and was obtained in March 2006.

not be compared.

Figure 2.8 presents the pixels in the stem of the cherry tree where xylem flow takes place and how this develops in time. For reference the amplitude image obtained in March 2006 is given (Fig. 2.8a). The time difference between these two experiments is 10 months. The difference in position between the two images along the stem is no more than one cm. The first measurement (Fig. 2.8b) have been done in May 2005, the second one (Fig. 2.8c) in March 2006. The differences in area and position of xylem flow between these 10 months are clear. In May 2005 the xylem flow is present in both the bright ring and in the internal part of stem (Fig. 2.8a), whereas in the beginning of spring (March 2006) the flow is observed in a ring only (Fig. 2.8b). At the present resolution it can not unambiguously be determined if this is a new annual ring or if it is the same ring of Fig. 2.8a. The differences can be explained by the differences in activity of processes which take place in the plant directly after winter period (March 2006) and after a few months of active growth (May 2005). It is possible that the internal part of the stem is not active any more or that it will transport water actively later in the season.

2.4 Conclusions

Both for the 3 T and for 0.7 T MRI systems the easy access to gradient system, its convenient geometry, openable construction of rf coil and vertical bore of magnet give the possibility to measure intact plants and trees in upright orientation. The climate control unit supports optimal conditions in the magnet during measurements. In this way images with high enough spatial resolution to observe spatially resolved xylem and phloem flows and flow conductive area (on a per pixel basis or as a total) during normal plant growth and in response to stress conditions.

Although there are clear susceptibility artifacts and shortening of relaxation times at 3 T, both 0.7 and 3 T flow MRI is possible in (non-water saturated, porous) tree

stems. Functional plant imaging by flow MRI offers exciting new possibilities for the physiological mapping of intact trees. For the first time, MRI allows the physiological state of individual plant organs to be described, as well as their inter-relationship at the whole plant level. By use of dedicated hardware xylem and phloem flow, and its mutual interaction, can be studied quantitatively in relation to the plant water balance.

In addition to flow parameters MRI also results in reliable values of sap flow conducting surface area. This conducting area is clearly not constant. This observation has clear consequences for the reliability of flow measurements based on heat-pulse methods.

References

- Bancal P., Soltani F. (2002) Source-sink partitioning. Do we need Münch? *Journal of Experimental Botany*, **53**, 1919-1928.
- Callaghan P.T., Eccles C.D., Xia Y. (1988) NMR microscopy of dynamic displacements: *k*-space and *q*-space imaging. *Journal of Physics E: Scientific Instruments*, **21**, 820-822.
- Callaghan P.T. (1993) *Principles of nuclear magnetic resonance microscopy*, Oxford, Oxford University Press.
- Clearwater M.J., Meinzer F.C., Andrade J.L., Goldstein G., Holbrook N.M. (1999) Potential errors in measurement of nonuniform sap flow heat dissipation probes. *Tree Physiology*, **19**, 681-687.
- Clearwater M.J., Clark C.J. (2003) In vivo magnetic resonance imaging of xylem vessels in woody lianas. *Plant Cell and Environment*, **26**, 1205-1214.
- Donker H.C.W., Van As H., Edzes, H.T., Jans A.W.H. (1996) NMR imaging of white button mushroom (*Agaricus bisporis*) at various magnetic fields. *Magnetic Resonance Imaging*, **14**, 1205-1215.
- Edzes H.T., Van Dusschoten D., Van As H. (1998) Quantitative T_2 imaging of plant tissues by means of multi-echo MRI microscopy. *Magnetic Resonance Imaging*, **16**, 185-196.
- Gullion T., Baker D.B., Conradi M.S. (1990) New compensated Carr-Purcell sequences. *Journal of Magnetic Resonance*, **89**, 479-484.
- Hoult D.I., Richards R.E. (1976) Noise and SNR in MRI. *Journal of Magnetic Resonance*, **24**, 71-85.
- Jenner C.F., Xia Y., Eccles C.D., Callaghan P.T. (1988) Circulation of water within wheat grain revealed by nuclear magnetic resonance micro-imaging. *Nature*, **336**, 399-402.

- Knoblauch M., Van Bel A.J.E. (1998) Sieve tubes in action. *Plant Cell*, **10**, 35-50.
- Koch G.W., Sillet S.C., Jennings G.M., Davis S.D. (2004) The limits to tree height. *Nature*, **428**, 851-854.
- Köckenberger W., Pope J.M., Xia Y., Jeffrey K.R., Komor E., Callaghan P.T. (1997) A non-invasive measurement of phloem and xylem water flow in castor bean seedlings by nuclear magnetic resonance microimaging. *Planta*, **201**, 53-63.
- Köckenberger W. (2001) Functional imaging of plants by magnetic resonance experiments. *Trends in Plant Science*, **6**, 286-292.
- Kuchenbrot E., Kahler E., Thürmer F., Deichmann R., Zimmermann U., Haase A. (1998) Functional magnetic resonance imaging in intact plants - quantitative observation of flow in plant vessels. *Magnetic Resonance Imaging*, **16**, 331-338.
- Lalonde S., Tegeder M., Throne-Holst M., Frommer W.B., Patrick J. W. (2003) Phloem loading and unloading of sugar and amino acids. *Plant Cell and Environment*, **26**, 37-56.
- Link J., Seelig J. (1990) Comparison of deuterium NMR imaging methods and application to plants. *Journal of Magnetic Resonance*, **89**, 310-330.
- MacFall J.J., Van As H. (1996) In: *Nuclear Magnetic Resonance in Plant Biology* (Shachar-Hill Y., Pfeffer P.E., eds). Rockville, The American Society of Plant Physiologists, 33-76.
- Peuke A.D., Rokitta M., Zimmermann U., Schreiber L., Haase A. (2001) Simultaneous measurement of water flow velocity and solute transport in xylem and phloem of adult plants of *Ricinus communis* over a daily time course by nuclear magnetic resonance spectrometry. *Plant, Cell and Environment*, **24**, 491-503.
- Peuke A.D., Windt C., Van As H. (2006) Effect of cold-girdling on flow in the transport phloem in *Ricinus communis*: is mass flow inhibited? *Plant and Cell Environment*, **25**, 15-25.
- Reinders J.E.A., Van As H., Schaafsma T.J. (1988) Water balance in *Cucumis* plants, measured by nuclear magnetic resonance, I. *Journal of Experimental Botany*, **39**, 1199-1210.
- Rokitta M., Zimmermann U., Haase A. (1999) Fast NMR flow measurements in plants using FLASH imaging. *Journal of Magnetic Resonance*, **137**, 29-33.

-
- Saxe H., Cannell M.G.R., Johnsen B., Ryan M.G., Vourlitis G. (2001) Tree and forest functioning in response to global warming. *New Phytologist*, **149**, 369-399.
- Schaafsma T.J., Van As H., Palstra W.D. (1992) Quantitative measurement and imaging of transport processes in plant and porous media by ^1H NMR. *Magnetic Resonance Imaging*, **10**, 827-836.
- Scheenen T.W.J., Van Dusschoten D., de Jager P.A., Van As H. (2000a) Microscopic displacement imaging with pulsed field gradient turbo spin-echo NMR. *Journal of Magnetic Resonance*, **142**, 207-215.
- Scheenen T.W.J., van Dusschoten D., de Jager P.A., Van As H. (2000b) Quantification of water transport in plants with NMR imaging. *Journal of Experimental Botany*, **51**, 1751-1759.
- Scheenen T. (2001) *Nuclear magnetic resonance imaging of water motion in plants*, Ph.D. thesis, Wageningen University.
- Scheenen T.W.J., Vergeldt F.J., Windt C.W., de Jager P.A., Van As H. (2001) Microscopic imaging of slow flow and diffusion: a pulsed field gradient stimulated echo sequence combination with turbo spin echo imaging. *Journal of Magnetic Resonance*, **151**, 94-100.
- Scheenen T.W.J., Heemskerk A.M., de Jager P.A., Vergeldt F.J., Van As H. (2002) Functional imaging of plants: a nuclear magnetic resonance study of a cucumber plant. *Biophysical Journal*, **82**, 481-492.
- Sevanto S., Vesala S.J., Peramaki M., Nikinmaa E. (2002) Time lags for xylem and stem diameter variations in Scots pine tree. *Plant and Cell Environment*, **25**, 1071-1077.
- Smith D.M., Allen S.J. (1996) Measurement of sap flow in plant stems. *Journal of Experimental Botany*, **47**, 1833-1844.
- Thompson M.V. (2006) Phloem: the long and the short of it. *Trends in Plant Science*, **11**, 26-32.
- Van Bel A.J.E. (2003a). The phloem, a miracle of ingenuity. *Plant, Cell and Environment*, **26**, 125-149.
- Van As H., Schaafsma T.J. (1984) Noninvasive measurement of plant water flow by nuclear magnetic resonance. *Biophysical Journal*, **45**, 469-472.
- Van Bel A.J.E. (2003b). Transport phloem: low profile, high impact. *Plant Physiology*, **131**, 1509-1510.

Windt C.W., Vergeldt F.J., de Jager P.A., Van As H. (2006) MRI of long-distance water transport: a comparison of the phloem and xylem flow characteristics and dynamics in poplar, castor bean, tomato and tobacco. *Plant, Cell and Environment*, **29**, 1715-1729.

Windt C.W., Vergeldt F.J., Van As H. (2007) Correlated displacement- T_2 MRI by means of a pulsed field gradient-multi spin echo method. *Journal of Magnetic Resonance*, **185**, 230-239.

Chapter 3

Flow characteristics and exchange in complex biological systems as observed by PFG-MRI

Water flow through model porous media was studied in the presence of surface relaxation, internal magnetic field inhomogeneities and exchange with stagnant water pools with different relaxation behavior, demonstrating how the apparent flow parameters average velocity, volume flow and flow conducting area in these situations depend on the observation time. To investigate the water exchange process a two component biological model system consisting of water flowing through a two component biofilm reactor (column packed with methanogenic granular sludge beads) was used, before and after a heat treatment to introduce exchange. We show that correction of the stagnant fluid signal amplitude for relaxation at increasing observation time using the observed relaxation times reveals exchange between the two fractions in the system. Further it is demonstrated how this exchange can be quantified.¹

3.1 Introduction

Fluid transport and processes of water exchange are of great importance in many areas of science and technology, e.g. flow in (woody) plants, perfusion in human and animal tissues, transport in geological media, two-phase flow in oil recovery, hydrodynamics in chromatographic columns for molecular separation, and flow in bio-reactors and catalysis systems. Nuclear magnetic resonance (NMR) has become an important method for characterizing such porous (bio-)systems. Pulsed field gradient (PFG) NMR is a powerful tool for investigating transport processes in such systems because it allows the measurement of the displacement propagator, the probability distribution of diffusive and advective molecular displacements (for some recent reviews

¹This Chapter is based on: Homan N.M., Venne B., Van As H. Flow characteristics and exchange in complex biological systems as observed by PFG-MRI.

see e.g. Mantle and Sederman, 2003, Stapf and Han, 2005). The combination of magnetic resonance imaging (MRI) and PFG methods allows flow to be spatially resolved and flow characteristics, like velocity, volume flow and flow conducting area, can be measured per pixel, even in pixels that contain flowing and non-flowing fluid (Scheenen *et al.*, 2000, Windt *et al.*, 2006, Van As 2007).

PFG NMR propagator measurements have been successfully applied to a direct and detailed experimental study of the topological and dynamic aspects involved in the exchange of small, nonsorbed fluid molecules between the intraparticle pore network and the interparticle void space in chromatographic columns packed with spherical-shaped, porous particles (Tallarek *et al.*, 1998 and 1999). The approach provided quantitative data of the diffusion-limited exchange kinetics for solute diffusion into and out of spherical particles. Using a systematic variation of the observation time, the time between the position encoding and decoding gradient pulses, the kinetics of mass transfer between the stagnant and flowing fluids within the packed bed could be recorded (Tallarek *et al.*, 1999). The system used in that study was in some sense ideal: no difference in relaxation between the flowing fluid in the voids and the fluid in the porous particles was observed. In addition, no surface relaxation was present in that system. Under these conditions, the signal amplitude of the stagnant fluid phase as a function of the observation time could be used directly to quantify the exchange. In many realistic (bio-)systems we have to deal with surface relaxation, internal field gradients due to susceptibility differences (e.g. between the fluid and matrix) and differences in relaxation times between pools of exchanging flowing and stagnant water.

In realistic systems internal field gradients result in attenuation of the NMR signal and shortening of the observed relaxation times. In order to measure the NMR signal accurately, suppression of the background gradients is crucial. For example, the effect of spatially constant gradients can be compensated for by a combination of bipolar gradients and refocusing pulses (Cotts *et al.*, 1989, van Dusschoten *et al.*, 1995, Zheng and Price, 2008). However, for long observation times (Δ) when the spin displacement becomes comparable to the length scale of local structures (pore size or particle length) the internal field gradients are not spatially constant. The measured NMR signal in a heterogeneous field for long Δ is therefore susceptible to a variation of background gradients. In addition, surface relaxation and differences in relaxation time between the exchanging flowing and stagnant fluid pools will affect the signals of the stagnant and flowing fluid. For these reasons in realistic (bio-)systems the propagator may be distorted and flow characteristics become dependent on the observation time (Scheven *et al.*, 2004). The effect of exchange under these conditions has not yet been investigated systematically. In this respect, the use of realistic model systems may help our understanding of the transport processes of fluid in porous media.

In this paper we focus on a range of Δ no longer than a few hundreds of milliseconds. This time range is typical for measurements where the asymptotic long-time limit for exchange cannot be reached because the relaxation times are too short. The main goal of this paper is to describe quantitatively how apparent parameters of flow (velocity, volume flow, flow conducting area) measured in a thin slice of fluid flowing in porous media depend upon the mechanisms causing the attenuation of the

PFG-MRI signal, including exchange. Based on this investigation we clearly show the limitation of the pulsed-field gradient stimulated echo (PGF-STE) method as well as its potential applicability for flow measurements in the porous media. We also investigate exchange between the flowing and stagnant fluid phases in a complex biological system with susceptibility and local gradient effects, surface relaxation and differences in relaxation between exchanging fluid pools and present a method to quantify this exchange.

3.2 Theory

In order to apply a wide range of Δ values, PFG-STE-TSE or -MSE was used, the latter being used for correlated displacement- T_2 measurements (Scheenen *et al.*, 2000, Homan *et al.*, 2007, Windt *et al.*, 2007). In the PFG-STE method the gradient pulses are separated by a storage interval. During the time the magnetization is in the x,y-plane (the periods between the first and second and between the third 90° and first 180° pulses), the magnetization vector is sensitive to T_2 relaxation decay, the applied field gradient and the (local) background fields produced by susceptibility differences between fluid and matrix. During the storage interval (between the second and the third 90° pulses) the magnetization is stored in the direction parallel to the main magnetic field, and the magnetization is only attenuated by T_1 relaxation.

For the ideal PFG-STE propagator experiment the echo amplitude can be written as

$$S(q, \Delta) = S(0, \Delta) \int_R dR P(R, \Delta) e^{i 2\pi q R}. \quad (3.1)$$

$S(0, \Delta)$ is the amplitude of the total proton magnetization in the measured volume. The displacement probability distribution (propagator) $P(R, \Delta)$ gives the probability that a molecule will travel a displacement R in time Δ in the direction of the applied magnetic field gradient pulse, that has an amplitude g and duration δ . g is defined by

$$q = \frac{1}{2\pi} \gamma \delta g. \quad (3.2)$$

Thus, $P(R, \Delta)$ can be reconstructed from the amplitude of the first echo as a function of g by Fourier transformation. Any molecule in a flowing fluid participates simultaneously in the coordinated mass flow and diffusional motion. The echo attenuation that occurs due to the diffusional motion, characterized by the diffusion coefficient D , over time Δ , including the longitudinal (T_1) and transverse (T_2) relaxation of magnetization, is written as (Callaghan, 1993)

$$S(q, \Delta) = S(0, \Delta) \exp \left(-4\pi^2 q^2 D \left(\Delta - \frac{\delta}{3} \right) - \frac{(\tau_2 - \tau_1)}{T_1} - \frac{2\tau_1}{T_2} \right). \quad (3.3)$$

τ_1 and τ_2 denote the time of the second and third 90° r.f. pulses in the PFG-STE experiment. In the experiments with differing observation time Δ τ_2 was varied, but τ_1 was fixed. Thus, the contribution of T_2 in echo signal attenuation at different

observation times was constant and the difference in echo amplitude at different Δ is due to T_1 relaxation only.

The flow conducting area (A) and the volume flow (Q) and the average flow velocity (v), can be calculated from the propagator (Scheenen *et al.*, 2000)

$$A = \sum_{R=0}^{R_{\max}} P_c(R, \Delta) A_{ref}, \quad (3.4)$$

$$Q = \sum_{R=0}^{R_{\max}} P_c(R, \Delta) R \frac{A_{ref}}{\Delta}, \quad (3.5)$$

$$v = \frac{Q}{A} = \frac{\sum_{R=0}^{R_{\max}} P_c(R, \Delta) R}{\sum_{R=0}^{R_{\max}} P_c(R, \Delta) \Delta}. \quad (3.6)$$

Here P_c is the propagator of flowing water P_F divided by the average pixel integral I_{ref} of a propagator of the pixels in a reference tube that is filled with pure water

$$P_c(R, \Delta) = \frac{P_F(R, \Delta)}{I_{ref}}. \quad (3.7)$$

In the real situation of flow through porous media the measured propagator can be distorted due for the following reasons (Scheven *et al.*, 2004).

- First, the diffusion of molecules across the streamlines and between the stagnant and flowing fluid. Diffusion does not result in a net displacement of the ensemble of molecules, but shifts the spectral weight from the undisplaced and the most displaced parts of the displacement spectrum toward its mean. However, diffusion does not result in a change in the calculated A_{app} , Q_{app} or v_{app} .
- Second, surface relaxation changes the shape of a propagator. Because of surface relaxation, the signal from spins located in small pores or next to the walls disappears. This results in an undercount of spins from the stagnant zones and the slowest flowing fluid located next to the walls and a corresponding overcount of the fast flowing spins. The net result is a shift of the spectral weight of the propagator towards longer displacements which, as a consequence, leads to an increase in v_{app} and Q_{app} .
- Third, susceptibility differences between fluid and matrix produces internal offset fields. The signal from moving spins can be lost from the measurement if during they displace into a position with a significantly different internal magnetic field (Song, 2000, Scheven *et al.*, 2004). The internal offset fields affect the faster flowing spins and lead to a shift of the spectral weight towards shorter displacement and a decrease in v_{app} and Q_{app} .

The effects of the susceptibility and relaxation mechanisms is a function of observation time (Donker *et al.*, 1996, Nestle *et al.*, 2002). For very short Δ the displacement of fluid due to both diffusion and flow is small compared to the length

scale of local structure. At such distances the magnetic field can be considered to be constant, the signal loss due to diffusion and flow motion is negligible, and the surface relaxation during short Δ is negligible. For an intermediate Δ the local magnetic field will change on the length scale of the diffusion and flow displacement and echo loss will be observed. The elongation of Δ will also result in the progressive increase of wall relaxation effects. For a long Δ , when the diffusion shift and flow displacement are larger than the local gradient length scale, all spins in the system will then sample all possible gradient amplitudes. Under this condition the loss of magnetization will become almost constant with increasing Δ .

Susceptibility and wall relaxation effects lead to systematic uncorrected loss of magnetization, resulting in an underestimation of A_{app} . The direction of shift in v_{app} and Q_{app} from the actual values depends on which of the two mechanisms, which have opposite effects, dominates in the system at given Δ (Scheven *et al.*, 2005).

In systems with exchange between stagnant and flowing fluid (e.g. fluid inside and outside porous particles/matrix, or flowing water in vessels and stationary water in parenchyma cells for water transport in plants) the situation becomes more complicated. If differences in relaxation can be neglected, exchange between the stagnant and flowing components results in a reduction or total disappearance of the stagnant fraction and an increase of flowing fluid in the propagator as Δ increases (Tallarek *et al.*, 1999, Kandhai *et al.*, 2002, Scheven *et al.*, 2005). That will result in an increase of A_{app} with increasing Δ if no susceptibility effects and differences in relaxation are present. In a system with surface relaxation the stagnant fraction disappears faster than in a system without significant surface relaxation. This effect becomes more noticeable when the measurement time scale is longer than the relaxation time of the stagnant fraction (Scheven *et al.*, 2004), and results in an additional decrease of the amplitude of the stagnant fraction. The T_1 and T_2 value for stagnant and flowing components usually varies quite significantly in different (bio-)systems. The relaxation time of fluid inside a porous matrix is in general shorter than the relaxation time of fluid outside the matrix (Lens *et al.*, 1999), so in tree stems the stationary water in parenchyma cells has shorter T_2 than the flowing water of the xylem vessels (Homan *et al.*, 2007, Windt *et al.*, 2007). Simulations of diffusion and relaxation behavior in multicompartment systems with significantly different T_2 values for the different compartments has shown that exchange between compartments results in an increase of the fraction with the longest T_2 and a decrease of the observed T_2 values (van der Weerd *et al.*, 2002). From these results we expect that exchange between components with different relaxation times will cause an increase of the fraction with the longest T_2 value (the flowing fraction) and can, therefore, lead to an increase of A_{app} .

The choice of spatial resolution and slice thickness can also affect the propagator in each pixel. When the spatial resolution is high and observation time is long, in plane dispersion during the time between two read out gradients can result in blurring and attenuation of the signal per pixel. The attenuation is stronger for fast moving molecules and weaker for slow moving spins. The signal that is lost due to dispersion cannot be compensated for by calculations. To estimate the signal loss

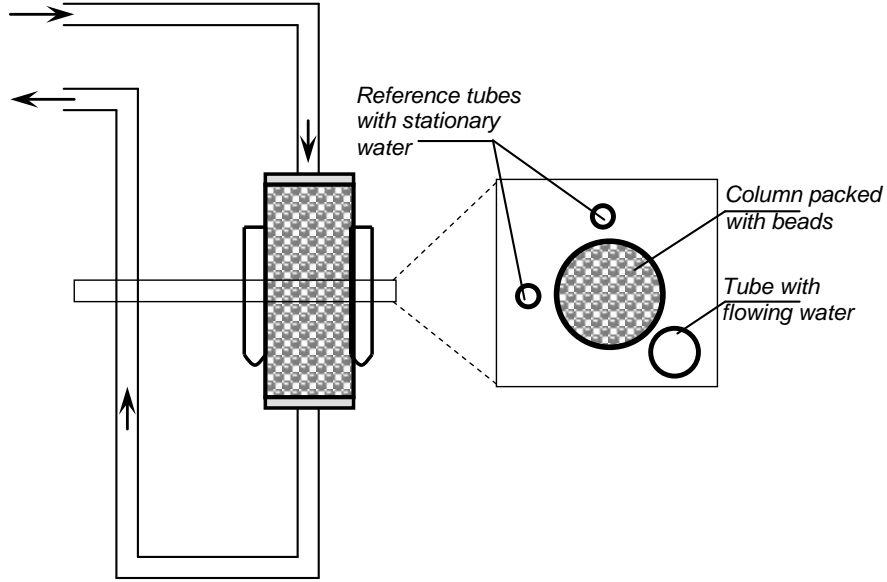


Figure 3.1 : Schematic representation of the phantom consisting of a column packed with porous beads, two references and a tube containing flowing water.

due to in-plane dispersion we assume that dispersion displacement does not exceed the maximum displacement due to flow. The displacement of the fastest flowing fluid measured at the longest Δ (320 ms) was comparable to the pixel dimension only in the experiment with the highest image resolution (0.312×0.312 mm, system 1, see Experimental for details). In all other experiments the longest displacement measured in the system was significantly smaller than the pixel size. Thus diffusion and dispersion blurring are small and, with respect to the pixel size, can be neglected.

In order to apply long Δ 's in the system with short relaxation times, PFG-STE was used. To minimize the artifacts that originate from the deviation of flip angles from 90° and 180° , three slice selective 90° pulses were applied with thickness of several (3-5 mm) millimeters. Due to flow in the direction perpendicular to the slice, part of the fluid can leave the slice during the displacement encoding time interval, which will result in an outflow effect that affects the signal intensity of fastest flowing spins. The loss of the signal from the fastest moving spins causes a shift of the spectral weight towards shorter displacements and a decrease of v_{app} , Q_{app} and A_{app} . In contrast to loss of magnetization due to susceptibility, the magnitude of signal attenuation due to outflow is a linear function of Δ and can be compensated by correcting the propagator for the amount of fluid that has flown out of the slice.

3.3 Experimental

We performed all experiments by passing distilled water through a column comprising of randomly packed particles (see Fig. 3.1). Three different types of particles were used: (i) porous aluminum oxide beads of 3.5 mm diameter packed in a column with 10 mm inside diameter and 420 mm length, (ii) silicone cylinders with a diameter of about 5 mm and length of 10 mm packed in a column with an inner diameter of 14 mm and a length of 800 mm, and (iii) methanogenic granular sludge particles with diameter about 2 mm packed into a column with an inner diameter of 14 mm and a length of 800 mm. These systems represent three different situations. The first one has strong surface relaxation effects (T_2 of water inside the pores of the beads is around 1 ms) and is expected to contain local gradients due to susceptibility effects between the fluid and the solid matrix. The second system presents a more ideal system without strong surface relaxation and susceptibility artifacts. The third system combines the effects of wall relaxation and observable stagnant water in the granules and flowing water outside the granules, with different relaxation time for the two water pools. In addition, the system can be manipulated to induce exchange between these two water pools by heating the complete packed column to 70°C for 30 mins. This treatment caused the bacterial cell membranes to become leaky allowing exchange between the intra-granular and extra-granular water pools.

To prevent loss of the particles due to flow and to provide an even distribution of fluid streamlines at the inlet, two cotton plugs were placed at the inlet and the outlet of the column. The column was connected to a reservoir by plastic tubes of 5 mm diameter. Tubes filled with 2% solution of agarose containing water doped with CuSO_4 served as references. The volume flow during a single set of measurements was constant.

A 3 T MRI system was used based on a superconducting magnet with a 50 cm vertical free bore (Magnex, Oxford, UK), in combination with an Avance console (Bruker, Karlsruhe, Germany) (Homan *et al.*, 2007). An openable gradient coil was used with a maximum gradient strength of 1 T/m. For T_2 relaxation time measurements a multi spin echo (MSE) sequence was applied (see details in Windt *et al.*, 2006); a 32×32 matrix was used, the field of view was 28.5×28.5 mm, and the slice thickness was 5 mm. Measurements were performed with an echo time (TE) of 4.8 ms and a repetition time (TR) of 6 s, and 256 echoes were acquired per echo train. For each image two acquisitions were averaged to improve the signal to noise ratio. For T_1 relaxation measurements a inversion recovery (IR) - turbo spin echo (TSE) sequence was used, with TE = 3.6 ms.

The propagators for all our measurements were obtained by PFG-STE-TSE sequences (Windt *et al.*, 2006). The PFG-STE-MSE was used for correlated displacement- T_2 measurements (Windt *et al.*, 2007). For the flow measurements in the column packed with porous aluminum oxide beads, the maximum gradient strength (g) was achieved in 32 equidistant steps. The duration of gradient pulses (δ) was 1.25 ms. Measurements were performed with slice thickness of 3 mm, TR = 1 s, turbo factor 8. For all other flow measurements g was achieved in 48 equidistant steps, δ = 4 ms, slice thickness 5 mm, TR = 2 s, and turbo factor 8. In correlated flow- T_2

measurements 64 echoes were acquired per echo train, with $TE = 8$ ms.

3.4 Results and discussion

The propagators for flow in the column packed with porous beads with strong relaxation sinks and in the tube (system 1) for different values of Δ are shown in Fig. 3.2. These propagators of the column and tube flow were extracted from the images by summing the propagators observed in all pixels in the column or tube, respectively. Since the signal from water inside the beads is not detectable due to having too short a T_2 (around 1 ms), the entire NMR signal in the column represents flowing fluid. The non-symmetrical shape of the propagators in Fig. 3.2(a) is typical for dispersive flow. The broad maximum at short displacements indicates a significant fraction of slow flowing water located near the beads. The propagators of the water flux in the tube (Fig. 3.2(b)) have an approximately rectangular shape typical of laminar flow smoothed by diffusional motion. Some deviation from rectangular shape for the propagator measured at the longest Δ may originate from the bend of the tube (see Fig. 3.1).

The values of v_{app} , A_{app} and Q_{app} extracted from the propagators shown in Fig. 3.2 decrease monotonically with increasing Δ (Figs. 3.3(a), (c) and (e)). The time dependence of these parameters is typical for susceptibility and surface relaxation effects in the column. We do not expect susceptibility effects in the tube with water and v_{app} is nearly the same for all Δ (Fig. 3.3(b)). A_{app} (Fig. 3.3(d)) and Q_{app} (Fig.

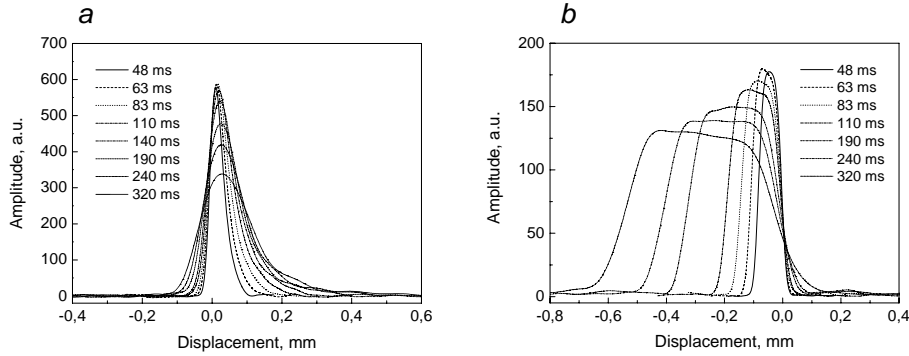


Figure 3.2 : The propagators in dependence of the observation time Δ for water flowing through a column packed with porous aluminum oxide beads of 3.5 mm diameter (a) and water flowing in the tube of 5 mm diameter (b). Experimental parameter: PFG-STE-TSE, resolution, 312 by 312 by 3000 μm ; spectral width 50 kHz; TE_1 , 6.1 ms; TE , 6ms; TR , 1000 ms; turbo factor 8; number of averages 2; 32 PFG steps, PFG duration $\delta = 1.25$ ms, labeling time $\Delta = 48, 63, 83, 110, 140, 190, 240, 320$ ms, and $PFG_{max} = 0.8, 0.61, 0.46, 0.35, 0.28, 0.2, 0.16, 0.12$ T/m, respectively.

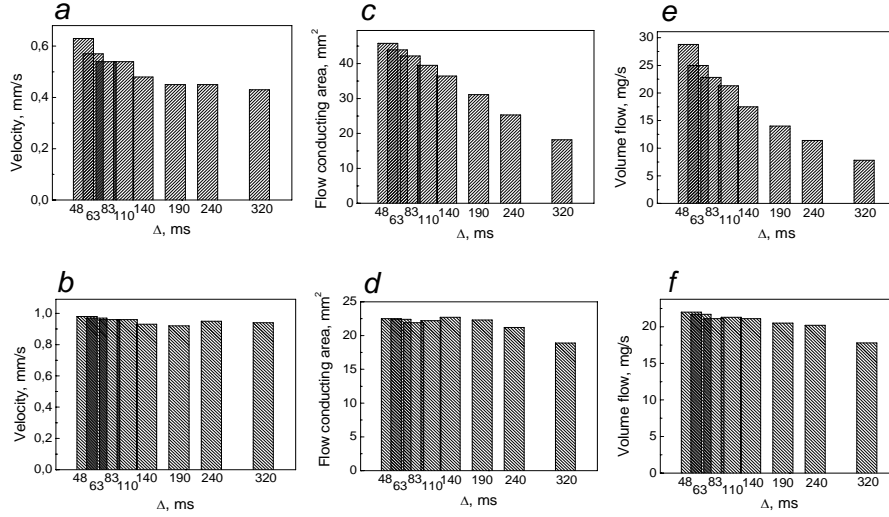


Figure 3.3 : Average flow velocity (a, b), flow conducting area (c, d) and volume flow (e, f) as a function of observation time Δ measured in the column packed with porous beads (a, c, e) and in the tube (b, d, f). Results extracted from the propagators presented in Fig. 3.2.

3.3(f)) slightly decreases at the longest Δ .

The summed signal amplitude of the first echo of all pixels in the column and in the tube corrected for T_1 (cf Eq. (3.3)) as a function of Δ are shown in Fig. 3.4 (solid symbols). The total signal in the reference tubes after correction for T_1 relaxation does not depend on Δ (data not shown). The total signal amplitude in the tube measured at the longest Δ (320 ms) is slightly lower than the signal amplitude at the shortest observation time of 48 ms. The signal amplitude in the column shows a significant decrease with increasing Δ . To estimate the actual magnetization in the tube and the column, the two T_1 corrected curves were mono-exponentially fitted to zero observation time (Fig. 3.4, dashed lines) and the amplitudes $S(0)$ obtained by extrapolation for both fractions were corrected for outflow effect (Fig 3.4, open symbols). For this correction we used the measured v_{app} of 1 mm/s in the tube (see Fig. 3.3(b)) and 0.63 mm/s in the column (Fig. 3.3(a)) and the slice thickness of 3 mm.

The difference between the outflow corrected $S(0)$ and the T_1 corrected amplitude arises from uncorrected signal loss. Since the silicon tube surface is not a strong relaxation sink, we do not expect a significant surface relaxation, and as the magnetic field is homogenous in the tube filled with water we do not any expect signal loss due to flow in offset fields. Though diffusion of molecules across streamlines does not shift the spectral weight of propagator, it can contribute to signal loss due to the read out gradient pulses. Since the first read out gradient was applied after first 90°

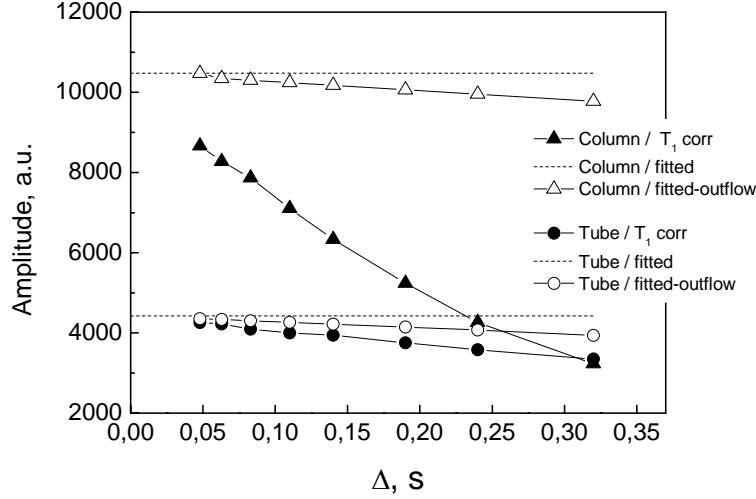


Figure 3.4 : Amplitude of 1st echo (corrected for T_1 , according to Eq. (3.3)) in the column packed with beads (\blacktriangle) and the tube with flowing water (\bullet) as a function of observation time Δ . Actual amplitudes (extrapolated to $\Delta = 0$) in column and tube with flowing water are shown as dashed lines. Actual amplitudes corrected for out-flow effect in column (\triangle) and tube with flowing water (\circ). The experimental parameters are the same as mentioned in Fig. 3.2.

pulse in the sequence we used, the in-plane diffusion over the longest Δ (320 ms) is comparable to the size of a pixel and this will result in uncompensated signal loss. In addition, there will be same saturation effect due to the short TR with respect to T_1 . The outflow effect results in an underestimation of signal from the fastest flowing spins, slightly shifting the spectral weight of the propagator towards lower v_{app} . The total signal loss due to both outflow and diffusion leads to a greater decrease of A_{app} and Q_{app} with increasing Δ in the tube with water. These effects are much stronger in the column. Strong uncompensated signal attenuation explains the decrease of A_{app} with increasing Δ and results from the susceptibility, wall relaxation and diffusion/dispersion mechanisms. The decrease of v_{app} with increasing Δ indicates that the outflow and susceptibility effects are stronger than the surface relaxation effect. It has also been shown in a system without outflow effects that for long Δ the loss of slow spins exceeds the suppression of signal of fast flowing spins (Scheven *et al.*, 2005) and this results in an increase of apparent displacement at increasing Δ . For measurements with slice selective rf pulses, the outflow effect progressively removes the signal of the fastest flowing spins, shifting the spectral weight of the propagator towards smaller values.

To confirm that the observed systematic changes of the flow parameters arise from the susceptibility in the system, we investigated flow in a column filled with

non-porous silicone cylinders (system 2). The latter have smooth walls, and in comparison to the porous beads this system has lower background gradients and hardly any surface relaxation. One can then expect that the magnetization loss due to susceptibility is significantly smaller. To minimize the outflow effect a lower velocity was used and the slice thickness was increased to 5 mm. The propagators of water flow through the column packed with these cylinders are shown in Fig. 3.5 for Δ ranging from 30 ms to 150 ms. They have a broad asymmetric shape indicating the predominance of slow flowing water similar to the flow through the column packed with porous beads. In Fig. 3.6 v_{app} , A_{app} and Q_{app} are presented for different Δ . The values of all these parameters do not change systematically with increasing Δ . The total signal corrected for T_1 is nearly independent of Δ in both the column and in the tube (Fig. 3.7). Since T_1 was the same (2 s) in the tube and in the column, the partial saturation effect arising due to the relatively short TR (2 s) was the same in both parts of the system. No outflow effect was observed (Fig. 3.7). Because the signal amplitude in the column does not depend on Δ we can conclude that there are no susceptibility effects. As a consequence, v_{app} , A_{app} and Q_{app} are also independent of Δ .

In porous systems wall relaxation, diffusion and flow motion in internal magnetic

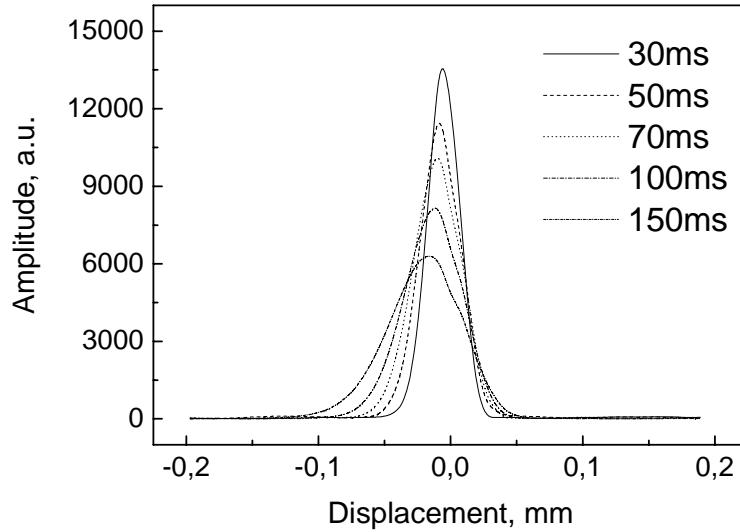


Figure 3.5 : The propagator at different observation time Δ for water flow in a column packed with silicon cylinders (diameter around 5 mm and length 10 mm). Experimental parameter: PFG-STE-MSE, resolution, 844 by 844 by 5000 μm ; spectral width 50 kHz; TE_1 , 13.5 ms; TE , 4.8ms; TR , 2000 ms; number of averages 2, 2, 2, 4, 4; 48 PFG steps, labeling time $\Delta = 30, 50, 70, 100, 150$ ms, PFG duration $\delta = 4$ ms, $PFG_{max} = 0.36$ T/m.

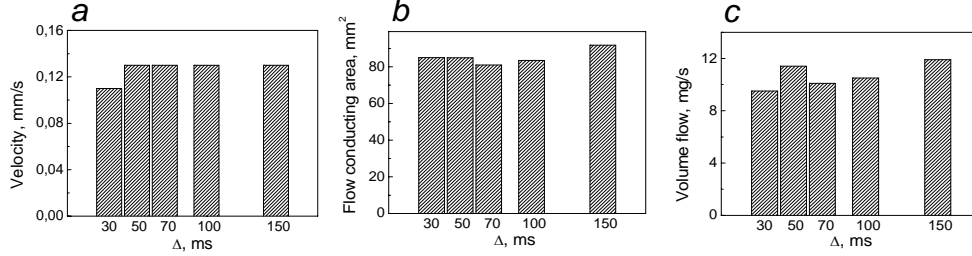


Figure 3.6 : Average flow velocity (a), flow conducting area (b) and volume flow (c) as a function of observation time Δ in a column packed with silicon cylinders. Results extracted from the propagators presented in Fig. 3.5.

field gradients result in significant uncorrected signal loss. To minimize the effect of susceptibility the background gradient suppression sequences were used (van Dusschoten *et al.*, 1995, Zheng and Price, 2008). However, there is no way to compensate these effects completely. The investigation of flow in porous media shows that susceptibility and wall relaxation result in systematic uncompensated signal loss and, as a consequence, to underestimation of A_{app} , Q_{app} and to shift of v_{app} from its real value. Since signal loss is time dependent, the deviation of apparent flow parameters from real ones increases with increasing Δ .

To investigate the effect of exchange in a multi-component system one can measure the change in relative water content (population) of the different fractions with increasing observation time (Tallarek *et al.*, 1999). This method requires very accurate determination of the signal amplitudes of the fractions present in the system. As demonstrated above, susceptibility and surface relaxation effects affect the observed signal amplitude of flowing water and exchange processes further complicates the measurements. To investigate this problem we performed the following measurements. Tap water was flushed through a glass column with inner diameter of 17 mm and packed with a methanogenic granular sludge, originating from an anaerobic waste water bioreactor. These biofilm granules consist of rigid, well-settling microbial (spherical) aggregates (diameter around 2 mm) that develop by the mutual attachment of bacterial cells in the absence of a carrier material. Since the relaxation times for the water flowing through the column and the water in the granules are different, flowing and stagnant water fractions can be discriminated on the basis of their T_2 . Correlated displacement- T_2 measurements (Windt *et al.*, 2007) were performed to obtain the propagators for both water fractions.

To avoid outflow effects a slice thickness of 5 mm, a low velocity and short Δ were used. As a result all the flow parameters for flowing water in the tube, i.e. v_{app} , A_{app} and Q_{app} , were nearly independent on Δ (data not shown). T_2 measurements by MSE imaging of water in the column revealed two components with T_2 of 12 and 695 ms, respectively, corresponding to water in the granules and extra-granular water

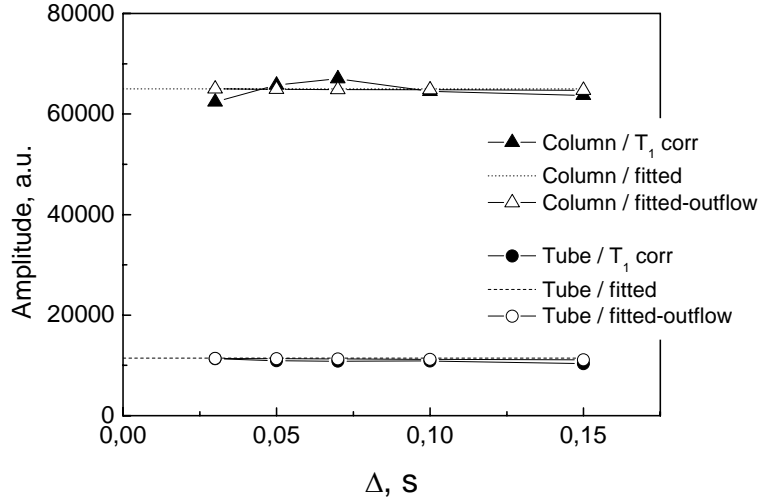


Figure 3.7 : The T_1 corrected first echo amplitude measured at observation time 30, 50, 70, 100 and 150 ms in the column packed with cylindrical particles (▲), tube (●). The dashed lines show the amplitude of the first echo obtained by fitting of the first echo amplitudes to zero observation time. Fitted amplitudes corrected for out-flow effect in column (△) and tube with flowing water (○). The experimental parameters are the same as mentioned in Fig. 3.5.

and in agreement with previous measurements (Lens *et al.*, 1999). T_1 was found to be 40 and 1074 ms, corresponding to the intra-granular and extra-granular water, respectively. Figure 3.8 shows the T_2 resolved propagators of each of these two fractions with increasing Δ . The propagators related to the shortest T_2 (Fig. 3.8(b)) are symmetrical and centered at zero, which is typical for non-flowing water. The propagators related to the longest T_2 (Fig. 3.8(a)) are not symmetrical around zero displacement, indicating fluid flow. The broad peak distributed at short displacements is related to slow moving fluid around periphery granules. The v_{app} , A_{app} and Q_{app} for Δ increasing from 30 to 100 ms are shown in Fig. 3.9; all three parameters decrease with increasing Δ . As demonstrated above, parameter behavior of this kind indicates strong susceptibility effects in the sample.

In a two-component system with no significant relaxation or susceptibility and no exchange between the stagnant and flowing water pools, the signal amplitude of both fractions corrected for relaxation will not depend on Δ . Exchange between the pools will result in a decrease of the relaxation times of both components (Windt *et al.*, 2007, van der Weerd *et al.*, 2002), and an increase of the amplitude of the flowing fluid, coupled with a corresponding decrease in the amplitude of the stagnant water, with increasing Δ (Tallarek *et al.*, 1999, Kandhai *et al.*, 2002). Since the signal from flowing fluid is sensitive to susceptibility effects, the amplitude of this component

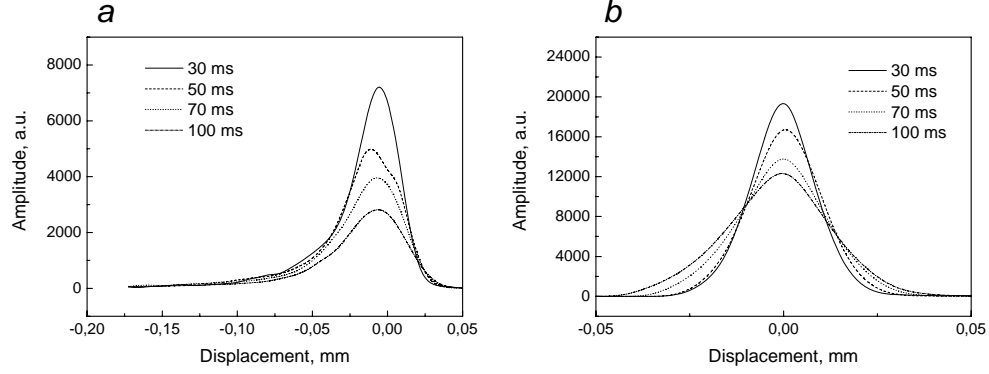


Figure 3.8 : T_2 resolved propagators in dependence of observation time Δ for the extra-granular ($T_2 = 695$ ms) (a) and intra-granular ($T_2 = 40$ ms) (b) components in a column packed with intact methanogenic biofilm granules. Experimental parameters: PFG-STE-MSE, resolution 891 by 891 by 5000 μm ; spectral width 50 kHz; TE1, 13.5 ms; TE, 8 ms; TR, 2000 ms; 48 PFG steps, labeling time $\Delta = 30, 50, 70, 100$ ms, and number of averages 2, 2, 2, 4, respectively; $\delta = 4$ ms, $\text{PFG}_{\text{max}} = 0.41$ T/m.

corrected for T_1 attenuation decreases with increasing Δ (see Fig. 3.10). Thus, the signal amplitude of flowing water cannot be used for the determination of exchange. At the same time the fluid inside the bacterial cells is hardly sensitive to the susceptibility effects because the displacement of spins due to diffusion inside the granules is much smaller than that due to dispersive flow outside the granules. Therefore, signal attenuation caused by the diffusive motion in magnetic field gradients inside the granules is lower than the attenuation for water flowing through the column. In Fig. 3.10 the first echo amplitude of stagnant granular water and of flowing water, both measured and T_1 corrected, are presented. Clearly, the T_1 corrected amplitude of the stagnant water in the granules is independent of Δ . This is typical for a system without exchange between the components.

The temperature treatment of the system resulted in a decrease of the apparent values for T_1 (29 and 988 ms) and T_2 (10 and 605 ms), revealing enhanced water exchange between the different water pools. The propagators of stagnant and flowing fluids for increasing Δ are similar to the propagators of the non-treated system (data not shown). The v_{app} , A_{app} and Q_{app} monotonically decrease with increasing Δ (data not shown), similar to those observed in the system before the heat treatment. The first echo amplitudes of the stagnant and flowing fractions as a function of Δ are shown in Fig. 3.11. The values of T_1 measured for the temperature treated system were used to correct the signal attenuation with increasing Δ . After this T_1 correction, an uncorrected amplitude loss is still observed for the flowing fraction due to susceptibility effects and wall relaxation. Surprisingly, the T_1 corrected amplitude of the first echo of the stagnant intra-granular water (strongly) increases with in-

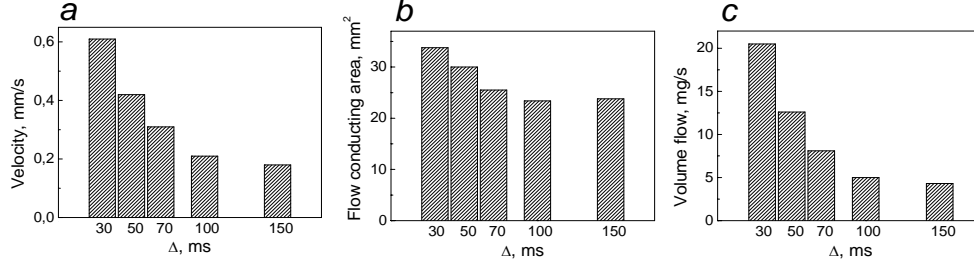


Figure 3.9 : Apparent average flow velocity (a), flow conducting area (b) and volume flow (c) for different observation time Δ measured for the water flow through the column packed with non-treated granules. Results extracted from the propagators presented in Fig. 3.8a.

creasing Δ , and this increase is significantly higher than the loss of amplitude for the flowing fraction. The total amplitude of these two fractions after T_1 correction increases with increasing Δ , which is physically impossible. If we correct the amplitude of the stagnant fraction using the T_1 of the granular water measured for the heat treatment the amplitude becomes independent on Δ , as expected for a system without exchange. Clearly, the observed T_1 is shortened by the exchange process and using this T_1 value to correct the amplitude of the stagnant water pool results in an overcorrection. If the observation times used in the measurements are of the same order as the T_1 of the stagnant fraction even a small decrease of T_1 due to exchange in the system will have a significant effect on the overcorrection of the amplitude of the non-flowing fluid. The temperature treatment clearly resulted in leakage of both the cell walls and the internal membranes of the bacterial cells, resulting in exchange of water inside the cells/granules with the flowing water pool and a decrease of the apparent T_1 of the stagnant water.

From this observation and our explanation a method can be devised to quantify the exchange. Exchange of water from the stagnant pool to the flowing pool will shorten the residence time in the stagnant pool. The observed T_1 is then given by $1/T_{1app} = 1/T_{1real} + 1/\tau$. Here τ is the mean residence time of a water molecule in the stagnant water fraction. T_{1real} is the T_1 value without exchange, which results in a corrected first echo amplitude of the stagnant water pool that is independent of Δ . τ can either be diffusion limited or defined by exchange over barriers, membranes, or similar. In the heat-treated column we find with $T_{1app} = 29$ ms, $T_{1real} = 40$ ms a mean residence time $\tau = 125$ ms.

3.5 Conclusions

We have shown that in porous media the outflow, the surface relaxation and susceptibility effects induced by the internal magnetic field gradients can (strongly) affect

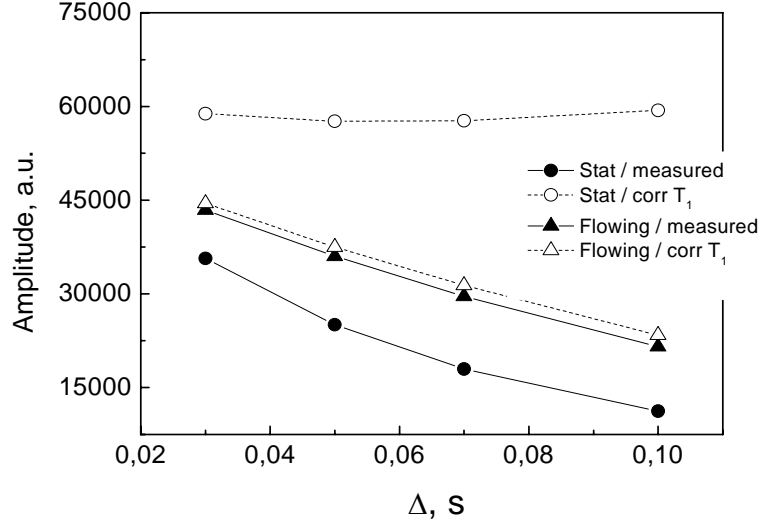


Figure 3.10 : T_1 corrected first echo amplitudes of intra-granular water and extra-granular water at observation time 30, 50, 70 and 100 ms measured in a column packed with non treated methanogenic biofilm granules. The experimental parameters are the same like mentioned in Fig. 3.8.

flow characteristics as measured by PFG-STE by removing the fastest and slowest moving spins from the NMR signal. Only the outflow effect can be corrected for by calculation. As a result, the apparent average velocity, v_{app} , the flow conducting area, A_{app} , and the volume flow, Q_{app} , as derived from the propagators, differ from their real values and become dependent on Δ . The non-corrected signal loss that remains after T_1 correction of the first echo amplitude always results in a systematic underestimation of A_{app} . Outflow and flow in local magnetic field gradients progressively remove the fastest flowing spins. When the total effect of these two mechanisms exceeds the magnetization loss from the slowest spins due to wall relaxation, the spectral weight of the propagator shifts towards lower values. That results in a reduction of v_{app} . Investigation of the dependence of the apparent flow parameters on Δ is essential for the selection optimal parameters for flow measurement in porous biological media.

The sensitivity of the signal amplitude of the flowing fluid in inhomogeneous media to susceptibility and wall relaxation makes it impossible to use it for the determination of exchange in the system. Since the signal amplitude of the stagnant water is hardly affected by uncompensated loss it can be used to reveal exchange between the stagnant and flowing water pools. If the T_1 corrected amplitude of the stagnant fraction is independent (or decreases) of Δ no exchange is present on that time scale. Exchange between fluids with different T_1 is accompanied by a decrease

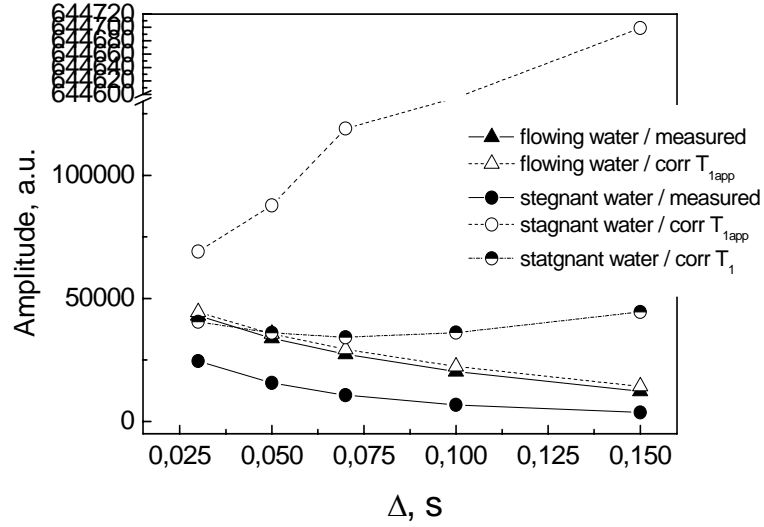


Figure 3.11 : Measured and T_1 corrected first echo amplitudes of intra-granular and extra-granular water for observation time 30, 50, 70, 100 and 150 ms, measured in the heat treated granular bed. Experimental parameter: PFG-STE-MSE, resolution, 875 by 875 by 5000 μm ; spectral width 50 kHz; TE_1 , 13.5 ms; TE , 4.8 ms; TR , 2000 ms; 48 PFG steps, labeling time $\Delta = 30, 50, 70, 100, 150$ ms, and number of averages 2, 2, 2, 4, 4, respectively; $\delta = 4$ ms, $PFG_{max} = 0.36$ T/m.

of the apparent T_1 values for both fractions. In these circumstances, the correcting the amplitude of stagnant water using the apparent T_1 will result in an increase of the signal amplitude of this fraction with increasing Δ . This overcorrection of the amplitude of stagnant fluid is a clear indication of exchange between the fractions. In a system with exchange it is necessary to use the value of T_1 for the system in the absence of any exchange to correct the signal amplitude of the stagnant water so that it becomes independent of Δ . From the difference between the observed T_1 and the T_1 without exchange the mean residence time of water in the stagnant pool can be obtained.

References

Callaghan P.T. *Principles of Nuclear Magnetic Resonance Microscopy*, Clarendon Press: Oxford, 1993; Chapter 6.3.

Cotts R.M., Hoch M.J.R., Sun T., Markert J.T. (1989) Pulsed field gradient stimulated echo methods for improved NMR diffusion measurements in heterogeneous systems. *Journal of Magnetic Resonance*, **83**, 252-266.

Donker H.C.W., Van As H., Edzes H.T., Jans A.H.W. (1996) NMR imaging of white button mushroom (*Agaricus bisporus*) at various magnetic fields. *Magnetic resonance imaging*, **14**, 1205-1215.

Homan N.M., Windt C.W., Vergeldt F.J., Gerkema E., Van As H. (2007) 0.7 and 3 T MRI and sap flow in intact trees: xylem and phloem in action. *Applied Magnetic Resonance*, **32**, 157-170.

Kandhai D., Hlushkou D., Hoekstra A.G., Slood P.M.A. Van As H., Tallarek U. (2002) Influence of stagnant zones on transient and asymptotic dispersion in macroscopically homogeneous porous media. *Physical Review Letters*, **88**, 234501.

Lens P., Vergeldt F., Lettinga G., Van As H. (1999) ¹H NMR Characterisation of the diffusional properties of methanogenic granular sludge. *Water Science and Technology*, **39**, 187-194.

Nestle N., Qadan A., Galvosas P., Süss W., Kärger J. (2002) PFG NMR and internal magnetic field gradients in plant-based materials. *Magnetic resonance imaging*, **20**, 567-573.

Scheenen T., van Dusschoten D., de Jager P.A., Van As H. (2000a) Microscopic displacement imaging with pulsed field gradient turbo spin echo NMR. *Journal of Magnetic Resonance*, **142**, 207-215.

Scheenen T.W.J., van Dusschoten D., de Jager P.A., Van As H. (2000b) A model-free quantification of water transport in intact plants with NMR imaging. *Journal of Experimental Botany*, **51**, 1751-1759.

- Scheven U.M., Seland J.G., Cory D.G. (2004) MNR propagator measurements on flow through a random pack of porous glass beads and how they are affected by dispersion, relaxation and internal field inhomogeneities. *Physical Review E*, **69**, 021201.
- Scheven U.M., Seland J.G., Cory D.G. (2005) NMR-propagator measurements in porous media in the presence of surface relaxation and internal fields. *Magnetic Resonance Imaging*, **23**, 363-365.
- Song Y. (2000) Detection of the high eigenmodes of spin diffusion in porous media. *Physical Review Letters*, **85**, 3878.
- Tallarek U., van Dusschoten D., Van As H., Bayer E., Guiochon G. (1998) Study of transport phenomena in chromatographic columns by pulsed field gradient NMR. *Journal of Physical Chemistry B*, **102**, 3486-3497.
- Tallarek U., Vergeldt F.J., Van As H. (1999) Stagnant mobile phase mass transfer in chromatographic media. *Journal of Physical Chemistry B*, **103**, 7654-7664.
- Van As H. (2007) Intact plant NMR for the study of cell water relations, membrane permeability, cell-to-cell and long-distance water transport. *Journal of Experimental Botany*, **58**, 743-756.
- van der Weerd L., Melnikov S.M., Vergeldt F.J., Novikov E.G., Van As H. (2002a) Modelling of self-diffusion and relaxation time NMR in multicomponent systems with cylindrical geometry. *Journal of Magnetic Resonance*, **156**, 213-221.
- van der Weerd L., Claessens M.M.A.E., Efde C., Van As H. (2002b) Nuclear Magnetic Resonance imaging of membrane permeability changes in plants during osmotic stress. *Plant, Cell and Environment*, **25**, 1538-1549.
- Van Dusschoten D., de Jager P.A., Van As H. (1995) Flexible PFG NMR desensitized for susceptibility artifacts using the PFG-multiple-spinecho sequence. *Journal of Magnetic Resonance, Series A*, **112**, 237-240.
- Windt C.W., Vergeldt F.J., de Jager P.A., Van As H. (2006) MRI of long-distance water transport: a comparison of the phloem and xylem flow characteristics and dynamics in poplar, castor bean, tomato and tobacco. *Plant, Cell and Environment*, **29**, 1715-1729.
- Windt C.W., Vergeldt F.J., Van As H. (2007) Correlated displacement- T_2 MRI by means of Pulsed Field Gradient - Multi Spin Echo method. *Journal of Magnetic Resonance*, **185**, 230-239.

Chapter 4

Dynamics of water transport and water content in storage pools in diffuse-porous trees during a dry-down period and recovery after watering

Xylem flow, flow conducting area and water content in the storage pools in the sapwood and cambial zone were investigated simultaneously and non-destructively by Magnetic Resonance Imaging (MRI) in diffuse-porous laurel (*Laurus nobilis*) and viburnum (*Viburnum tinus*) trees during a dry-down period and recovery after watering. The development of the drought stress was detected by the decrease in average velocity, volume flow and flow conducting area as observed by MRI flow imaging. The decrease in flow conducting area occurred one day later than the reduction of average velocity, volume flow and water content in the cambial zone. Water content in the sapwood region did not decrease during the dry-down period. The re-watering of the plants resulted in a fast restoration of the flow conducting area to the value observed under well watered conditions, demonstrating that if cavitations had been induced they refilled quickly. In addition, though a significant increase of the average velocity and volume flow was observed after rewatering, they did not recover to their pre-water stress values. Images of water content in the cambial zone revealed a gradual decrease of the water content even before the drought stress, but which speeded up during the stress. The rate of decrease was dependent on day/night conditions. Watering resulted in the partial restoration of the water content of this zone. The water content of the sapwood showed a clear diurnal variation; it decreased quickly at the beginning of the photoperiod but fully recovered during the day and evening. Drought stress did not change the character of diurnal variation of water content significantly, but it increased the amplitude of the diurnal variation. Re-watering of the tree resulted in a 10% loss of water content in the sapwood. The oldest annual ring was

rather inactive in long distance water transport. We found that the transport activity of this ring was insensitive to any environmental changes and that the variation of water content in sapwood was uniform in all annual rings.¹

4.1 Introduction

Studies on plant water relations have shown that intrinsic water storage capacities in roots, stem and leaves contribute significantly to buffering water transport fluxes during daily fluctuations in water demand by transpiring tissues (mainly the leaves) and during seasonal water deficits. This capacitive effect has been demonstrated indirectly by the simultaneous measurement of the xylem flow near the base of the trunk and in the crown of intact (woody) plants in the morning hours, when transpiration increases at the beginning of the photoperiod. The rise of the basal flow was delayed relative to the increase of the flow measured in the crown (Andrade *et al.*, 1998, Meinzer *et al.*, 2003), and changes in water content at different positions in the stem were delayed relative to each other and with respect to the change in flow (Van As *et al.*, 1994). The water potential drop initiated by the transpiration in leaves induces water transport from the storage compartments into the transpiration stream. That helps to compensate rapid water loss and temporal imbalance between the water supply and demand (Holbrook, 1995). Internal storage water can contribute from 5% up to 65% of the total daily transpiration water loss (Waring and Running, 1978, Tyree and Yang, 1990, Goldstein *et al.*, 1998, Phillips *et al.*, 2003, Čermak *et al.*, 2007). In the morning, when the transpiration reaches its maximum value, up to 75% of transpired water can be withdrawn from the internal storage compartments in the crown and stem. (Zweifel and Häslér, 2001, Čermak *et al.*, 2007, Zweifel *et al.*, 2001).

In the stem three water storage reserves can be distinguished (Zimmermann, 1983): (i) the xylem vessels, (ii) cell wall capillaries and inactive xylem elements, and (iii) elastic, living cells in the bark, parenchyma, phloem, cambium and ray cells. Investigations of different types of trees have shown that sapwood is the main water storage pool in the stem (Phillips *et al.*, 2003). The capacity of this pool increases with the age of trees. The capacitance of the storage pool in elastic tissues can be estimated from the daily changes in stem diameter. Diurnal variations in stem dimension occur mainly in the tissues outside the sapwood (Molz and Klepper, 1973, Zweifel *et al.*, 2000) and are proportional to the water content in these elastic tissues (Zweifel and Häslér, 2001). Depending on the balance between water supply and demand three general patterns have been observed from the daily stem diameter changes (Hinckley and Bruckerhoff, 1975, Brough *et al.*, 1986, Zweifel and Häslér, 2001): (i) When soil water content is high and evaporative demand is low, the stem diameter can increase overall from one morning to the next with either no decrease, or only a reduction of the rate of increase, in stem diameter in the intervening daylight

¹This Chapter is based on: Homan N.M., Gerkema E., Van As H. Dynamics of water transport and water content in storage pools in diffuse-porous trees during a dry down period and recovery after watering.

period when transpiration is active; (ii) when both soil water content and evaporation demand are high, the stem diameter can increase from one morning to the next, but during the intervening period of daylight the stem diameter can decrease; (iii) at low soil water content and high evaporative demand the stem diameter can decrease during the day and only partly recover during the night.

All the water storage elements have different locations in a trunk and water is withdrawn from them at different water potential values. Capillary water is withdrawn at water potentials from 0 to about -0.2 MPa (Tyree and Yang, 1990). Zweifel *et al.* (Zweifel *et al.*, 2000) reported that when water potential is higher than -2.3 ± 0.3 MPa, water is withdrawn almost solely from bark and other elastic cells of stem. A further decrease of water potential results in cavitations and depletion of xylem vessels (Tyree and Yang, 1990). Thus, the water storage pools of different tissues contribute differently to plant adaptation occurring in response to changing of environmental conditions. However, the interaction between storage pools and xylem flow characteristics under dynamic (stress) conditions is still not well understood. A completely non-invasive measurement of sap flow and the active flow conducting area in intact plants is needed that will permit the dynamics (day/night, stress responses) of these processes to be investigated in relation to the water content of the adjacent tissues. Non-invasive intact plant MRI hardware and methods have been recently developed for this purpose (Homan *et al.*, 2007, Van As, 2007, Van As *et al.*, 2009). In this paper we present for the first time results obtained by applying such non-invasive MRI methods to measure the correlation between sap flow and water distribution in different internal storage pools in diffuse-porous trees under well watered conditions, during the development of a drought stress, and during recovery after watering.

4.2 Materials and methods

4.2.1 Plant material

A laurel (*Laurus nobilis*) and a viburnum (*Viburnum tinus*) tree (3-4 years old) were obtained from a local nursery. The trees were about 1 m tall with trunk diameter of about 1.5 cm and were rooted in 5 liter pots. The plants were kept well-watered before measurements. After insertion into the MRI setup watering was stopped. Water content and xylem flow were measured by MRI at approximately 90 minute intervals. Plant water status was estimated using the flow parameters measured by MRI. During the measurements supplemental halogen lighting was used to create day-night cycle (14 h light / 10 h dark). As soon as there was no flow increase in the stems upon starting the photoperiod the drought was terminated by rewatering the plants.

4.2.2 The NMR imaging setup

The laurel tree was measured using a 3 T vertical bore MRI system as described elsewhere (Homan *et al.*, 2007, Van As, 2007). An openable gradient coil (Bruker) generating maximum gradient strengths of 1 T/m and an openable radio frequency

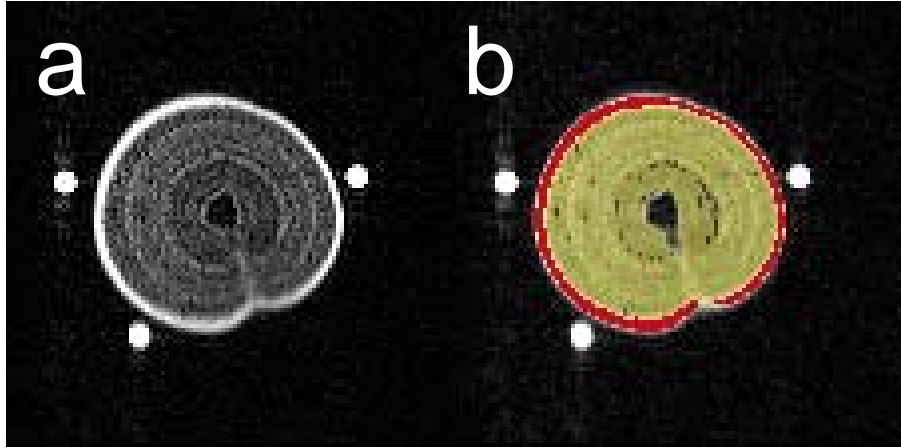


Figure 4.1 : (a) MRI T_2 weighted water content image in a cross sectional slice of the stem of a laurel tree. (b) The same image with the mask of active sapwood (yellow) and the mask of cambium and phloem (red). Due to too short T_2 values the bark is hardly observed in these images.

(RF) coil with inner diameter of 4 cm were mounted around the stem at ca. 40 cm above the pot surface. Image resolution was set to 128×128 pixels at a field of view of 40 mm, resulting in a pixel dimension of $312 \times 312 \mu\text{m}^2$. The slice thickness of the cross sectional images was chosen to be 3 mm.

The viburnum tree was imaged using a 0.7 T system (Homan *et al.*, 2007, Windt *et al.*, 2007). A gradient system with planar geometry and 5 cm air gap between the gradient plates was used, generating maximum gradient strengths of 1 T/m. The planar geometry of the gradient system allows easy access to the center of the magnet from the front and back as well as from above and below. A home made 9-turn RF coil of 1.5 cm diameter was centered around the stem at ca. 40 cm above the pot. The coil was connected to a tuning circuit and shielded. The tree with the coil in place was inserted into the magnet in an upright orientation. Imaging resolution was set at 128×128 pixels at a field of view of 16.5 mm. The in plane pixel dimension was $129 \mu\text{m} \times 129 \mu\text{m}$. Cross sectional images were measured with a slice thickness of 5 mm.

4.2.3 MRI flow measurements

A pulsed field gradient - spin echo - turbo spin echo sequence (PFG-SE-TSE) (Windt *et al.*, 2007) was used to measure xylem flow in the trees. This method allows us to measure the displacement distribution, or propagator, during the displacement labeling time Δ of all spins in each pixel (Scheenen *et al.*, 2000, Windt *et al.*, 2007, Homan *et al.*, 2007, Van As, 2007). The following experimental parameters were

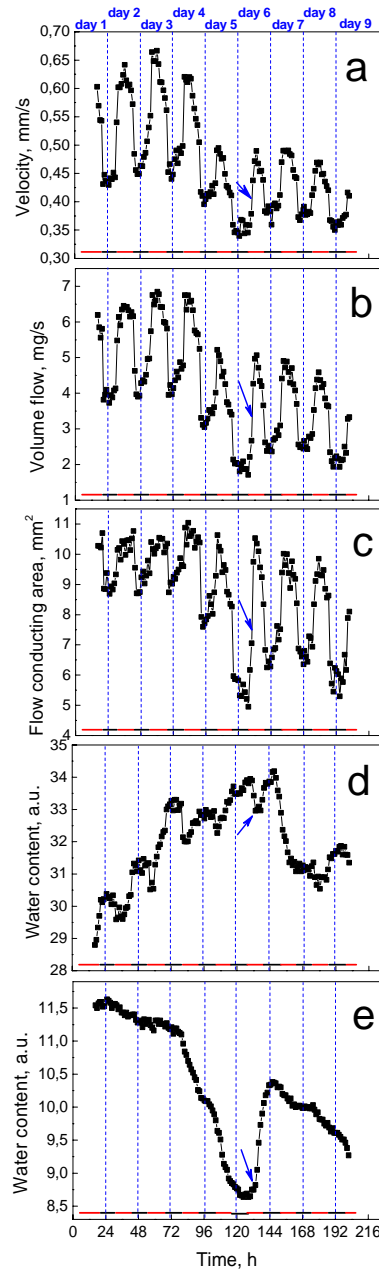


Figure 4.2 : Average flow velocity (a), volume flow (b) and flow conducting area (c) of xylem sap as well as water content in the xylem tissue (d) and in the cambial zone (e) in a laurel tree measured during a drydown period and recovery after watering. The arrows indicate the time of watering.

used: $\Delta = 60$ ms, $\delta = 3$ ms, 32 PFG steps, $\text{PFG}_{\text{max}} 0.36$ T/m, echo time (TE) was 3.7 ms, repetition time (TR) was 2 s.

The spatial resolution that has been chosen in these MRI measurements cannot resolve individual vessels containing flowing water from adjacent cells containing non-flowing water in either the laurel or viburnum plants. The symmetry of the displacement distribution of non-flowing water around zero displacement (typical for diffusion) is used to separate non-flowing and flowing fluids (Scheenen *et al.*, 2000). To do this the signal in the non-flowing direction was mirrored around zero and subtracted from the signal in the flowing direction. The resulting propagator presents the flowing water only.

4.2.4 Water content imaging

The calculation of water content in different tissues in the stem of laurel was done on the basis of part of the data set for flow imaging: PFG-SE-TSE images with zero pulsed-field gradient amplitude. The T_2 weighted MRI signal in each pixel correlates to proton density and consequently to water content (Van As *et al.*, 2009). Since the encoding time in flow measurements was 60 ms, during that time T_2 relaxation was active and can affect the signal intensity (Van As, 2007). The amplitude of the signal in each pixel is T_2 weighted and correlates to the amount of water with relaxation time long enough to be detected. The T_2 relaxation time for water in bark is significantly shorter than 60 ms (Homan *et al.*, 2007) and is therefore not reliable for water content determination. The mask of xylem, representing the functionally active xylem as observed by the flow measurements, was used to estimate the water content in the sapwood. Pixel dimension in these measurements was $312 \mu\text{m} \times 312 \mu\text{m}$, which was too large to allow the cambium and phloem to be distinguished. The mask for these two types of tissues was obtained by selecting the pixels with high proton density just surrounding the sapwood (Fig. 4.1) and we will call this region the cambial zone. These masks were selected from the initial MRI measurements during the photoperiod of the first day of the experiment when the tree was well watered. The same areas corresponding to xylem and cambium and phloem were applied to all measurements during the drydown and recovery periods.

4.3 Results

4.3.1 Variation in axial flow

Average velocity, flow conducting area and volume flow were measured in laurel and viburnum under well watered conditions, and during the development of a drought stress and recovery after watering. All these parameters show a diurnal fluctuation associated with the day-night light cycle (Fig. 4.2a-c). In order to minimize variations of flow parameters during the day time, constant light, and nearly constant temperature and humidity were used. In both types of trees all measured flow parameters decreased during the drought period (the results for viburnum are not shown, but are very comparable to those of laurel). On day 4 the average velocity and volume

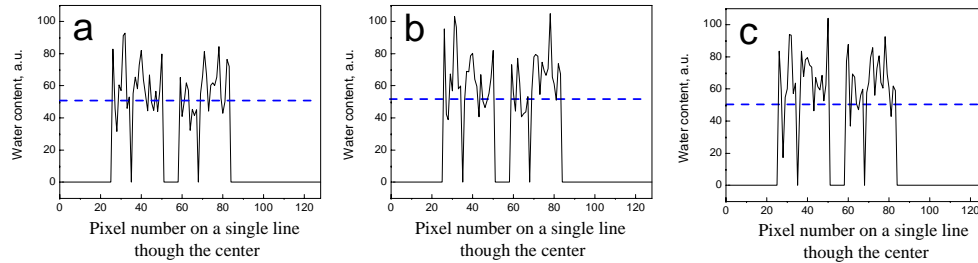


Figure 4.3 : Water content profiles through the center of sapwood of the laurel tree measured under favorable water condition (a), during the drought stress just before watering of the tree (b) and immediately after watering (c).

flow started to decrease simultaneously. The decrease of the flow conducting area began on day 5, one day later than the decrease of average velocity and volume flow. In response to watering, the flow conducting area, average velocity and volume flow increased immediately. Flow conducting area both in laurel and viburnum recovered to the value observed on days 2-4, while average velocity and volume flow increased to 75% and 70% of the initial values, respectively.

4.3.2 Water content in sapwood and cambial zone

Using the water content maps, the total amount of water in the selected regions was estimated by the summing signal intensity of all pixels in the regions of interest. Figures 4.2d-e show for laurel the total water content in the sapwood and the cambial zone during the whole measuring period. For different types of trees we observed an increase of water content in sapwood during the first few days after insertion of the plant into the magnet. We assume that such a behavior is related to the adaptation of the (well watered) trees to the new environment. After the third day the increase in water content in the sapwood leveled off. The watering of the tree on day 6 did not influence the diurnal variation in water content in this tissue. After watering, at the start of the light period on day 7 when the daily maximum of water content was reached, the amount of water in the sapwood started to decrease and continued to decrease during that day, dropping down by about 10%. During the next night it became constant and on day 8 a diurnal variation was observed around that level. The radial distribution of the water content in the sapwood at the times of maximum and the minimum water content in either the well watered tree (Figs. 4.3a and b) or during the period of minimum water content (day 7) (Fig. 4.3c) does not show preferential decline of water in any growth ring. The day/night cycle in water content had recovered by day 8 (Fig. 4.2d) while the amount of water was significantly lower than the amount detected during the stress.

The water content in the cambial zone was decreased from the first day of measurement. A clear day/night difference in the rate of decrease can be observed. From

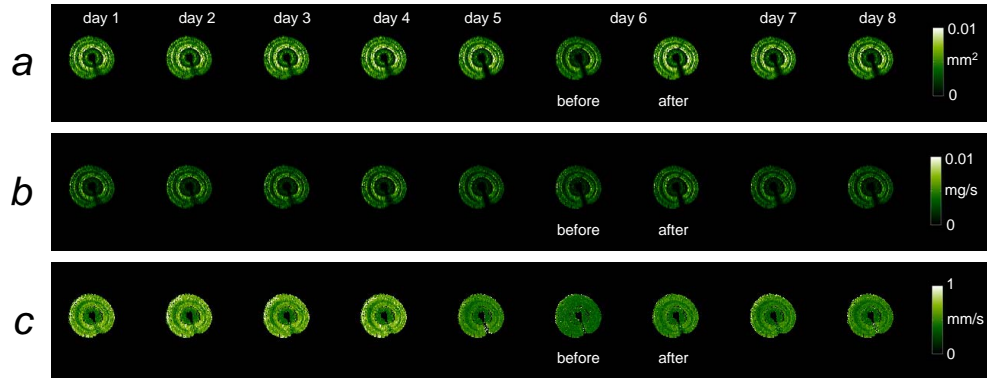


Figure 4.4 : Maps of flow conducting area (a), volume flow (b) and average flow velocity (c) for the stem of a laurel tree at different times during the experiment: favorable water conditions, developing drought stress and recovery after watering.

the fourth day, when the behavior of average velocity and volume flow indicated drought stress, the decrease became steeper. In response to the watering, the water content in the cambial zone increased immediately, and kept increasing for the rest of the day, reaching about 90% of the water content on day 1. After watering on the following day the water content again decrease, but the rate of decrease was notably lower than that recorded during stress conditions, though it was, however, faster than the decrease under well watered conditions (day 1 and 2).

4.3.3 Radial variation in sap flow

In Figure 4.4 maps of flow conducting area, volume flow and average velocity in laurel are presented. In the oldest growth-ring all these parameters were lower than in the younger rings. The lower flow conducting area can be related to a lower density of functional xylem vessels in the oldest sapwood. The average velocity, which was one and a half times lower in the oldest sapwood than in the youngest rings, may be due to the smaller vessels in this region, which, according to Poiseuille's law for laminar flow in a cylindrical tube and assuming equal pressure drop over all vessels, should result in a lower average velocity. Under well watered conditions the velocity in the oldest sapwood hardly showed any day-night changes (Figs. 4.5a and b). Even drought stress did not result in any change in velocity in the oldest annual ring, even though it caused a reduction of the velocity in the youngest sapwood (see Fig. 4.5c). Figure 4.5d shows that the flow velocity immediately increased in the outer sapwood in response to watering on day 6.

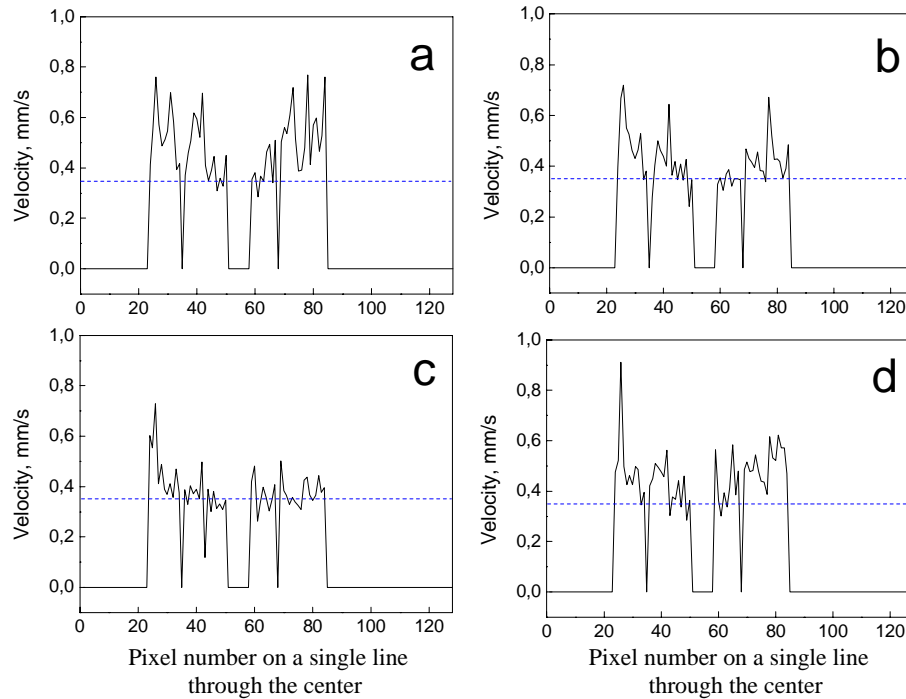


Figure 4.5 : Flow velocity profile through the center of the stem of the laurel tree measured on day 1 (well watered) day time (a) and night time (b) and before watering of the tree on day 6 (c) and immediately after watering (d).

4.3.4 Diurnal variation of water content in sapwood and cambial zone

The diurnal variation of water content of the different laurel stem tissues on day 2 (well watered) is shown in Fig. 4.6a. The amount of water in the xylem decreased immediately at the start of the photoperiod, and then increased gradually during the rest of the photoperiod to a level even higher than that just preceding the start of the photoperiod at which it remained during the night. In the sapwood the total water includes water in vessels, xylem parenchyma, tracheids and ray cells. In this type of experiment it is not possible to distinguish the water in vessels from that in any other xylem cells. As sapwood is rigid it cannot undergo any significant diurnal changes in size. In addition, in a well watered tree we did not observe changes in flow conducting area during the photoperiod of days 1-4 (see Fig. 4.2). Thus, when the flow conducting area is constant we can conclude that any change in water content corresponds to the change in amount of water in all tissues in the sapwood except the functionally active vessels. The water content in the cambial zone gradually decreased at the start of the photoperiod and continued to decrease slightly during the remainder of the photoperiod and the night-time.

The fourth day of the experiment is particularly interesting because the decrease of average velocity and volume flow indicated that there was a shortage of water in the system while the flow conducting area did not yet show any reduction (see Fig. 4.2). Thus, we can conclude that the change of water content in the xylem was not related to cavitated conduits. The reduction of water content in the xylem region in response to the light was about two times higher than under well watered conditions (cf Figs. 4.6a and b). During the day and in the evening this water pool restored to its initial level. The decrease of water content in the cambial zone was three times stronger and did not recover.

4.4 Discussion

4.4.1 Variations in axial flow

Diurnal fluctuations in flow velocity, volume flow and flow conducting area in well watered trees were observed for different species and presumably result from the day-night changes of stomatal conductance and transpiration rate (Windt *et al.*, 2006). A decrease in flow velocity (Fig. 4.2a) and volume flow (Fig. 4.2b) in response to a developing drought stress preceded a decrease in flow conducting area (Fig. 4.2c). Our findings are in agreement with the observation that stomatal control of water loss is a fast response to water deficit (Buckley, 2005). Under water limiting conditions the stomata are thought to be controlled by ABA signaling from the roots (Tardieu, 2003) or to respond to a decrease in the conductance of the hydraulic pathway. In *Laurus nobilis* L. xylem vessels in leaves are more vulnerable to cavitation than conduits in the stem so they will be the first to cavitate under conditions of water deficit (Salleo *et al.*, 2000, Salleo *et al.*, 2001). This observation is consistent with the observed delay in the decrease in flow conducting area in the stem compared to the decrease in velocity or volume flow.

Unfortunately, we do not have data on the tree water potential during drought stress. Nonetheless the measurement of stem water potential and water content in cambial zone in oak (see Appendix to Chapter 5) showed a very good, approximately linear correlation between these two parameters during dry-down period. In oak a decrease of water potential by 1 MPa corresponds to a 16% decrease of water content in the cambial zone. Here we observed a maximum decrease of water content in the cambial zone during drought stress of about 24%. Assuming a comparable relationship between water content and water potential in oak and in laurel in the cambial zone, this decrease corresponds to a decrease of water potential of about 1.5 MPa. In diffuse-porous trees like birch and aspen, a 50% loss of xylem conductance was observed at a plant water potential of -1.0 to -1.6 MPa (Sperry *et al.*, 1994). Thus, we can conclude that drought stress may have resulted in cavitation in xylem vessels. After watering, the flow conducting area fully recovered within 30 minutes to its value under well watered conditions. This shows that the embolisms were repaired by a fast refilling of cavitated vessels. The latter conclusion is in good agreement with the fast embolism recovery previously observed in young trees of *Laurus nobilis*

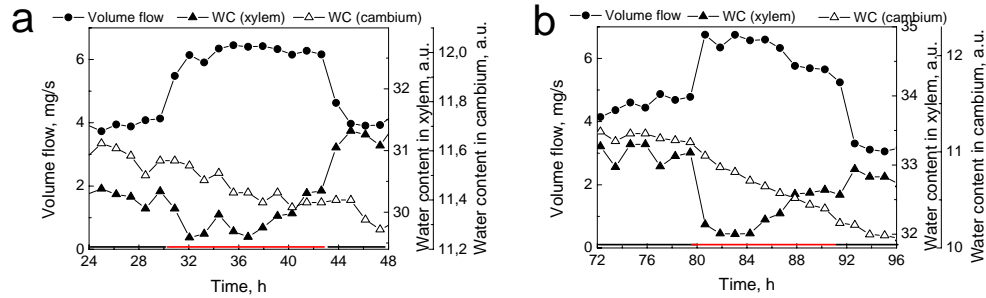


Figure 4.6 : Diurnal variation of volume flow (●), water content in xylem (▲), water content in cambium and phloem (△) on the second day (a) and on the fourth day of measurements (b).

(Salleo *et al.*, 1996). After watering, the average velocity and volume flow increased, but did not return to their initial values. Since flow conducting area recovered almost completely, the decrease in average velocity is not related to an increase in xylem resistance and most probably results from the change in resistance in roots, leaves or both. We note that after watering the flow conducting area during the night period is significantly lower than that in the well watered tree. This reduction in flow conducting area was probably caused by a reduction in the number of flow conducting xylem vessels (Windt *et al.*, 2006). The slowest moving water will be found in the vessels with the smallest diameters. It is likely that, under conditions of low transpiration, the flowing water in these vessels will be the first to become indistinguishable from stationary water (see Appendix).

4.4.2 Water content in sapwood and cambial zone during drought stress and recovery

Below we discuss the result of water content measurement. Since the signal intensity is T_2 -weighted, we do this under the assumption of constant T_2 values for the storage pools. This assumption should be tested by optimized amplitude measurements, e.g. by MSE imaging (see Chapter 5). An increase of water deficit in the tree, which is detected by a decline in sap flow, is accompanied by a withdrawal of water from mainly the elastic tissues in the cambial zone. Under drought stress, the start of the photoperiod initiated a faster decrease of water content in storage pool in the sapwood than under well watered conditions, and the loss of water was completely replenished during the day. We suggest that under moderate water deficit this replenishment takes place by water from the storage pools in elastic tissues. The water store in the sapwood very likely serves as the last reserve that is used only if the cambial zone buffer drops below a certain water content. This assumption agrees with the results obtained for drying stem segments (Zweifel *et al.*, 2000) and for living trees (Holbrook, 1995), which show that water loss mainly occurs in elastic cells at small

decrease of xylem water potential. Only when xylem water potential decreases below a certain transition point is water withdrawn from the rigid sapwood.

After re-watering, water content in the cambial zone recovered to 90% of its value before the stress. In contrast, the water content in the xylem tissues decreased significantly in response to rewatering and there had been no decrease of water content during the dry-down. Recovery after drought stress in oak (see Appendix to Chapter 5) showed that water potential recovered after complete replenishment of water content in cambial zone. Since water content in the cambial zone of the laurel tree did not restore completely, we can not exclude the possibility that watering of the tree was not sufficient to replenish all water storage pools. Depletion of water in the sapwood storage pool may be related to redistribution of water between storage pools in stem and the crown. Zweifel *et al.* (Zweifel *et al.*, 2001) have shown for Norway spruce tree that the diurnal increase in transpiration resulted in the depletion of water reserves in the crown that was followed by a depletion of the elastic stem storage pool. The replenishment of water occurred in the reverse order to depletion. At the same time it was observed that recovery of photosynthesis that was inhibited during the stress was promoted by recovery of leaf water content (for review see Yordanov *et al.*, 2000). Thus, the decrease in water content in the xylem buffer during recovery from the stress may be related to refilling of the water storage reservoir in the crown, which is needed for the recovery of the photosynthetic activity.

4.4.3 Radial variation in sap flow

Diffuse-porous trees have very broad sapwood. Until now the spatial and temporal use of the sapwood for water transport have not been well understood. Experiments with heat pulse techniques have shown significant variation in sap flow with respect to the radial position in the trunk. The sap flow velocity had a maximum value in the outermost rings and then declined in inner sapwood for different woody plant species; laurel (Jimenes *et al.*, 2000), beech (Granier *et al.*, 2000) and poplar (Wullschlegel and King, 2000). It has been suggested that the decline of the water transport activity with radial depth depends upon the age of the sapwood (Phillips *et al.*, 1996). Our observation of a decrease in sap velocity in the inner annual ring is in agreement with these previous investigations. We observed a variation in xylem flow only in the outer sapwood. In the inner sapwood flow was not sensitive to any environmental changes. An interesting hypothesis explaining this behavior of the inner sapwood was proposed by Dye *et al.* (Dye *et al.*, 1991). They assumed that the inner xylem, which is formed early in the life of the tree, supplies water to the first-formed branches. When the tree gets older these branches die or become shaded, and the sap flow in the oldest xylem declines because inner sapwood no longer participates in the supply of water to transpiring surfaces. Consequently water flow in the oldest xylem should not depend on changing environmental conditions. The results of our measurements for the inner sapwood agree rather well with their hypothesis.

4.4.4 Diurnal variation of water content in sapwood and cambial zone

The water storage reserve in xylem tissue consists of three types of storage compartments. Firstly, there is capillary water in cell walls and in inactive xylem elements. Secondly, there is water in living cells, such as the rays and xylem parenchyma. The third type of storage water is that of the xylem vessels. The sites of water storage outside the sapwood are mainly in living cells and to a lesser extent the cell walls. Since the relaxation time of water in the cell wall matrix in woody plants is too short to be observed by a conventional MRI experiment only intracellular water is usually detected (Van der Toorn *et al.*, 2000).

Withdrawal of water from sapwood, which during the first few days of the experiments reported here was observed at the start of the photoperiod, should be related to the depletion of water stored in cell walls and inactive xylem elements because capillary water is released at high values of water potential (Tyree and Yong, 1990). We therefore assume that the fast decrease of water content in sapwood (see Fig. 4.5a) should be related to the withdrawal of water from inactive xylem vessels. Water is withdrawn from sapwood and the cambial zone simultaneously, which results in a further decrease of water content in these tissues. When the transpiration rate decreases in the afternoon, the water content of the sapwood recovers. It is reasonable to assume that the capillary storage compartment replenishes first as suggested by the increase of water content in sapwood in the afternoon. At the same time the decrease in water content in the living cells of the cambial zone continued, but with a rate of decrease lower than that during the period of active transpiration in the morning. The water loss from these living cells during the photoperiod did not fully recover during the night period, in contrast to the storage water pool in sapwood that was refilled completely.

On the fourth day of measurements, when the decrease of flow velocity and volume flow indicated that water uptake had become limiting (see Fig. 4.5b), the capillary storage compartment and water storage buffer in living cells were depleted more strongly than under well watered conditions. Even under this water-limiting condition a day-night rhythm was still visible in the water content of sapwood and it was replenished daily. This shows that the storage buffer of this tissue closest to the active xylem vessels is used to dampen the imbalance between water supply and demand at the peak of transpiration.

Čermak *et al.* (Čermak *et al.*, 2007) proposed that functionally less-active sapwood can be used as a resource of storage water. If this is true, the variation in water content of the oldest xylem would be more pronounced under the diurnal transpiration cycle and during drought stress. However in our measurements we did not observe any noticeable difference of water content between the functionally more active youngest annual rings and the less active oldest sapwood either under well watered conditions or during the water-limiting drought period. Thus, we conclude that while xylem vessels are active in long-distance water transport, the buffer in the sapwood is mainly used for compensation of diurnal imbalance between the water demand and availability in the same vessels. Under the moderate drought stress, as applied here, this water reserve was not used as an additional storage pool for more active xylem.

4.5 Conclusion

For the first time the coupling between water flow in xylem vessels and water content in storage pools was demonstrated. We analyzed the behavior of different storage tissues in response to short- and long-term variations of environmental conditions.

The fast decrease in water content of the cambial zone during drought stress indicated that this storage water is used to compensate for the imbalance between foliar transpiration and water uptake by roots. The diurnal depletion and replenishment of the water storage pool in sapwood suggests that this water reservoir is needed to buffer the rapid loss of water that occurs during the morning increase of transpiration. The daily replenishment of this storage pool shows that the sapwood pool is not used to compensate dehydration under moderate drought stress. It might be that water stored next to xylem vessels is the last water reserve and used only when more remote buffers have already been depleted. The difference between the behavior of the water content in sapwood and in cambial zone during drought stress may indicate a difference in water potential between these tissues.

The inner annual ring is less active in sap transport than the outer rings. The sap flow in the less active oldest part of sapwood was neither sensitive to day/night rhythm nor to water deficit during drought stress. This can be explained if one assumes that the sap in the oldest sapwood is not transported to the transpiring leaves. We did not observe any variation in water content between the active and inactive parts of sapwood, indicating that the oldest sapwood is not used as the additional water reservoir.

Appendix

Subtraction of the signal from xylem vessels and surrounding cells in the basis of correlated flow- T_2 measurements

Introduction

A crucial step in quantification of the flow and flow conducting area is to discriminate stationary and flowing water. The propagator for free, unhindered, diffusing water has a Gaussian shape, centered around $R = 0$ (Fig. 4.7a). The root mean square displacement of diffusing protons, observed by NMR, is proportional to the root of Δ times D , and is directly related to the width of the Gaussian distribution (Fig. 4.7a). In contrast, the mean displacement R of flowing protons is linearly proportional to Δ times v_{av} , the average flow velocity of the flowing protons. The fact that the propagator for stationary water is symmetric around zero is used to separate stationary from flowing water. The signal in the non-flow direction is mirrored around zero displacement and subtracted from the signal in the flow direction, to produce the displacement distribution of the flowing and the stationary water (Fig. 4.7b). Doing so the probability (amplitude) of the propagator of flowing water at $R = 0$ is zero. For laminar flow in small capillaries ($r < 100 \mu\text{m}$) at the actual values of Δ this is a correct assumption (Tallarek *et al.*, 2000) (Fig. 4.7b). At increasing Δ diffusion averaging results in a shift of the lower velocities (or stationary water at the wall) towards higher velocities.

Here we will discuss the method which allows us to distinguish water in xylem vessels and in the surrounding tissues on the basis of its differences in T_2 relaxation for a better discrimination of stationary and flowing water.

Materials and methods

T_2 relaxation measurement

T_2 maps were measured using the MSE pulse sequence (Van As, 2007), $\text{TR} = 3000$ ms, $\text{TE} = 5$ ms. A 128×128 matrix was used, $\text{FOV} = 21.5 \times 21.5$ mm, slice thickness

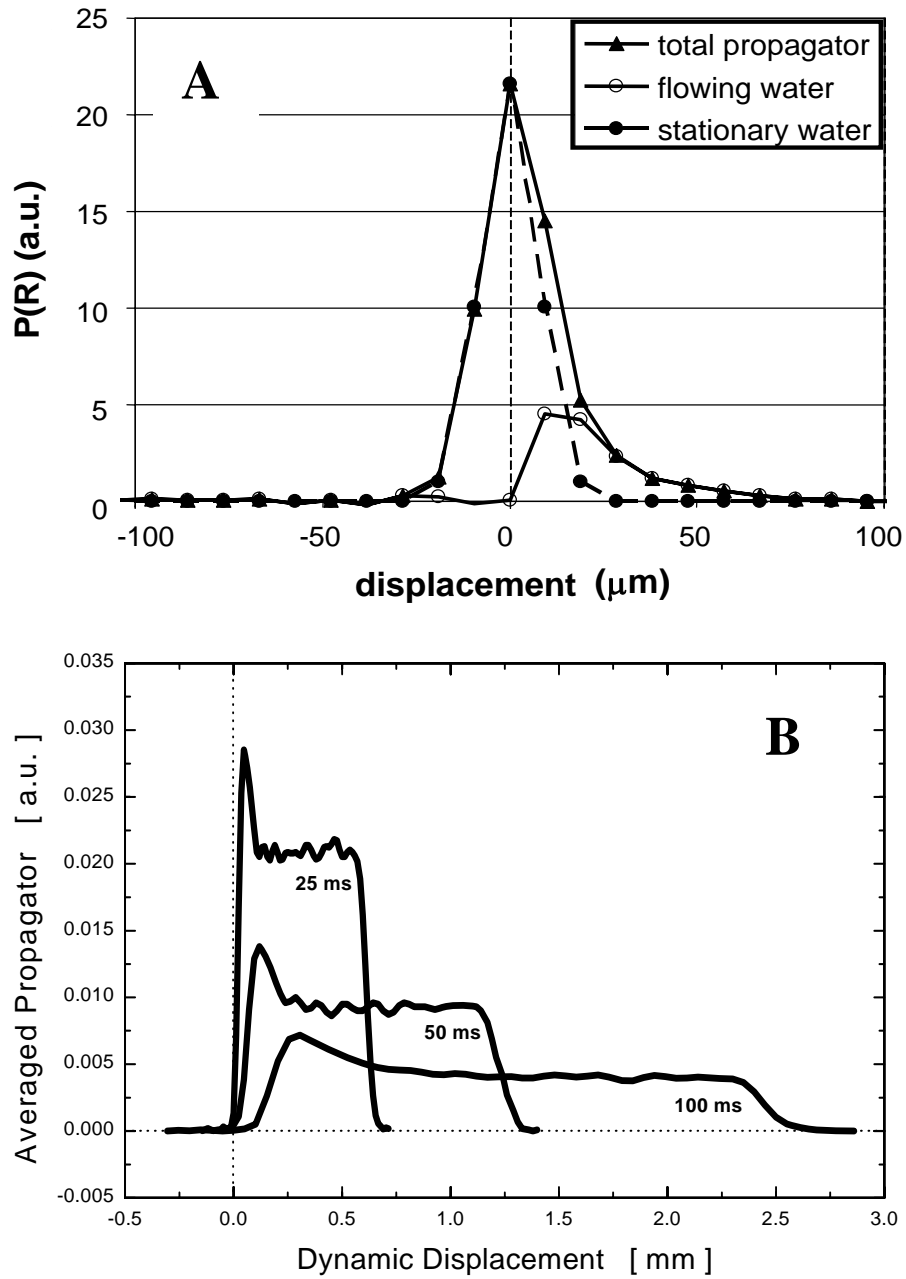


Figure 4.7 : (A) Total propagator and the propagators of flowing and non-flowing water deduced from it in the xylem region in the stem of a plant. (B) Propagator of laminar flow in a capillary of $100\ \mu\text{m}$ radius as a function of Δ (Van As et al., 2009).

3 mm. 128 echoes were acquired per echo train. For each image two acquisitions were averaged to improve the signal to noise ratio.

Correlated flow- T_2 measurement

Flow- T_2 correlated measurements were done using the PFG-STE-MSE sequence as described elsewhere (Windt *et al.*, 2006). The following experimental parameters were used. Field of view (FOV) 15.5×15.5 mm, slice thickness 5 mm, matrix size 128×128 . Flow encoding settings: flow encoding time $\Delta = 30, 40, 60$ and 100 ms, PFG duration $\delta = 4$ ms, 32 PFG steps, $\text{PFG}_{\max} = 0.486$ T/m. For T_2 echo train detection 48 echoes were acquired, first echo time (TE1) 12.7 ms, echo time (TE) 6 ms, repetition time (TR) 1500 ms. All MRI measurements were performed with a spectral bandwidth of 50 kHz.

Data analysis

The signal in all pixels with xylem (either selected on base of anatomy (T_2) or flow) was summed up to improve signal-to-noise ratio.

The curves of T_2 relaxation measurements were fitted with a bi-exponential function of the form

$$M(n) = M_1(0) e^{-(TE1+(n-1)TE)/T_{2,1}} + M_2(0) e^{-(TE1+(n-1)TE)/T_{2,2}}. \quad (4.1)$$

Here $M(n)$ is the amplitude of the echo number n ; $M_1(0)$ and $M_2(0)$ are the initial amplitudes; $T_{2,1}$ and $T_{2,2}$ are T_2 relaxation times of the different components.

Fitting T_2 relaxation curves with a mono-exponential function led to χ^2 values higher than those obtained from a bi-exponential fit. A tri-exponential fit did not result in significant decrease of χ^2 values as compared to the bi-exponential fit. Therefore, we chose the latter to analyze T_2 relaxation.

Results and discussion

The cross-sectional optical microscopy image of pith and xylem of the stem of *Viburnum tinus* is presented in Figure 4.8. The xylem vessels are about the same diameter with a slight tendency to decreased diameter at the end of the growing season. All vessels are generally solitary. The density of the xylem vessels is higher in the early wood and slightly decreases in the late wood. The conduits are surrounded by parenchyma cells. The rays are almost not observable.

In the diffuse-porous tree there is no significant variation in the vessel diameters. T_2 of the signal that originates from different vessels should then be about equal. The cells of other xylem tissues also have comparable size. Analysis of the T_2 attenuation curve that is obtained after summation of the signal in xylem tissue, gives us two components with relaxation times 25 ms and 100 ms, and with relative amplitudes 58% and 42%, respectively. We assume that the component with T_2 equal to 100 ms corresponds to the water in vessels. The relaxation time of 25 ms originates from

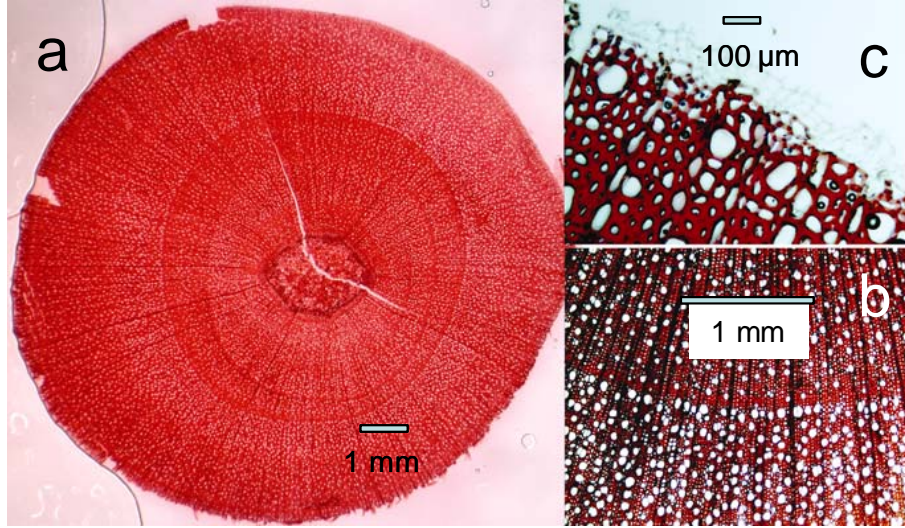


Figure 4.8 : Optical microscopic cross-sectionional images of the wood anatomy of *Viburnum tinus*: magnification 1.5 (a), 40 (b), and 100 (c).

parenchyma cells that are the smallest cells in the xylem. In order to determine to which of the two components the signal from tracheids should be related we have done the following calculations. According to Brownstein and Tarr (Brownstein and Tarr, 1977, 1979) T_2 of a cell compartment is determined by the bulk T_2 ($T_{2,bulk}$), the compartment (or cell) radius R and the rate of wall relaxation or surface sink strength density H . Assuming cylindrical symmetry the T_2 relaxation time is then given as follows (Homan *et al.*, 2007)

$$\frac{1}{T_2} = \frac{1}{T_{2,bulk}} + \frac{2H}{R}, \quad (4.2)$$

where $T_{2,bulk}$ for water at 25°C is 2 s. The calculated sink strength parameter H for xylem vessel with T_2 equal to 100 ms and the conduit radius 50 μm and less (see Fig. 4.8) is $23.8 \times 10^{-5} \text{ m s}^{-1}$. H reflects the permeability of pit membranes and the cell wall relaxation. Since the vessels and tracheids have very comparable cell wall structure and we do not expect essential differences in the permeability of pit membranes, we assume that these two types of cells have the same H . Then, T_2 of tracheids with R about 15 μm should be 31 ms. Since this value is close to the shortest measured T_2 we conclude that T_2 for parenchyma and for tracheids are comparable and the signal from these two types of cells is detected as one component with T_2 about 25 ms.

These assumptions can be tested by correlated flow- T_2 measurements (Windt, 2007). Results of correlated displacement- T_2 measurements are presented in Figure 4.9. The T_2 relaxation curve for zero displacement was fitted by a bi-exponential

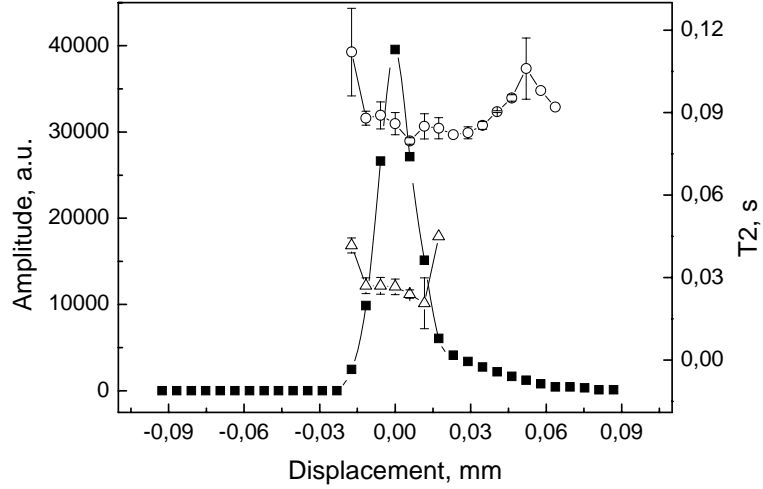


Figure 4.9 : Total propagator of signal in the xylem flow mask (■) and velocity- T_2 correlation plots (Δ and \circ) of total water within xylem. Experimental parameters: PFG-STE-MSE; resolution, 121 by 121 by 5000 μm ; spectral width 50 kHz; TE1, 12.672 ms; TE, 6 ms; TR, 1500 ms; number of echoes 48; number of averages 2; 32 PFG steps, labeling time $\Delta = 40$ ms, PFG duration $\delta = 4$ ms, $\text{PFG}_{\text{max}} = 0.486$ T/m.

decay curve. T_2 was found to be 27 and 86 ms, respectively. These values are in a good agreement with the T_2 values obtained from the T_2 measurement. Analysis of relaxation decay for three displacement steps around zero also resulted in two components whereas the relaxation curve of the signal with higher displacement could be fitted with a mono-exponential decay only, with T_2 close to 90 ms. The signal to noise ratio is getting lower and the accuracy of the fit drastically decreases when the intensity of the signal is low or the intensity of one of the component is minor. That results in significant scatter in the fitted T_2 values.

Based on the amplitudes of each T_2 component for each displacement step we constructed the T_2 resolved propagators (Fig. 4.10). The propagator of water with shorter relaxation time is symmetric around zero and clearly represents non-flowing fluid. The propagator of the fluid characterized by the longer relaxation time contains non-flowing and flowing water. From this follows that significant amount of water on xylem vessels is stagnant or very slow flowing fluid. The displacement distribution reaches its maximum at zero displacement. The amount of water in each T_2 fraction was calculated by the integration of the corresponding propagators. The amount of fluid with shorter and longer T_2 is 60% and 40%, respectively. These values are in a good agreement with the result of T_2 measurements.

The velocity distribution of liquid in xylem conduits (longest T_2 value) obtained with the labeling time of 30 ms shows a large peak centered around zero velocity

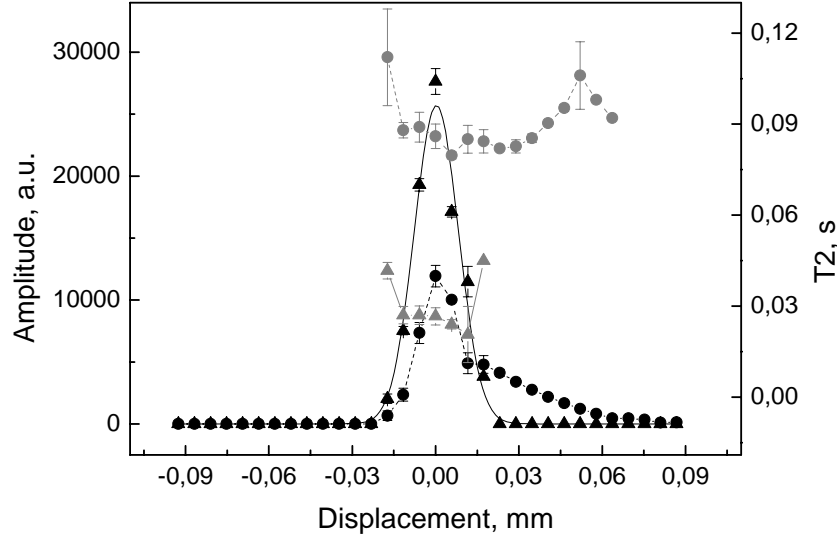


Figure 4.10 : Propagators ($-\blacktriangle-$ and $-\bullet-$) constructed on the basis of the relative amplitudes of the velocity- T_2 distribution ($--\blacktriangle--$ and $--\bullet--$) for the component with shorter (triangles) and longer (circles) relaxation times.

(Fig. 4.10). Such a shape of the propagator points out a significant amount of stagnant or very slow flowing water. It is well known that larger xylem vessels contribute substantially more to the total conductivity than smaller vessels (Ellmore and Ewers, 1986, Steppe and Lemeur, 2007). The comparison between the conduit lumen cross-sectional area as observed by optical microscopy and flow conducting area calculated based on MRI flow measurements for pine, castor bean, grape and tomato shows that only part of the total xylem lumen cross-sectional area (from 86% to 31%) was involved in the water conductance (Windt, 2007). This means that the signal from non-functional conduits is detected as diffusing fluid and gives a peak at zero displacement. At the same time, the total propagator of flowing water in the vessels is not rectangular, due to the spread in diameters of the xylem vessels. The microscopic image of the cross-section of the stem shows that there is small deviation in vessels diameter. The hydraulic resistivity of a xylem conduit is the sum of the lumen and end wall resistivity. Lumen resistivity is a function of the inner vessel diameter and can be quantified by the Hagen-Poiseuille law. According to this law lumen resistivity is proportional to $1/d^4$, where d is inner conduit diameter. That means that even a small difference in the vessel diameters leads to a significant difference of its resistance and, as a consequence, substantial differences in the flow velocities. The end wall resistivity is a function of the conduits length and the flow resistance through the end walls. It was found (Sperry *et al.*, 2005) that the length of the conduits is proportional to the conduits d^2 and the wall resistance is

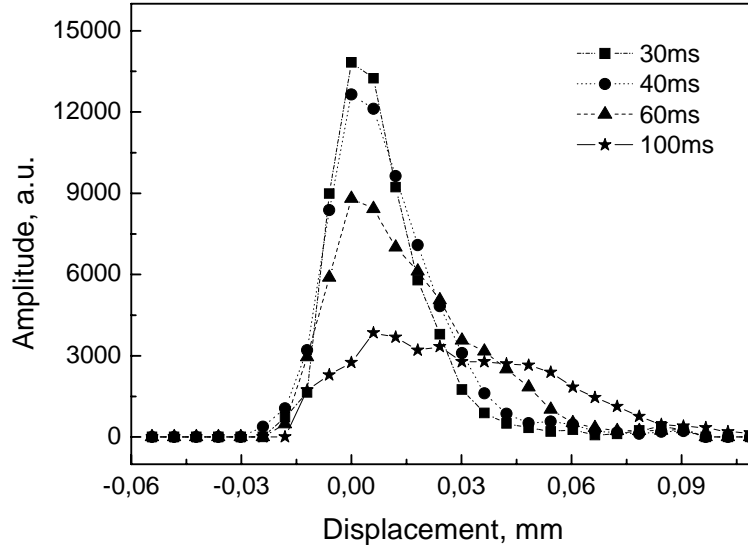


Figure 4.11 : Propagators of water with the longest T_2 relaxation time (around 100 ms), as a function of labeling time 30 ms (■), 40 ms (●), 60 ms (▲) and 100 ms (★).

inversely proportional to vessel length. This all shows that small even variations in vessel diameter results in considerable differences in flow velocity and makes the flow distribution with lower velocity more probable.

To answer the question if part of the water in the vessels is really non-flowing or flows at a very low velocity, we repeated correlated flow- T_2 measurements with increasing flow labeling time (Fig. 4.11). The shape of the propagator obtained from the measurement with labeling time 30 ms has a maximum at zero displacement. At longer labeling times the area under this peak decreased and the shape of the propagator became elongated toward longer displacements. All fluid molecules participate simultaneously in two types of motion, which are random diffusion motion and flow motion. Based on the diffusion coefficient of bulk water ($2 \cdot 10^{-9} \text{ m}^2/\text{s}$) the diffusion displacement during the shortest observation time 30 ms is $11 \mu\text{m}$. The average flow displacement calculated from the propagator for the same Δ is $7 \mu\text{m}$. Thus, at short observation time the diffusion displacement is comparable or even exceeds the flow displacement for the water molecules with low flow rate. For longer times the flow displacement prevails over the diffusive motion, the shape of propagator becomes more elongated. All xylem conduits in diffuse-porous trees are solitary and a direct vessel-vessel water exchange between them is therefore impossible. So the decrease of signal at zero displacement at longer Δ and the increase of displacements of the flowing part of the propagators indicate that a significant part, but not all, of the xylem vessels participates in long-distance water transport. Due to a relatively slow

flow velocity this water can not be properly discriminated from non-flowing fluid when Δ is short. In the presence of a large signal from non-flowing water in cell surrounding the xylem vessels (total propagator) the discrimination of stationary and flowing water becomes based on the total propagator is less accurate. T_2 -resolved propagators clearly improves the discrimination, on the cost of measurement time.

References

- Andrade J.L., Meinzer F.C., Holbrook N.M., Cavelier J., Jackdon P. (1998) Stem water storage and diurnal patterns of water use in tropical forest canopy trees. *Plant, Cell and Environment*, **21**, 397-406.
- Brough D.W., Jones H.G., Grace J. (1986) Diurnal changes in water content of the stem of apple trees, as influenced by irrigation. *Plant, Cell and Environment*, **9**, 1-7.
- Brownstein K.R., Tarr C.E. (1977) Spin-lattice relaxation if a system governed by diffusion. *Journal of Magnetic Resonance*, **26**, 17-24.
- Brownstein K.R., Tarr C.E. (1979) Importance of classical diffusion in NMR studies of water in biological cells. *Physical Review A*, **19**, 2446-2453.
- Buckley T.N. The control of stomata by water balance. *New Phytologist*, 2005, **168**, 275-291.
- Čermak J., Kučera J., Bauerle W.L., Phillips N., Hinkley T.M. (2007) Tree water storage and its diurnal dynamics related to sap flow and changes in stem volume in old-growth Douglas-fir trees. *Tree Physiology*, **27**, 181-198.
- Dye P., Olbricht B.W., Poulter A.G. (1991) The influence of growth rings in *Pinus patula* on heat pulse velocity and sap flow measurement. *Journal of Experimental Botany*, **42**, 867-870.
- Ellmore, G.S., Ewers, F.W. (1986) Fluid flow in the outermost xylem increment of a ring-porous tree, *Ulmus-Americana*. *American Journal of Botany*, **73**, 1771-1774.
- Goldstein G., Andrade F.C., Meinzer N.M., Holbrook J. Calier J., Jackson P., Celis A. (1998) Stem water storage and diurnal patterns of water use in tropical forest canopy trees. *Plant, Cell and Environment*, **21**, 397-406.
- Granier A., Biron P., Lemoine D. (2000) Water balance, transpiration and canopy conductance in two beech stands. *Agricultural and Forest Meteorology*, **100**, 291-308.

- Hinckley T.M., Bruckerhoff D.N. (1975) The effects of drought on water relation and stem shrinkage of *Quercus alba*. *Canadian Journal of Botany*, **53**, 62-72.
- Holbrook N.M. (1995) Stem water storage. In: Gartner B.L. (Ed.), *Plant stems: physiological and functional morphology*. Academic Press, San Diego, 151-174.
- Homan N.M., Windt C.W., Vergeldt F.J., Gerkema E., Van As H. (2007) 0.7 and 3 T MRI and sap flow in intact trees: xylem and phloem in action. *Applied Magnetic Resonance*, **32**, 157-170.
- Jimenes S.M., Nadezhkina N., Čermak J., Morales D. (2000) Radial variation in sap flow in five laurel forest tree species in Tenerife, Canary Islands. *Tree Physiology*, **20**, 1149-1156.
- Meinzer F.C., James S.A., G., Woodruff D. (2003) Whole-tree water transport scales with sapwood capacitance in tropical forest canopy trees. *Plant, Cell and Environment*, **26**, 1147-1155.
- Molz F.J., Klepper B. (1973) On the mechanism of water-stress-induced stem deformation. *Agronomic Journal*, **65**, 304-306.
- Phillips N., Oren R., Zimmerman R. (1996) Radial patterns of xylem sap flow in non-, diffuse- and ring-porous tree species. *Plant, Cell and Environment*, **19**, 983-990.
- Phillips N.A., Ryan M.G., Bond B.J., McDowell N.G., Hinckley T.M., Čermak J. (2003) Reliance on stored water increases with tree size in three species in the Pacific Northwest. *Tree Physiology*, **23**, 237-245.
- Salleo S., Lo Gullo M.A., De Paoli D., Zippo M. (1996) Xylem recovery from cavitation-induced embolism in young plants of *Laurus nobilis*: a possible mechanism, *New Phytologist*, **132**, 47-56.
- Salleo S., Nardini A., Pitt F., Lo Gullo M.A. (2000) Xylem cavitation and hydraulic control of stomatal conductance in Laurel (*Laurus nobilis* L.). *Plant, Cell and Environment*, **23**, 71-79.
- Salleo S., Lo Gullo M.A., Raimondo F., Nardini A. (2001) Vulnerability to cavitation of leaf minor veins: any impact on leaf gas exchange? *Plant, Cell and Environment*, **24**, 851-859.
- Scheenen T.W.J., van Dusschoten D., de Jager P.A., Van As H. (2000) Quantification of water transport in plants with NMR imaging. *Journal of Experimental Botany*, **51**, 1751-1759.

Sperry J.S., Nichols K.L., Sullivan J.E.M., Eastlack S.E. (1994) Xylem embolism in ring-porous, diffuse-porous, and coniferous trees of northern Utah and interior Alaska. *Ecology*, **75**, 1736-1752.

Sperry J.S., Hacke U.J., Wheeler J.K. (2005) Comparative analysis of end wall resistivity in xylem conduits. *Plant, Cell and Environment*, **28**, 456-465.

Stapf S., Han S.-I. (2005) *NMR imaging in chemical engineering*. Wiley, Weinheim.

Steppe K., Lemeur R. (2007) Effect of ring-porous and diffuse-porous stem wood anatomy on the hydraulic parameters used in water flow and storage model. *Tree Physiology*, **27**, 43-52.

Tallarek U., Rapp E., Scheenen T., Bayer E., Van As H. (2000) Electroosmotic and pressure-driven flow in open and packed capillaries: velocity distribution fluid dispersion. *Analytical Chemistry*, **72**, 2292-2301.

Tardieu F. (2003) Virtual plants: modeling as a tool for the genomics of tolerance to water deficit. *Trends in Plant Science*, **8**, 9-14.

Tyree M.T., Yang S. (1990) Water-storage capacity of *Thuja*, *Tsuga* and *Acer* stem measured by dehydration isotherms: the contribution of capillary water and cavitation. *Planta*, **182**, 420-426.

Van As H., Reinders J.A.E., de Jager P.A., van de Sander P.A.C.M., Schaafsma T.J. (1994) *In situ* plant water balance studies using a portable NMR spectrometer. *Journal of Experimental Botany*, **45**, 61-67.

Van As H. (2007) Intact plant MRI for the study of cell water relations, membrane permeability, cell-to-cell and long distance water transport. *Journal of Experimental Botany*, **58**, 743-756.

Van As H., Homan N., Vergeldt F.J., Windt C.W. (2009) MRI of water transport in the soil-plant-atmosphere continuum. *Magnetic resonance microscopy: spatially resolved NMR techniques and applications*. Ed. S. Codd, J.D. Seymour. Wiley-VCH, 566 p.

Van der Toorn A., Zemah H., Van As H., Bendel P., Kamenetsky R. (2000) Developmental changes and ware status in tulip bulbs during storage: Visualization by NMR imaging. *Journal of Experimental Botany*, **51**, 1277-1287.

Waring R.H., Running S.W. (1978) Sap wood water storage: its contribution to transpiration and effect upon water conductance through the stem of old growth Douglas-fir. *Plant, Cell and Environment*, **1**, 131-140.

- Windt C.W., Vergeldt F.J., De Jager P.A., Van As H. (2006) MRI of long-distance water transport: a comparison of the phloem and xylem flow characteristics and dynamics in poplar, castor bean, tomato and tobacco. *Plant Cell and Environment*, **29**, 1715-1729.
- Windt C.W. (2007) *Nuclear magnetic resonance imaging of sap flow in plants*. PhD Thesis, Wageningen.
- Windt C.W., Fergeldt F.J., Van As H. (2007) Correlated displacement- T_2 MRI by means of a Pulsed Field Gradient-Multi Spin Echo method. *Journal of Magnetic Resonance*, **185**, 230-239.
- Wulschleger S.D., King A.W. (2000) Radial variation in sap velocity as a function of stem diameter and sapwood thickness in yellow-poplar trees. *Tree Physiology*, **20**, 511-518.
- Yordanov I., Velikanov V., Tsonev T. (2000) Plant responses to drought, acclimation, and stress tolerance. *Photosynthetica*, **38**, 171-186.
- Zimmermann M.N. (1983) *Xylem structure and ascent of sap*. Springer, Berlin Heidelberg New York.
- Zweifel R., Item H., Häsler R. (2000) Stem radius changes and their relation to stored water in stem of young Norway spruce trees. *Trees*, **15**, 50-57.
- Zweifel R., Häsler R. (2001a) Dynamic of water storage in mature, subalpine *Picea abies*: temporal and spatial patterns of change in stem radius. *Tree Physiology*, **21**, 561-569.
- Zweifel R., Item H., Häsler R. (2001b) Link between diurnal stem radius changes and tree water relations. *Tree Physiology*, **21**, 869-877.

Chapter 5

Cavitation in ring-porous xylem: magnetic resonance imaging exposes potential artifacts in vulnerability curve measurements

Non-destructive measurements of cavitation were made with Magnetic Resonance Imaging (MRI) methods to test whether large earlywood vessels of ring-porous xylem are as vulnerable as some standard methods have suggested. Potted, 3-4 year old *Quercus robur* L. trees were droughted to water potentials measured with temperature-corrected stem psychrometers. Imaging of (vessel) water content indicated that earlywood cavitation in trunks was not detectable until water potentials dropped below -3 MPa. Most earlywood vessels were cavitated below -4 MPa. Dye perfusions through excised branch segments gave comparable results. Imaging of flow conducting area (FCA) indicated a gradual decline in trunk water conduction that was not solely associated with cavitation, but probably resulted from stomatal closure and too low velocities to be discriminated from non-flowing water. Dye perfusions and FCA indicated a significant portion of earlywood vessels were non-conducting even at the most favorable water potentials. No refilling of embolized vessels was detected in rewatering experiments. Contradictory to the MRI results, standard centrifuge and air-injection methods on *Q. robur* stem segments indicated complete cavitation at xylem pressures at or below -1 MPa. An artifact in these destructive methods was revealed by experiments on the related species *Q. gambelii* Nutt. When earlywood vessels became air-filled during collection prior to being refilled in the lab, they became much more vulnerable to cavitation. Residual bubbles left behind in the refilled vessels may be responsible. These results suggest revised protocols for measuring vulnerability curves by destructive methods.¹

¹This Chapter is based on: Sperry J.S., Homan N.M., Smith D.S., Christman M., Van As H. Cavitation in ring-porous xylem: magnetic resonance imaging exposes potential artifacts in vulnerable curve measurements.

5.1 Introduction

How vulnerable are the large early-wood vessels of ring-porous trees to cavitation by water stress? There is debate on the question, and the answer depends on the validity of various methods for measuring cavitation. Some studies suggest that these large vessels are quite vulnerable, cavitating significantly at normal mid-day sap pressures (Hacke *et al.*, 2006). Other results point to the difficulties of reliably measuring cavitation pressure in large vessels, particularly when many of these vessels must be cut open during the measurement process (Cochard *et al.*, 2005). Here, we use the non-destructive method of magnetic resonance imaging (MRI) to address the question a ring-porous oak species, *Quercus robur*.

Most measures of cavitation are destructive and require excision of plant parts. An exception is acoustic detection, but it suffers from the difficulty of separating the sound of cavitating xylem conduits from other noises (Tyree and Sperry, 1989). The simplest destructive method is the "native embolism" technique, and it is arguably the least prone to artifact (Sperry *et al.*, 1988). Branches are cut from the plant in such a way as to prevent air from getting into the severed xylem conduits, and the conducting capacity of the branch is assessed either by perfusing a dye or measuring the hydraulic conductivity. Precautions are taken to avoid re-filling any naturally embolized vessels during these procedures.

Recent work on a ring-porous oak (*Quercus gambelii*) and ash (*Fraxinus pennsylvanica*) found that native embolism was extensive at mid-day, with dye perfusions or conductivity measurements indicating over 50% of the current year's earlywood being non-conducting (Li *et al.*, 2008, Taneda and Sperry, 2008). These results were statistically consistent with the extensive cavitation predicted from "vulnerability curves." Vulnerability curves measure the loss of hydraulic conductivity as a function of negative sap pressure. The conclusion from this work is that at least some large ring-porous vessels are quite vulnerable, with many of them cavitating at typical mid-day xylem pressures. Native embolism in *Q. gambelii* was less extensive at pre-dawn, which suggested that some of these cavitated earlywood vessels were able to refill (Taneda and Sperry, 2008). Other studies, however, report lower levels of native embolism in twigs from four other ring-porous oak species: on the order of 10 to 50% depending on degree of water stress (Cochard *et al.*, 1992a).

The accuracy of vulnerability curves has been questioned for ring-porous species where vessels can be so large as to run through half or more of the stem segment. The criticism comes from clearly anomalous vulnerability data using a recently developed "flow-centrifugation" method on a ring-porous *Fraxinus* species (Cochard *et al.*, 2005). In this technique, water flows through the stems while they are spinning in a custom centrifuge rotor. The spinning creates a minimum negative pressure in the stem center, and the hydraulic conductivity is measured while the stems are spinning. Microbubbles or other impurities in the perfusing solution could be swept into the center of the stem and prematurely nucleate cavitation in long-vesseled material. In short-vesseled diffuse-porous material or tracheid-bearing conifers, pit membranes would exclude such nucleators from penetrating very far into the spinning stem.

However, in one of the studies cited previously (Li *et al.*, 2008), the flow-centri-

fugation method compared favorably with other methods, even for a sampling of three ring-porous species. In the older "static-centrifugation" method, there is no sustained flow through the stems during spinning, and stems are removed from the rotor to make conductivity measurements on a gravity-feed apparatus. In the even older "air-injection" method, stems were sealed in a double-ended pressure chamber with both ends protruding to allow the measurement of conductivity by gravity-feed. The air pressure in the chamber is raised in steps, until the conductivity falls to near zero. The correspondence between the three vulnerability curve methodologies in three ring-porous species suggests that either all are accurate, or all suffer from the same artifact. Their accuracy is supported by their agreement with native embolism. The air-injection results also argue against an artifact because the sap is never under any negative pressure in this technique: the embolism is thought to result from air being forced into the vessel network. Correspondence between embolism caused by air-injection and cavitation caused by negative pressure is evidence for cavitation being caused by gas-phase air entry into the xylem vessels (Cochard *et al.*, 1992b, Sperry *et al.*, 1996).

Nevertheless, it is difficult to accept without further proof that early-wood vessels are so vulnerable that many of them cavitate at typical mid-day water potentials. MRI as a cavitation-detection method is promising because it is non-destructive and yet can potentially localize embolized vessels (Van As, 2007, Van As and Windt, 2008). The technology can detect embolized vs. water-filled vessels as long as the pixel dimension is similar to or smaller than the vessel diameter. MRI has been used to detect cavitation in drying plants, as well as refilling of embolized vessels after rewatering (Clearwater and Clark, 2003, Scheenen *et al.*, 2007). The technology has also been used to detect flowing water in xylem vessels and phloem sieve tubes at sub-pixel resolution (Scheenen *et al.*, 2000, Windt *et al.*, 2006).

In this paper, we paired MRI with non-destructive and continuous measurements of water potential to construct the first *in situ* vulnerability curves of intact plants. MRI vulnerability curves should be free of any artifacts that might plague standard destructive methods. We imaged the early-wood vessels of a ring-porous oak, *Quercus robur*, for comparison with native embolism measured by dye perfusion, and with vulnerability curves using the static-centrifugation method and the air-injection method. In addition to imaging trees during a dry-down phase, we also imaged after re-watering to look for refilling of earlywood vessels.

5.2 Materials and methods

5.2.1 Plant Material

Quercus robur L. plants 3-4 years old were obtained from a nursery (Bomenland Schiphorst bv, Bennekom, NL) and kept well-watered prior to MRI imaging. Imaging experiments took place at the Wageningen NMR Centre of Wageningen University (The Netherlands). The treelets were about 2 m tall with trunks between 1.5 and 2.5 cm wide at the base. They were rooted in 5 liter pots. Ring-porous anatomy in the

trunk was well established by the third year. The basal 60-80 cm of the trunks were relatively free of major side-branches which made them easy to insert into the MRI apparatus. Tree water status was controlled by reducing or withholding water, and spot checks of xylem pressure were made on branchlets using a pressure chamber.

5.2.2 Single-pressure protocol

A tree was inserted into the MRI and one "intact" water content image was taken. For most trees, we also imaged the flow-conducting area. Water potential was measured every 5 minutes during imaging with 1-3 stem psychrometers (see below). The imaged trunk section was cut from the tree in a 1.5 cm long piece and air was gently blown through at ca. 50 kPa for 2-5 minutes to empty all the earlywood vessels. The piece was re-imaged to obtain an "empty" control image. Finally, the same piece was flushed with deionized water to refill the earlywood vessels. The piece was imaged a third time to obtain a "filled" control image. By experience, we learned that complete refilling required at least 20 minutes of flushing the stem piece while it was underwater to thoroughly saturate the tissues. Both stem surfaces were coated with silicone vacuum grease to hold the water in the vessels and prevent dehydration during imaging. Four trees at various water potentials from -0.65 to -3.2 MPa were imaged in this way.

5.2.3 Drydown protocol

A tree at a relatively high water potential was inserted in the MRI, fitted with 3 psychrometers, and water was withheld. Water content and flow images were sampled roughly every hour as the tree dehydrated over a period of days until significant cavitation was detected. Water potentials were measured every 5 minutes. Four trees were imaged in this way. Two were re-watered after cavitating and imaged until water potentials returned to near zero.

5.2.4 MRI procedures

All trees except one were imaged using a 0.7 Tesla electromagnet with parallel magnetic field gradient plates for convenient installation of intact trees (Windt *et al.*, 2006). Cross-sectional MRI images were obtained of the trunk at ca. 40-50 cm above the pot surface. At this point, the trunk was between 1.4 and 1.8 cm in diameter. In a few trees a small side branch or two had to be removed near the imaging point. A reference tube of agarose gel representing 100% (v/v) water content was fixed vertically next to the stem, and a 9-turn RF coil of about 5 cm length was centered around the imaging region. A copper foil shield enclosed the coil, and the trunk was positioned between the two flat poles of the magnet of the MRI apparatus. The gap between the poles was ca. 10 cm wide. The pot sat below the magnets, and the crown of the treelet was fully exposed above them. During some drydown experiments, supplemental halogen lighting was used in conjunction with a fan to enhance

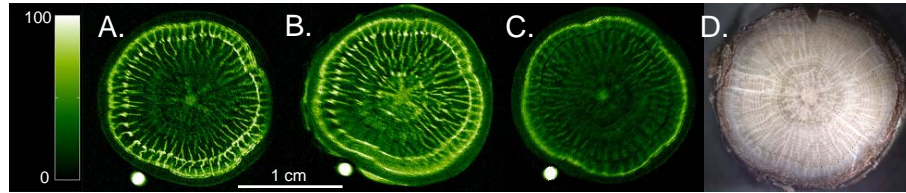


Figure 5.1 : A. MRI water content image of intact *Quercus robur* trunk at -0.65 MPa. B. Same trunk section flushed to fill all earlywood vessels with water. C. Same trunk with earlywood vessels emptied by air injection. D. Cross section of the same trunk at image position. Color scale at left is percentage water content relative to the agarose gel reference tube (imaged in cross section).

dehydration. After centering the tree within the magnetic field, imaging was initiated. Imaging resolution was set at 256×256 pixels at a field of view ranging from 21.5 to 19 mm on a side. Pixel dimensions ranged from 74 to 84 microns on a side. Cross-sectional images were taken with a slice thickness of typically 3 mm, and the MRI information is averaged over this thickness.

One tree for the drydown protocol was imaged in a 3 Tesla MRI system with a 50 cm vertical bore cryo-magnet (Homan *et al.*, 2007) over a period of 13 days (including a 3 day re-watering period). The tree with reference tubes and 4 cm RF coil was positioned within the magnet. The crown emerged from the top of the cylindrical magnet and continuous supplemental halogen lighting was eventually used to speed dehydration. The resolution used in this machine was 512×512 , which at the field of view of 24×24 mm yielded a pixel dimension of 47 microns on a side. Cross sectional images were averaged over 3 mm thickness.

5.2.5 Water content imaging and analysis

Water content maps (proton density per pixel) were obtained by the Multi-Spin-Echo sequence (Van As, 2007). Experimental details: first echo time 9.6 ms, inter echo time $TE = 6.8$ ms, number of echoes 64, $TR = 2$ s, number of averages 4. We restricted analysis of water content to the earlywood vessels because their average dimension (grand mean diameter: $70 \pm 9 \mu\text{m}$, $n = 8$ trees) was similar to the maximum pixel dimension of 74-84 μm in the 0.7 Tesla machine. Earlywood was defined as the ring of large vessels at the inner boundary (towards stem center) of the current year's growth ring (e.g., Fig. 5.1).

To identify pixels containing water-filled earlywood vessels, we examined T_2 images at progressively longer relaxation times. Bulk water held in large spaces retains a stronger signal for longer relaxation time than water bound in cell walls and protoplasm (Windt *et al.*, 2007). Signals with T_2 values longer than 80 and 100 ms relaxation time were used to locate pixels that included earlywood vessels. Selected earlywood pixels composed the image "mask," the pixels that were sampled for their

water content in the water content map. Mask pixel water content was calculated relative to the average water content signal of pixels within the reference tube. We assumed that the percent water content of the mask pixel equaled the percent of the pixel area occupied by a water-filled vessel. This represents a deliberate over-estimation of vessel area because many pixels will also include tissue surrounding the vessel. This tissue has a lower water content than the filled vessel and we do not expect significant variation of water content in these cells (Chapter 4). This estimate of the filled vessel area per pixel was added up across the entire mask to yield the total area of filled vessels, also referred to as the "mask area."

In the "drydown" protocol, the mask was selected from the initial MRI image at the beginning of the dry down when the tree was at relatively high water potential. The same mask was applied to successive images, which assumes a minimal shift in sample orientation within the magnet. The mask area for each water content image was expressed relative to the initial mask area. In the "single-pressure" protocol, separate masks had to be selected for the "intact," "filled," and "empty" images because sample orientation changed for each image. The mask area of the "intact" image was expressed relative to the mask area of the "filled" image. The necessity of selecting separate masks made the single-pressure protocol less precise than the dry-down method.

5.2.6 Imaging and analysis of xylem flow

We also used the presence of detectable bulk water flow as an indicator of water conduction in the same trees imaged for water content. We used the q-space or propagator method to resolve flow conducting area (FCA) at the sub-pixel level and to calculate volume flow rate (PFG-SE-TSE sequence, see e.g. Van As *et al.*, 2009). Experimental details: inter echo time TE 4.2 ms, TR = 1.5 s, turbo factor 8, gradient steps 32, $\delta = 4$ ms, $\Delta = 30$ ms, $G_{\max} = 0.49$ T/m, number of averages 2. Importantly, the absence of water conduction in a vessel does not necessarily mean that the vessel is embolized because it could be filled with stationary water (Scheenen *et al.*, 2007). The signal was calculated over a 3 mm axial distance, and the absolute value of the FCA is influenced by any deviation of the vessel from perfectly vertical. For a vessel of 100 μm in diameter, a 2 degree tilting of the vessel increases FCA by factor 2. The relative error increases with smaller vessel size. The FCA was measured for the earlywood pixels only, except for the tree in the 3 T MRI system, where FCA was also measured in the late-wood pixels.

For the trees imaged in the 0.7 T system by either the single-pressure or dry down method we report the maximum FCA measured. For the tree imaged in the 3 T system we report the full time course of FCA under conditions of continuous light provided by a bank of halogen bulbs suspended above the narrow crown. This tree took 8 days for its water potential to drop from near zero to below -0.5 MPa. Continuous lighting was initiated on day 6 of the dry down.

5.2.7 Water potential (Ψ) measurements

Temperature-corrected stem psychrometers (PWS Instruments, Guelph Ontario; similar devices are currently available from ICT international, Armidale, Australia) were used to make minimally-invasive measurements of stem water potential. These instruments correct for the temperature difference between stem surface and the air around the thermocouple junction that measures the wet-bulb temperature (Dixon and Tyree, 1984). Psychrometers were calibrated with NaCl solutions. They were mounted on the main trunk above the imaged section. After the tree was positioned in the MRI, a sharp razor blade was used to shave flat a 2 cm length of stem surface, just exposing the cambium. The exposed surface was wiped, and the psychrometer chamber clamped over it. Care was taken to insure that the thermocouple junction for measuring stem surface temperature was protruding from the chamber and thus would contact the stem surface. The junction between the psychrometer and exposed stem surface was sealed with silicone vacuum grease to prevent leaks, and any remaining exposed tissue was also sealed to avoid local desiccation. Psychrometers were connected to a datalogger (CR7, Campbell Scientific, Logan, UT, USA) and read every 5 minutes.

Two (four trees) or three (four trees) psychrometers were installed per tree, on different sides of the stem. Sensitivity to the magnetic and electrical fields in the vicinity of the MRI was tested in two experiments. First, by putting salt solutions of known water potentials in the psychrometer and measuring water potential as a function of proximity to the magnet. Second, after some trees were imaged, the section of trunk containing the mounted psychrometers was cut from the tree, and positioned in various ways relative to the magnet. In neither experiment did psychrometer position have a detectable effect on water potential. Accuracy of the *in situ* water potential readings was periodically checked against measurements of shoot xylem pressure with a pressure chamber. The psychrometer calibration was checked between successive installations with salt solutions. In two cases we detected anomalous readings: one was traceable to corrosion of a thermocouple junction, the other was possibly caused by a leaky seal with the stem surface.

In the single-pressure protocol, stem water potential was averaged from all psychrometers across the imaging period. For the dry-down protocol, each psychrometer was represented by a running 15 minute mean, and stem water potential was the average of the running mean across all psychrometers.

5.2.8 Dye perfusions

Fifteen of the potted *Q. robur* treelets were harvested at various stem xylem pressures ranging from -0.4 to below -4 MPa for dye perfusions of their trunks. Three shoot tips per tree were covered in foil to promote equilibration with the stem xylem pressure, and shoot xylem pressure was measured with the pressure chamber. The chamber used was only judged safe to -4 MPa. Three of the drier trees did not exude at this pressure so their xylem pressure could only be said to be below -4 MPa. Once the xylem pressure was measured, a 27 cm long section of trunk was cut from the

tree underwater. The ends were shaved smooth with a razor blade, and attached to water-filled tubing at one end. The free end was submerged in filtered 0.1% w/w safranin dye, and the dye was siphoned through the stem at 1.5 kPa of suction. This pressure is less than that required to displace an air-water meniscus from the largest vessels present (150 μm), and therefore would not cause artificial refilling of embolized vessels in the segment. Dye was perfused for at least 45 minutes, and then followed by at least 45 minutes of water. Segments were stored frozen until sectioned and photographed.

5.2.9 Centrifuge and air-injection tests

Stem segments 40-50 cm long were cut from seven *Q. robur* trees (cuts were not made underwater), wrapped in plastic bags, and transported to the University of Utah for centrifuge and air-injection experiments. Stems spent four days in transit prior to the first measurements. Segments were cut back to 27 cm long underwater and flushed with filtered (0.2 μm) 20 mM KCl solution at ca. 80 kPa for at least one hour. This flushing refilled any vessels that were embolized, but otherwise not occluded (Sperry *et al.*, 1988). After flushing, the segments' maximum conductivity was measured by dividing the flow rate through the segment by the pressure gradient generated by a ca. 1.5 kPa hydraulic head. Flow rate was measured gravimetrically on an electronic balance interfaced with a computer. An Excel Visual Basic macro was written to communicate with the balance and compute conductivity (available on request from the senior author). Conductivity was expressed per cross sectional area of the entire stem, based on the mid-section average diameter.

Some stems were then secured in a custom built centrifuge rotor (Alder *et al.*, 1997) and spun to -1 or -2 MPa for 5 minutes. Stem ends were submerged in the same KCl solution used to measure conductivity during spinning. Conductivity was re-measured after spinning (the "static" centrifugation protocol). Comparison of pre- vs. post-spinning conductivity indicated the extent of xylem cavitation caused by centrifugation. Stems were then dyed with Safranin using the same protocol described above.

Other stems were sealed in a double-ended pressure chamber (Sperry and Salendra, 1994) with both ends protruding and the center portion of the stem exposed to an elevated air pressure of 1 MPa for 20 minutes. After slow release of pressure, the stem conductivity was re-measured and stems were dyed with safranin. Embolism caused by the air-injection was quantified by comparing pre- vs. post-injection conductivity.

5.2.10 Anatomical measurements

Imaged and dyed *Q. robur* stems were cut transversely, shaved smooth with a razor blade, and the surface photographed with a digital camera (model RT KE; Diagnostic Instruments) under a stereomicroscope. A low magnification image captured the entire cross section. Multiple higher magnification images made around the complete earlywood circumference were used for measuring early-wood vessel diameters and

lumen areas. Lumen perimeters were traced, and image analysis software (ImagePro, Media Cybernetics) was used to calculate cross sectional area and equivalent circle diameter. Imaged stems were photographed as close to the MRI image plane as possible. Dyed stems were photographed at ca. 18 cm from the end of the 27 cm long segment that was submerged in dye.

5.2.11 Experiments on *Quercus gambelii*

A major discrepancy between the MRI/dye perfusion results and the centrifuge/air injection results (see Results section) for *Q. robur* was investigated in the related white oak, *Quercus gambelii* Nutt. which grows in the wild near the University of Utah. *Q. gambelii* treelets of 3-6 years of age were studied in the Red Butte Canyon Research Natural Area (40° 47' 08" N 111° 47' 31" W, 1775m) adjacent to the University of Utah. These experiments tested the effect of centrifugation with vs. without the prior exposure of vessels to air on the conductivity of test segments.

Native xylem conductivity was measured on 27 cm test segments cut from 10 trees. In some trees, the segments were cut from the rooted trees under-water using split funnels sealed around the trunk and filled with water. In other trees, the entire tree was cut near the base in the air, and then the conductivity segment was subsequently cut from the tree underwater. The conductivity segment was located at least 1.5 m from the cut base of the tree.

Native conductivity was measured in the field by attaching one end of the test segment to tubing filled with filtered 20 mM KCl solution, and measuring the volume flow rate in a graduated pipette at a pressure head of ca. 1.5 kPa. The conductivity (flow rate/pressure gradient) was expressed per total stem cross sectional area, based on the average stem diameter at the center of the test segment. Native stem xylem pressure was measured with a pressure chamber on three bagged shoot tips immediately prior to harvesting the tree. Measurements were made at midday on a clear day. The test segments were kept submerged in water and transported to the laboratory where they were subsequently spun in the centrifuge at their native stem pressure using the static centrifugation protocol. In this experiment, no additional drop in conductivity should occur after spinning because stems should not have been exposed to a negative pressure any lower than what they had just experienced in the field. Assuming accurate assessment of the native xylem pressure, only a measurement artifact would change the conductivity. Stems were then flushed to their maximum conductivity and then spun once again to their native xylem pressure and the conductivity measured.

In a subsequent experiment, we simulated the manner in which the *Q. robur* centrifuge segments were collected. We collected four 27 cm long test segments from the same *Q. gambelii* population by cutting short 40-50 cm sections from the trees in air and stored them for four days before flushing them to maximum conductivity, spinning to -1 MPa, and then measuring the post-spin conductivity (the "static" protocol).

Finally, we collected *Q. gambelii* test segments by cutting them underwater to avoid embolizing vessels, and then purposefully embolized them by blowing air through

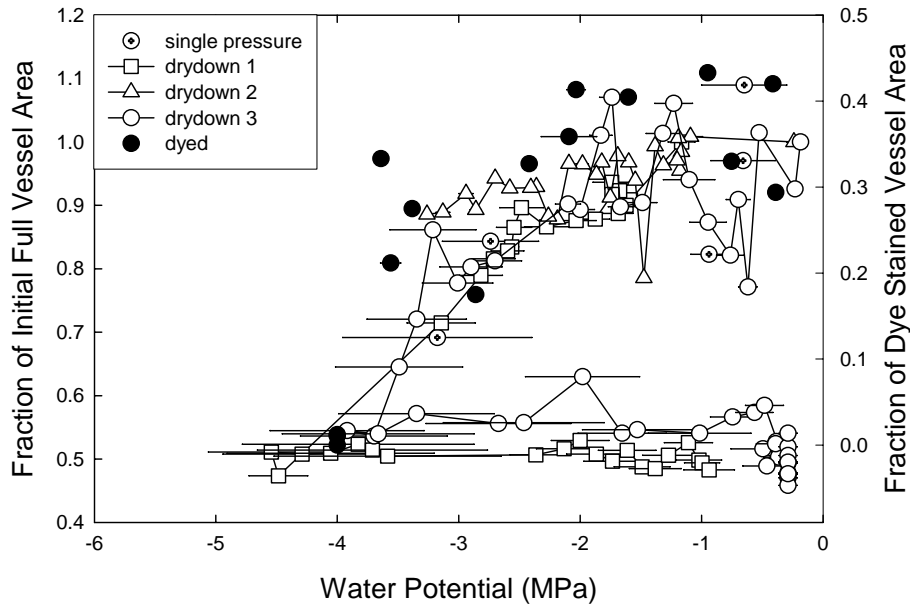


Figure 5.2 : Loss of water-filled early-wood vessel area vs. water potential. Open symbols represent MRI images of early-wood vessels expressed as a fraction of their initial water-filled area (left "y" axis). Dotted circles are separate trees measured at a single water potential ("single pressure" protocol). Other open symbols are three trees imaged as they dried down to a minimum water potential ("drydown" protocol). Two of the drydown trees were rewatered to test for refilling. Solid symbols are separate trees dried down to various water potentials, perfused with dye, and then measured for the fraction of dye-stained earlywood vessel area (right "y" axis).

the segments briefly at low (ca. 30 kPa) pressure until we could see bubbles coming from the other end. We then flushed the segments to maximum conductivity, spun to -1 MPa, and measured the post-spin conductivity.

5.3 Results

5.3.1 Water content imaging

The ring of large earlywood vessels were clearly identified by comparing "intact" images taken at given xylem pressure with the corresponding "filled," and "empty" images of the same trunk section (Fig. 5.1A-C). The intact image in Figure 5.1A, for example, was taken at a water potential of -0.65 ± 0.29 MPa (mean \pm SE) and visually, there was no obvious embolism relative to the filled image (1B). Mask areas tended to over-estimate actual vessel areas as expected due to some signal from cells

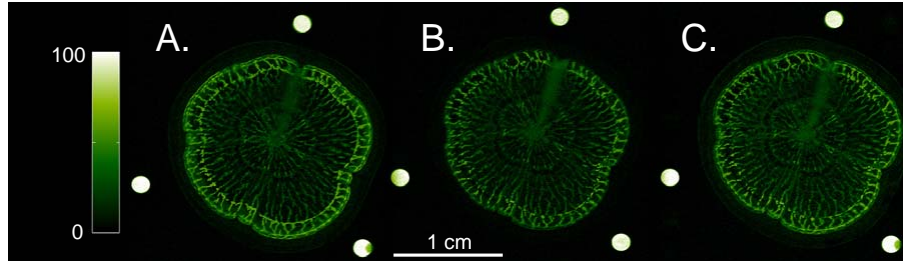


Figure 5.3 : Water content maps of drydown 3 from Fig. 5.2 (Fig. 5.2, open circles) in the 3 T MRI system. A. Initial water content at ca. -0.3 MPa. B. Water content at minimum water potential of -3.9 MPa showing extensive embolism of earlywood vessels. C. Water content of rewatered tree at ca. -0.3 MPa showing no obvious refilling of earlywood vessels.

surrounding vessels (see methods). Filled mask area for T_2 relaxation time longer than 100 ms averaged 1.8 ± 0.4 times the total area of earlywood vessels measured on the same stems. The mask area was even larger for the 80 ms relaxation, so we only report the 100 ms data which better reflects the water content of the vessels as opposed to the adjacent tissues.

For the tree imaged in Figure 5.1, the intact mask area was 8% greater than the filled mask, consistent with the qualitative impression of no significant embolism at the modest -0.65 MPa pressure. The fact that the intact mask area was greater than the filled mask area does not necessarily mean that the intact stem had less embolism than the filled stem. The 8% difference probably reflected the fact that masks had to be selected separately for each image for the single-pressure protocol. Selecting different pixels in one image from another introduced variation in mask area that was independent of a difference in embolism. This inevitability of the single-pressure protocol made it a less sensitive method for quantifying embolism. Nevertheless, when embolism was visually obvious, it was reflected by declining mask area. For example, the "empty" image (1C) showed complete embolism of the earlywood ring, and the corresponding mask area was 2% of the filled mask area. Single-pressure images taken at progressively lower water potentials indicated little significant loss of intact mask area (relative to filled mask area) until water potentials dropped below -3 MPa (Fig. 5.2, filled circles).

Progression of earlywood embolism was more easily visualized and quantified by the drydown protocol where a single tree was imaged as it dehydrated (Fig. 5.2, open symbols). In this protocol, there was only one mask, which was selected for the initial image taken at the highest water potential. Changes in filled vessel area during dehydration were based on this one mask. As for the single-pressure measurements, significant loss of mask area was not seen until pressures fell below -2.5 to -3 MPa. By -4, signal intensity had dropped to 50% of the initial value (Fig. 5.2, open symbols). Cavitation of earlywood vessels was also obvious by comparing images of

water content at the beginning of the drydown (Fig. 5.3A) with -4 MPa (Fig. 5.3B). Crisping of leaves was observed when water potentials fell below -4 MPa.

The two re-watered trees showed no significant recovery of signal intensity indicating no vessel refilling. This was despite the full recovery of stem water potential to near zero values and several hours (2 days in drydown 3) at full hydration (Fig. 5.2). Lack of refilling was also evident from the similarity between the water content images taken before (Fig. 5.3B) and after complete water potential recovery (Fig. 5.3C).

Stem water potentials tended to show more variation when trees were relatively dry, as evidenced by the larger error bars (SE) in the drier trees (Fig. 5.2). Psychrometers on different sides of the stem at similar heights could give water potentials differing by as much as 1 MPa or more. Several observations suggested that this was real variation and not measurement artifact. Checks after the experiments confirmed that psychrometer calibration had not drifted. In some cases, the trunk containing the mounted psychrometers was cut from the tree after imaging, and bagged in plastic. The variable psychrometer readings gradually converged, as expected for water potential equilibration, and the mean value was similar to pressure bomb measurements of adjacent leaf-bearing short shoots.

5.3.2 Flow conducting area and volume flow rate imaging

The FCA is resolvable at the sub-pixel scale and should be equal to or less than the measured vessel area, barring an over-estimate caused by a tilted axis (see Methods). In all but one tree the maximum earlywood FCA was less than the measured earlywood vessel area, with the maximum FCA averaging $65 \pm 10.0\%$ of the earlywood vessel area ($n = 5$). In the exceptional tree the maximum FCA was 1.94 times the measured area, suggesting a tilting artifact on the order of 2 degrees from vertical. Tilting, however, does not influence the relative change in FCA with water potential and transpiration rate.

The tree in the high resolution 3 Tesla machine took 8 days for its stem water potential to drop below -0.5 MPa. During this period of favorable water status, the volume flow rate through the trunk increased during first several days (most probably in a response to new environmental conditions) and reached its maximum on day 8. Volume flow rate fluctuated daily, presumably because of diurnal changes in stomatal conductance and transpiration rate associated with the day-night light cycle. The FCA fluctuated in step with changes in volume flow rate (data not shown). To minimize diurnal variation in FCA as the tree began to dry out, we maintained constant lighting and approximately constant temperature conditions during the remaining dry-down and re-watering period (Fig. 5.4 data for continuous light).

Roughly 80% of the total FCA in this tree was in the earlywood throughout the dry-down and re-watering cycle. The FCA was more sensitive to declining stem water potential than the filled vessel area (Fig. 5.4A, solid circles): as water potential dropped, the FCA in both early- and late-wood declined in an essentially linear manner with decreasing water potential (Fig. 5.4A, solid circles). Filled vessel area during this same time was relatively constant in the same tree (Fig. 5.2, open circles,

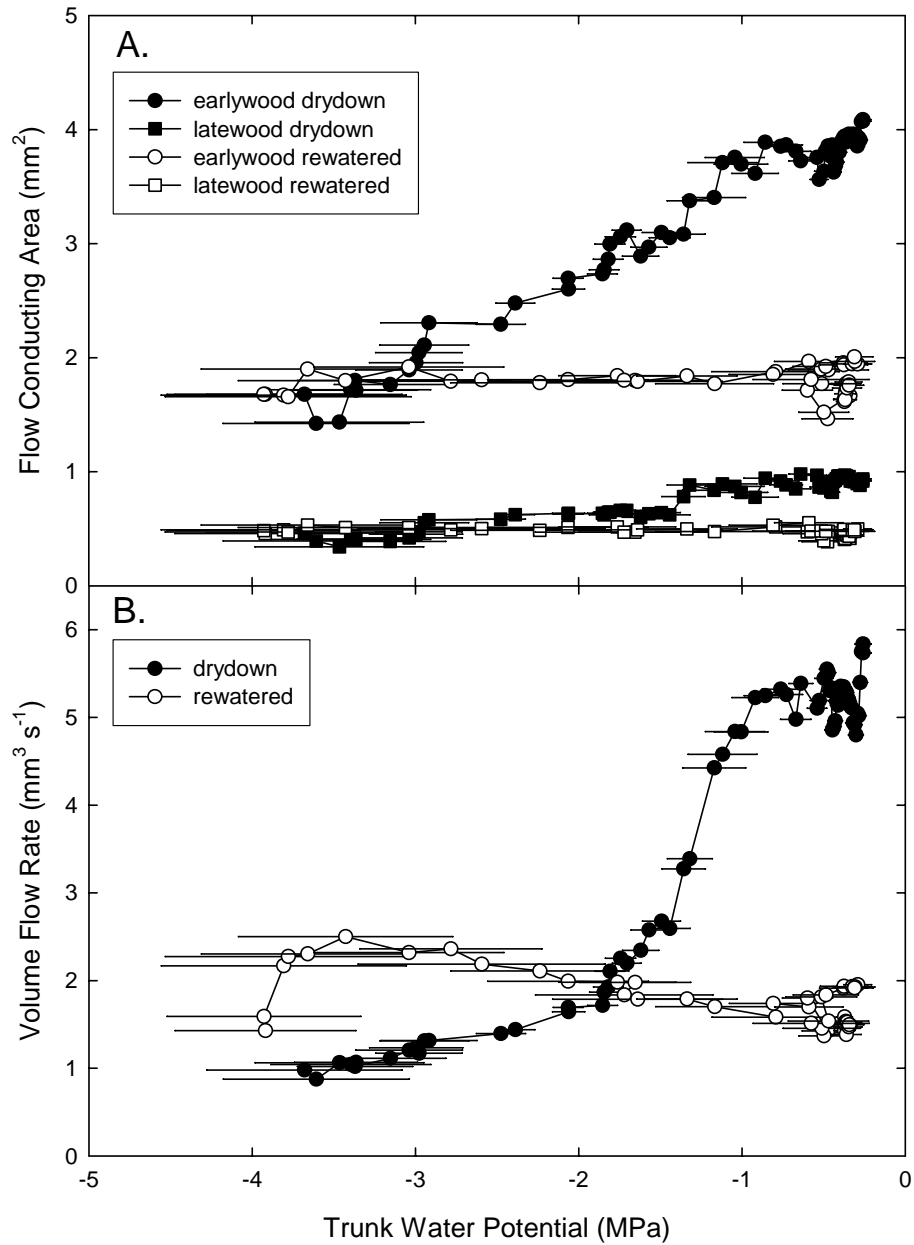


Figure 5.4 : A. Flow conducting area vs. trunk water potential for drydown 3 imaged in the 3 T MRI system (Fig. 5.2, open circles). The solid symbols are the drying phase, the open symbols after rewatering. Circles are earlywood, squares are latewood. B. Volume flow rate for the same tree.

drydown 3). The total drop in FCA over the drought was similar in magnitude to the approximately 50% drop in filled vessel area (Fig. 5.2). The earlywood FCA showed a 59% drop as water potential fell to -4 MPa, and the latewood FCA also dropped by 50% over the same interval (Fig. 5.4A, solid squares). The volume flow rate through the trunk fell by 80% during the dry-down period (Fig. 5.4B, solid circles).

After re-watering, the FCA remained essentially unchanged from its drought-induced minimum (Fig. 5.4A, open symbols). The volume flow rate doubled on re-watering, but then declined steadily as trunk water potentials rose to their pre-

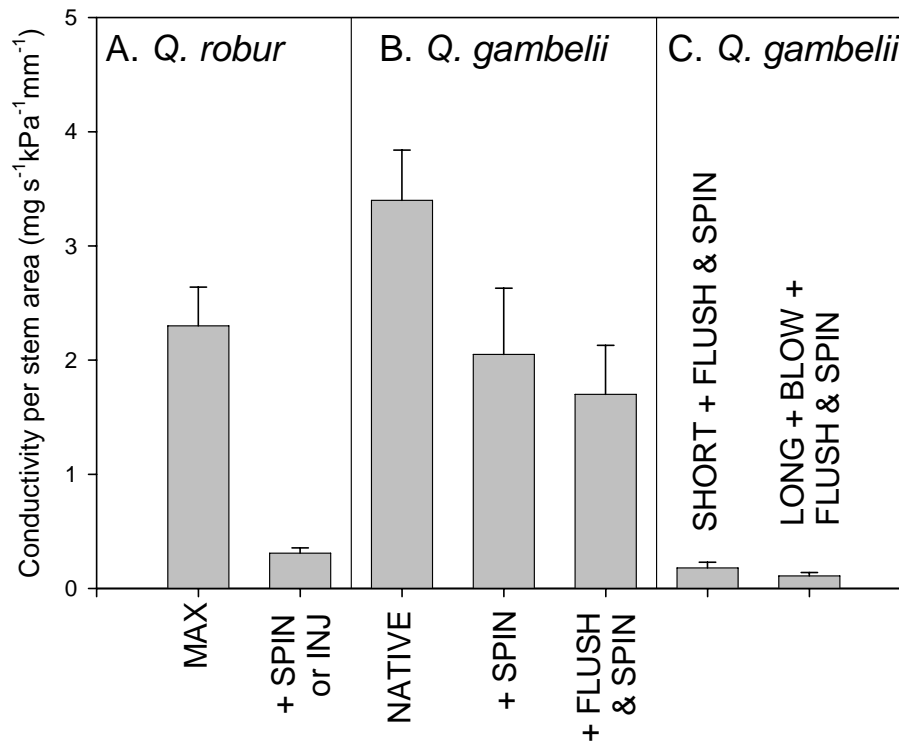


Figure 5.5 : Hydraulic conductivity of stem segments per stem cross sectional area. A. *Quercus robur* stems before (MAX, $n = 10$) and after (+SPIN or INJ) spinning in a centrifuge at -1 or -2 MPa or injection with air at 1 MPa. B. *Quercus gambelii* stems cut long at harvest to avoid causing embolism (NATIVE, $n = 10$); after spinning to the native xylem pressure (+SPIN); and after a second spin to the same pressure following a flush treatment to refill vessels (+FLUSH & SPIN). C. *Q. gambelii* stems cut short to expose earlywood vessels to air, then flushed and spun to native xylem pressure (SHORT + FLUSH & SPIN, $n = 4$); or cut long as in the "native" measurement but then blown out with air followed by a flush and spin treatment (LONG + BLOW + FLUSH & SPIN, $n = 8$).

drought value. At the conclusion of the experiment when trunk water potentials had risen to pre-drought values, volume flow rate was about 1/3 of its original level (Fig. 5.4B, open symbols).

When the soil water potential was zero at the beginning and end of the experiment, we were able to calculate the soil-to-trunk conductance ($\Delta Q = \text{trunk volume flow rate} / \text{trunk water potential}$). Conductance values were calculated for 20°C to correct for the 1.5° increase in temperature over the period (which changes viscosity and hence conductance). Soil-to-trunk conductance averaged $18.57 \pm 0.228 \text{ mm}^3 \text{ s}^{-1} \text{ MPa}^{-1}$ over the first three successive readings of the dry-down period in Fig. 5.4. At the conclusion of the re-watering period, the last three readings averaged $7.47 \pm 0.142 \text{ mm}^3 \text{ s}^{-1} \text{ MPa}^{-1}$, indicating a 60% drop in hydraulic conductance caused by the drought.

5.3.3 Dye perfusions

Dye perfusions of trunk segments cut from *Q. robur* treelets during dehydration showed a drop in dye-stained area of earlywood vessels with stem water potential (Fig. 5.2, solid symbols). Unstressed stems (-2 MPa or above) averaged $38.2 \pm 2.31\%$ of total vessel area stained. This indicated somewhat less functional earlywood than the maximum FCA which averaged $65 \pm 10.0\%$ of the earlywood vessel area. As pressures dropped from -2 to below -4, the dye stained area dropped to zero (Fig. 5.2, solid symbols). The trend paralleled the drop in filled vessel area with stem water potential (Fig. 5.2, open symbols). Because of safety concerns with the pressure chamber, we could not determine the exact water potential of the fully embolized dye stems, only that it was below -4 MPa. Nevertheless, the dye perfusions agreed with the water content imaging in indicating a significant fraction of functional earlywood down to below -3 MPa.

5.3.4 Centrifuge and air-injection of *Q. robur* trunk segments

Trunk segments transported to Utah and flushed to refill embolized vessels showed high maximum conductivity per stem cross sectional area ($2.3 \pm 0.34 \text{ mg s}^{-1} \text{ kPa}^{-1} \text{ mm}^{-1}$) and conducted dye readily (Fig. 5.5A, "max" $n = 10$). However, these stems uniformly had minimal hydraulic conductance and no dye conduction after being centrifuged to -1 MPa (conductivity = $0.41 \pm 0.047 \text{ mg s}^{-1} \text{ kPa}^{-1} \text{ mm}^{-1}$, $n = 4$) or -2 MPa (0.47 ± 0.071 , $n = 2$), or air-injected at 1 MPa ($0.20 \pm 0.066 \text{ mg s}^{-1} \text{ kPa}^{-1} \text{ mm}^{-1}$, $n = 4$; Fig. 5.5A, "+ spin or inj," pooled mean) This result dramatically contradicted the MRI and dye perfusion data which indicated significant xylem function at xylem pressures well below -2 MPa (Fig. 5.2).

5.3.5 *Quercus gambelii* experiments

In the first experiment, native stem pressure and conductivity were measured in trunk segments from ten *Q. gambelii* trees prior to centrifugation of the segments at native pressures. Native stem xylem pressure averaged $-1.84 \pm 0.06 \text{ MPa}$, and

native stem-area specific conductivity averaged $3.4 \pm 0.44 \text{ mg s}^{-1} \text{ kPa}^{-1} \text{ mm}^{-1}$ (Fig. 5.4B, "native"). This result indicated very significant xylem conductivity at -1.8 MPa of negative pressure. There was no significant difference in native conductivity whether the trunk was initially cut in air vs. under-water. The lack of a difference indicated two things: first, that inter-vessel pit membranes in the air-cut branches were not being penetrated by air at the native xylem pressure; and second, that if any vessels exposed by the initial cut in air were long enough to extend into the test segment (ca. 1 m distant) their embolism did not significantly reduce the native xylem conductivity.

When the same test segments were spun to their native xylem pressure in the lab, the conductivity fell to $61 \pm 11.2\%$ of the native value (average drop computed on individual stem basis, $n = 10$). Although centrifugation caused a reduction in conductivity on average, it did not come close to causing the near-zero conductivity observed for *Q. robur* stems spun at similar pressures (Fig. 5.4B "+ spin" vs. Fig. 5.4A "+ spin or inj"). Flushing the *Q. gambelii* stems to the maximum conductivity and then re-spinning them to the native xylem pressure resulted no further statistical change in the percentage conductivity relative to the native value (Fig. 5.4B "+ flush & spin"). Therefore, flushing itself did not cause any abnormal sensitivity of xylem conductivity to subsequent centrifugation.

We simulated the procedure used to collect the *Q. robur* stems by cutting relatively short *Q. gambelii* trunk segments in the air and storing for four days. In this case, we observed a very different response to the flushing plus centrifugation treatment. Stem area-specific conductivity after spinning flushed stems to -1.5 MPa was extremely low ($0.18 \pm 0.051 \text{ mg s}^{-1} \text{ kPa}^{-1} \text{ mm}^{-1}$; Fig. 5.4C "short + flush & spin", $n = 4$) and similar to the response of *Q. robur* segments (Fig. 5.4A, "+ spin or inj").

Further tests indicated that the exaggerated response to centrifugation resulted from vessels being air-filled prior to flushing and spinning. *Q. gambelii* trunk segments were harvested from long branches so as to avoid air-filling the vessels in the segment. Segments were cut from the branches underwater, and then air was briefly blown through the segments at low pressure ($< 20 \text{ kPa}$) to fill vessels with air. Vigorous bubbling was observed from the other segment end when held under water, indicating many vessels open at both ends. Segments were flushed and spun to -1.5 MPa. The conductivity fell to very low values ($0.111 \pm 0.0282 \text{ mg s}^{-1} \text{ kPa}^{-1} \text{ mm}^{-1}$, $n = 8$; Fig. 5.4C, "long + blow + flush & spin") that were no different from the stems harvested at short lengths before flushing (Fig. 5.4C "short+ flush & spin"). This result indicates a "refilling artifact" in the static centrifuge protocol: once emptied, refilled vessels did not regain their native resistance to cavitation.

5.4 Discussion

The MRI technology proved adequate for compiling *in situ* vulnerability curves in ring-porous material, and it was essential for revealing an important problem in standard vulnerability curve protocols. The technique, however, was not without its own ambiguities. Chief among them was the difficulty of assigning pixilated MRI

data to specific cells in the tissue (Van As and Windt, 2008). Pixel location cannot be precisely mapped to the anatomical cross section. Superimposed on this basic issue were limitations on minimum pixel size which was constrained by the need for a field of view large enough to encompass the entire stem and to avoid excessive imaging time. It is in principle possible to further resolve the signal in the xylem mask, e.g. by bi-exponential fitting of the total T_2 decay curve (cf. Scheenen *et al.*, 2002), or by correlated T_1 - T_2 or displacement- T_2 measurements. Water in the vessels will in general have a quite different T_2 value with respect to water surrounding the vessels and in this way can be discriminated (see Chapter 4) The FCA imaging was resolvable at the sub-pixel level, but has the shortcoming that FCA is not a direct proxy for water-filled vessel area (Scheenen *et al.*, 2007). Changes in FCA thus do not necessarily result from cavitation or refilling.

The "drydown" protocol was much more efficient and accurate for detecting cavitation than the single-pressure method. In the drydown method, one trunk was continually imaged as it became more stressed, and changes in water content in the same earlywood pixels (presumably at nearly the same anatomical location) could be tracked over time. Tracking the same pixels allowed more precise relative measurements of the water content of earlywood vessels than the single-pressure method where pixels had to be selected separately for the intact image and the reference "filled" image. In addition, installation of the stem was time consuming, and the number of installations per data point was much less in the drydown protocol.

Three main conclusions can be drawn from our results. First: dye perfusions and FCA measurements indicate that a substantial portion of earlywood vessels in the current growth ring were not conducting fluid at even the highest (least negative) of water potentials in *Quercus robur*. Second: water content and dye perfusion data showed that the functional earlywood vessels did not cavitate significantly until water potentials fell below -3 MPa, and no refilling of earlywood vessels was detected in re-watered trees. Third: centrifuge and air-injection measurements contradicted the MRI and dye perfusion data by predicting nearly complete embolism at water potentials as high as -1 MPa. Experiments on *Q. gambelii* identified a "refilling artifact" by way of explanation.

The first conclusion, that a portion of current-year earlywood vessels were not conducting in *Q. robur*, is consistent with previous results from ring-porous species showing high native embolism and incomplete dye conduction through current year's earlywood (Li *et al.*, 2008, Taneda and Sperry, 2008). Lower native embolism reported for current-year twigs of ring-porous oaks (Cochard *et al.*, 1992a, Cochard and Tyree, 1990) might result from the fact that the large-vesseled ring-porous anatomy does not develop until the second or third year of growth. The embolized earlywood we detected were either so vulnerable to cavitation that they lost function soon after maturation, or they cavitared during a previous water-stress event and were never refilled *in situ*. We measured our trees in September, and we would have to measure trees soon after vessel maturation to know how vulnerable *all* of the earlywood vessels were. As it was, the MRI and dye data only gave us the vulnerability of the still functioning vessels.

The best evidence for empty earlywood vessels in well-watered trees was from the

dye perfusions, but they were also suggested by maximum FCA being generally less than the early-wood vessel area. Although FCA was found to vary independently of the area of functional vessels with variation in sap flow rate, the maximum FCA should approach the water-filled vessel area. Previous studies have also noted that maximum FCA is less than the cross sectional area of all vessel lumens (Windt, 2007). The discrepancy was greatest (FCA 31% of total) for material with larger conduits than for stems with narrower ones (FCA 86% of total). It seems that species with large conduits may operate with many of them non-functional, perhaps because a subset of the larger vessels is very susceptible to cavitation and/or a substantial number has too low velocity to allow a good discrimination of flowing and non-flowing water. The latter can also, at least partly, explain the discrepancy between the water content and FCA behavior as a function of water potential: average flow velocity become too low (for details and solutions see Appendix to Chapter 4). In contrast to our FCA data, our water content data gave maximum filled vessel areas in excess of total earlywood vessel area. The coarse pixel-scale resolution of water content data apparently prevented the detection of any originally empty vessels. The water content imaging was most reliable for detecting relative changes in filled vessel area with water potential rather than absolute values.

The second conclusion, that the water-filled earlywood vessels of *Q. robur* were relatively resistant to cavitation, seemingly contradicts centrifuge and air-injection vulnerability curves on ring porous species that show over 90% loss of hydraulic conductivity at water potentials less negative than -1 MPa (Li *et al.*, 2008, Taneda and Sperry, 2008). Our dye perfusion and MRI water content data were both convincing in showing no marked decrease in filled vessel area until below -3 MPa. Furthermore, there was no crisping of leaves until water potentials fell below -4 MPa, at which point the dye perfusions indicated no functional earlywood. These results are comparable with vulnerability curves on *Q. robur* using the "bench dehydration" method which measures only the cavitation in vessels functional at the time of collection (Cochard *et al.*, 1992a). The bench dehydration method is free of the refilling artifact that we identified in the centrifuge and air-injection methods. The FCA data (Fig. 5.4) are less reliable for detecting cavitation because FCA could decrease without any cavitation occurring either via a drop in transpiration rate or a shut-down in flow due to cavitation occurring upstream or downstream from the imaged vessels.

The lack of evidence for *in planta* refilling in re-watered *Q. robur* contrasts with diurnal fluctuations in native embolism suggestive of nocturnal refilling in ring-porous *Q. gambelii* (Taneda and Sperry, 2008). The refilling in this species was observed in mid-summer, but was not evident by September. We also did our *Q. robur* measurements in September, which could explain why we saw no refilling.

The third conclusion, that there is potential for a refilling artifact in the vulnerability curve protocol, provides part of an explanation for the discrepancy between the MRI results and vulnerability curves using centrifuge or air-injection methods. The refilling artifact is the artificially extreme vulnerability to cavitation exhibited by air-filled vessels that have been refilled by the flushing procedure. The evidence is most clearly shown by the comparison between *Q. gambelii* stems collected so as to avoid the air-filling of functional vessels vs. stems collected in exactly the same way but

then purposefully blown full of air (Fig. 5.5B,C). The large quantity of air observed passing through the 27 cm long segments indicated numerous vessels running entirely through. When both sets of stems were flushed and spun in the centrifuge, the ones that had been purposefully air-filled before flushing had essentially no conductivity (Fig. 5.5C, long blow flush & spin) while the ones that were not air-filled had much greater conductivity (Fig. 5.5B, + flush & spin). The refilling artifact cannot be attributed to contaminants in the perfusing solution, because the stems that did not have their vessels refilled but were otherwise spun on the centrifuge had significantly higher conductivity (though not as high as native values; Fig. 5.5B).

The refilling artifact explains the anomalously near-zero conductivity of *Q. robur* stems that were flushed and spun in the centrifuge (Fig. 5.5A + spin or inj). The *Q. gambelii* stems cut to similarly short lengths as *Q. robur* exhibited similarly low and anomalous conductivity when flushed and spun (Fig. 5.5C, short + flush & spin). In both species, the longest vessels exceed 1 meter (Cochard *et al.* In review; Sperry and Sullivan, 1992). Cutting short stem pieces from the trees in the air would allow air to enter the long vessels of both species and penetrate the test segments prior to being refilled by flushing. The refilling artifact apparently also applies to the air-injection method, because it gave the same anomalously low conductivities in *Q. robur* as did the centrifuge method.

The simplest explanation for the refilling artifact is that micro-bubbles remain trapped in the vessel after refilling, probably attached to the walls or retained within the pit chambers. Such bubbles would serve to prematurely nucleate cavitation when the refilled vessel was spun in the centrifuge. Similarly, bubbles could serve as sites for the out-gassing of dissolved air in the air-injection method. Confirmation of this putative mechanism requires further experimentation. But regardless of the cause of the artifact, our results were unambiguous in showing that the air injection as well as centrifugation methods were both vulnerable to the artifact.

The discovery of the refilling artifact has major implications for conducting and interpreting vulnerability curves. Clearly, the vulnerability of any vessel that was refilled by flushing prior to either centrifugation or air-injection cannot be assessed with confidence unless a method can be found that eliminates the artifact. In the meantime, the artifact can be avoided by cutting the segments from large branches or the tree itself under-water so as to avoid air-filling any functional vessels in the segment. This was impossible in the case of our *Q. robur* segments which had to be transported from The Netherlands to Utah before measurement. Flushing should probably be avoided prior to conducting vulnerability curves because it does not reliably restore the vessel to its original cavitation resistance. Flushing is still required for measuring native embolism (Sperry *et al.*, 1988), but there is currently no way to reliably determine the vulnerability of the embolized and refilled xylem.

We suspect that the refilling artifact is responsible for what has been termed "cavitation fatigue" in previous work (Hacke *et al.*, 2001). This phenomenon refers to the often markedly greater vulnerability of xylem after it has been stressed to extreme cavitation and then refilled and tested again. The fact that the refilled xylem was as vulnerable to cavitation by centrifugation as it was to air-filling by air-injection was originally taken as evidence that previous cavitation had made the vascular system

more permeable to air entry (as opposed to leaving micro-bubbles behind). Stretching of inter-vessel pit membranes was proposed as the mechanism. However, here we saw the same phenomenon when vessel lumens were air-filled without experiencing stress-induced cavitation. We propose that expansion of micro-bubbles is responsible, which occurs because of out-gassing in the air-injection experiments and because of cavitation nucleation in the centrifuge. The possibility that vessels can become air filled by air-injection without gas-phase penetration of vessel walls has not been explicitly recognized before, and the proposed role of microbubbles in nucleating the out-gassing process during air injection requires further study.

Notably, not all species exhibit cavitation fatigue (Hacke *et al.*, 2001) which suggests that the refilling artifact may be more of a problem for some species than others. The difference may lie in details of vessel wall chemistry and structure which suppress the retention of micro-bubbles. The many species which refill naturally must have mechanisms to suppress the artifact, and how they do so would be interesting to know.

Our results also expose a second, though less dramatic, artifact associated with the centrifuge method in large-vesselled material. The evidence is seen in the *Q. gambelii* stems that were collected so as to avoid any air-filling of functional vessels (Fig. 5.5B). The conductivity after spinning these stems to their native pressure was only 61% of the native conductivity (Fig. 5.5B, native vs. + spin). We refer to this as the "spinning artifact." If there were no artifact associated with spinning the stems, and if the centrifugally-induced pressure was no more negative than the native pressure, the post-spin conductivity should have been 100% of the native value. Flushing and repeating the spin had no significant further effect, indicating that the flushing procedure alone had no dramatic effect on the cavitation.

It is possible that our estimates of native xylem pressure were too negative, because they were measured on shoots attached near the test segment. Although the shoots were bagged to reduce transpiration and promote equilibration with the stem, a residual pressure gradient could have remained. If so, we were centrifuging the stems to an overly negative pressure which may have induced additional cavitation. Spinning itself could also potentially cause artifacts.

During spinning, the ends of the stem are in reservoirs that hold the same filtered KCl solution used to measure conductivity. As the rotor accelerates, the solution rises up to submerge the stem ends (Alder *et al.*, 1997). Some filled vessels could lose their water prior to submergence and become embolized by simple displacement. Alternatively, some of the perfusing solution could flow into the spinning stem and if the solution contained microbubbles or other nucleators it could cause cavitation if not filtered by pit membranes. This is the artifact proposed in relation to the flow-centrifugation protocol (Cochard *et al.*, 2005, Cochard *et al.*, In review), but it could also influence static centrifugation. Short vesselled material would be less susceptible to either source of the spinning artifact.

It is difficult to say how much these artifacts have influenced previous vulnerability curves, but the refilling artifact is the most serious one. Large-vesselled material (vines, ring-porous trees, roots) would be most prone to both artifacts. Importantly, both centrifugal and air-injection methods, as different as they are in operation, seem

to be equally susceptible to the refilling problem. In our previous work on ring porous trees (Li *et al.*, 2008; Taneda and Sperry, 2008), material was usually collected so as to minimize air-filling of functional vessels in the test segment. Thus, the portion of the curve extending from the native xylem pressure to more negative pressures would be immune to the refilling artifact, but still susceptible to the less critical spinning artifact for centrifugal curves. Such curves may be at least approximately accurate for pressures at or below native xylem pressure. This would explain why they agreed statistically with native embolism measurements which are immune to either artifact. However, the portion of such curves above (less negative) than the native xylem pressure would be suspect. Also suspect would be any curves where a substantial number of originally functional vessels in the test segment became emptied during collection. A priority for future work is the development and testing of improved methods for obtaining vulnerability curves on large-vesseled material.

In conclusion, the MRI and dye perfusion results indicated that a substantial fraction of the earlywood vessels of *Q. robur* were very resistant to cavitation. But, there was also evidence for a similar fraction of earlywood vessels that were non-functional even at the highest of water potentials. The latter observation is consistent with the high native embolism reported in some ring-porous trees, and is possible that these non-functional vessels are relatively susceptible to cavitation. More observations are necessary to discover the vulnerability of the full set of earlywood vessels in ring-porous species.

Appendix

The correlation between water potential and water content in different tissues in the stem of oak

Apart from the vulnerability curves we can also correlate for the first time the water content in the different tissues observed in the stem of oak (*Quercus robur* L.) with the water potential as measured by the psychrometers as described above. Water content in different tissues was calculated by summing the signal amplitude of all pixels in each tissue, which were selected on the basis of tree anatomy.

Figure 5.6 shows the correlation between the water potential in the stem and the amount of water in the bark, the cambial zone and xylem vessels (the pixels with the highest intensity) in earlywood and late wood during drought stress and recovery after watering. The time of watering is indicated by the dashed line. Water content in the bark started to decrease simultaneously with the decrease of water potential. Initially it decreased quite fast, but it slowed down in approximately 100 hours. In response to watering water content in the bark increased immediately and reached the initial amount at the same time when the water potential restored to its initial level.

Water content in the cambial zone constantly decreased when water potential went down, and restored very fast after watering.

Water content in early xylem vessels started to decrease at a water potential of around -2 MPa, whereas the water content in late xylem vessels started to decrease at a water potential of around -2.5 MPa. Early xylem vessels reached its minimum in water content faster than the late xylem vessels. The decrease of water content in vessels directly relates to xylem cavitations. Watering after the drydown period did not result in an increase in water content in the xylem vessels.

During this experiment we observed about linear correlation between water potential and decrease in water content in the cambial zone. A decrease in water potential of 1 MPa corresponded to a decrease in water content in this tissue approximately by 16 - 20% of its amount in the well watered tree (when the water potential was about zero).

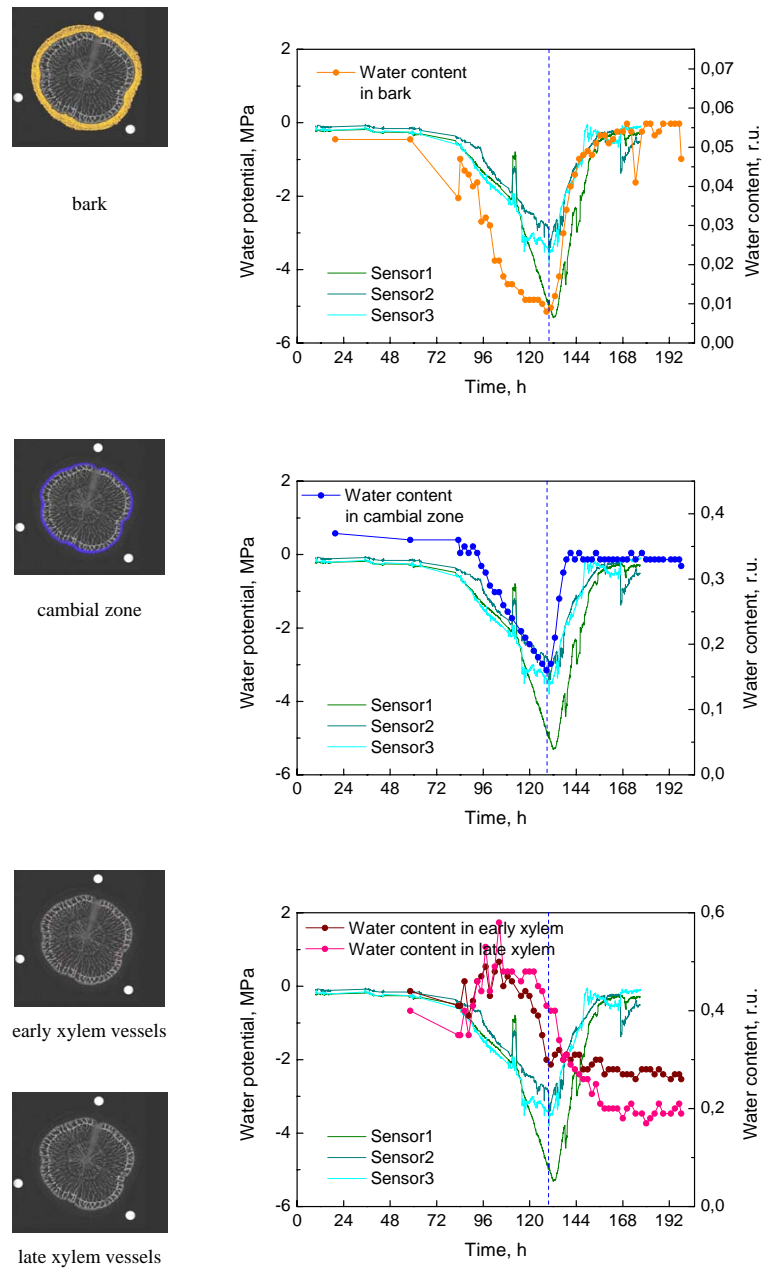


Figure 5.6 : Water potential and water content in bark, cambial zone, and early and late xylem vessels measured during drought and recovery.

References

- Alder N.N., Pockman W.T., Sperry J.S., Nuismer S. (1997) Use of centrifugal force in the study of xylem cavitation. *Journal of Experimental Botany*, **48**, 665-674.
- Clearwater M.J., Clark C.J. (2003) In vivo magnetic resonance imaging of xylem vessel contents in woody lianas. *Plant Cell and Environment* **26**, 1205-1214.
- Cochard H., Tyree M.T. (1990) Xylem dysfunction in *Quercus*: Vessel sizes, tyloses, cavitation and seasonal changes in embolism. *Tree Physiology*, **6**, 393-408.
- Cochard H., Breda N., Granier A., Aussenac G. (1992a) Vulnerability to air embolism of three European oak species (*Quercus petraea* (Matt) Liebl, *Q. pubescens* Willd, *Q. robur* L). *Annales des Sciences Forestieres*, **49**, 225-233.
- Cochard H., Cruiziat P., Tyree M.T. (1992b) Use of positive pressures to establish vulnerability curves: Further support for the air-seeding hypothesis and implications for pressure-volume analysis. *Plant Physiology*, **100**, 205-209.
- Cochard H., Gaele D., Bodet C., Tharwat I., Poirier M., Ameglio T. (2005) Evaluation of a new centrifuge technique for rapid generation of xylem vulnerability curves. *Physiologia Plantarum*, **124**, 410-418.
- Cochard H., Herbette S., Barigah T., Vilagrosa A. (In review) *A pitfall in the centrifugation techniques for measuring xylem vulnerability to cavitation*.
- Dixon M.A., Tyree M.T. (1984) A new stem hygrometer, corrected for temperature gradients and calibrated against the pressure bomb. *Plant Cell and Environment*, **7**, 693-697.
- Hacke U.G., Stiller V., Sperry J.S., Pittermann J., McCulloh K.A. (2001) Cavitation fatigue: embolism and refilling cycles can weaken cavitation resistance of xylem. *Plant Physiology*, **125**, 779-786.
- Hacke U.G., Sperry J.S., Wheeler J.K., Castro L. (2006) Scaling of angiosperm xylem structure with safety and efficiency. *Tree Physiology*, **26**, 689-701.

- Homan N., Windt C.W., Vergeldt F.J., Gerkema E., Van As H. (2007) 0.7 and 3 T MRI and sap flow in intact trees: xylem and phloem in action. *Applied Magnetic Resonance*, **32**, 157 - 170.
- Li Y., Sperry J.S., Bush S.E., Hacke U.G. (2008) Evaluation of centrifugal methods for measuring xylem cavitation in conifers, diffuse- and ring-porous angiosperms. *New Phytologist*, **177**, 558-568.
- Scheenen T.W.J., van Dusschoten D., de Jager P.A., Van As H. (2000) Microscopic displacement imaging with pulsed field gradient turbo spin-echo MRI. *Journal of Magnetic Resonance*, **142**, 207-215.
- Scheenen T.W.J., Heemskerk A.M., de Jager P.A., Vergeldt F.J., Van As H. (2002) Functional imaging of plants: a nuclear magnetic resonance study of a cucumber plant. *Biophysical Journal*, **82**, 481-492.
- Scheenen T.W.J., Vergeldt F.J., Van As H. (2007) Intact plant magnetic resonance imaging to study dynamics in long-distance sap flow and flow-conducting surface area. *Plant Physiology*, **144**, 1157-1165.
- Sperry J.S., Donnelly J.R., Tyree M.T. (1988) A method for measuring hydraulic conductivity and embolism in xylem. *Plant Cell and Environment*, **11**, 35-40.
- Sperry J.S., Sullivan J.E.M. (1992) Xylem embolism in response to freeze-thaw cycles and water stress in ring-porous, diffuse-porous, and conifer species. *Plant Physiology*, **100**, 605-613.
- Sperry J.S., Saliendra N.Z. (1994) Intra-and inter-plant variation in xylem cavitation in *Betula occidentalis*. *Plant Cell and Environment*, **17**, 1233-1241.
- Sperry J.S., Saliendra N.Z., Pockman W.T., Cochard H., Cruiziat P., Davis S.D., Ewers F.W., Tyree M.T. (1996) New evidence for large negative xylem pressures and their measurement by the pressure chamber method. *Plant Cell and Environment*, **19**, 427-436.
- Taneda H., Sperry J.S. (2008) A case-study of water transport in co-occurring ring-versus diffuse-porous trees: contrasts in water-status, conducting capacity, cavitation and vessel refilling. *Tree Physiology*, **28**, 1641-1652.
- Tyree M.T., Sperry J.S. (1989) Characterization and propagation of acoustic emission signals in woody plants: Towards an improved acoustic emission counter. *Plant Cell and Environment*, **12**, 371-382.
- Van As H. (2007) Intact plant MRI for the study of cell water relations, membrane

permeability, cell-to-cell and long distance water transport. *Journal of Experimental Botany*, **58**, 743 - 756.

Van As H., Windt C.W. (2008) Magnetic resonance imaging of plants: water balance and water transport in relation to photosynthetic activity. *In Biophysical techniques in photosynthesis II* (eds T.J. Aartsma & J. Matysik), pp. 55-75. Springer, Berlin.

Van As H., Homan N., Vergeldt F.J., Windt C.W. (2009) MRI of water transport in the soil-plant-atmosphere continuum. *In Magnetic Resonance Microscopy* (eds S. Codd & J.D. Seymour), pp. 315-330. Wiley-VCH, Weinheim.

Windt C.W., Vergeldt F.J., de Jager P.A., Van As H. (2006) MRI of long distance water transport: a comparison of the phloem and xylem flow characteristics and dynamics in poplar, castor bean, tomato and tobacco. *Plant Cell and Environment*, **29**, 1715-1729.

Windt C.W. (2007) *Nuclear magnetic resonance imaging of sap flow in plants*. PhD Thesis, Wageningen.

Windt C.W., Vergeldt F.J., Van As H. (2007) Correlated displacement- T_2 MRI by means of a pulsed field gradient-multi spin echo method. *Journal of Magnetic Resonance*, **185**, 203-239.

Chapter 6

Summarizing discussion

Due to their long life span, changing climatic conditions are of particular importance for trees. Climate changes will affect the water balance, which can become an important limiting factor for photosynthesis and growth. Long-distance water transport in trees is directly related to the transpiration stream and very sensitive to changes in the soil-plant-atmosphere water continuum. Therefore the study of long distance transport gives information about tree response to changing climatic conditions. Here the dynamic behaviour of water transport processes in trees has been studied by the MRI method, which is a direct and non-invasive tool. MRI flow imaging has been applied to diffuse- and ring-porous trees to study drought stress and the occurrence of xylem vessel cavitations.

World-wide unique dedicated MRI hardware is described that allows imaging of sap flow in intact trees with a maximal trunk diameter of 4 cm and height of several meters. This setup is used to investigate xylem and phloem flow in an intact tree quantitatively. Flow is quantified in terms of (averaged) velocity, volume flow (flux) and flow conducting area, either in imaging mode or resolved on the level of annual rings.

Results obtained for the same tree, imaged at two different field strengths (0.7 and 3 T), are compared. An overall shortening of observed T_2 values is manifest going from 0.7 to 3 T. Although susceptibility artefacts may be present at 3 T, the results are still reliable and the gain in sensitivity due to the higher magnetic field strength results in shorter measurement time (or a better spatial resolution or a higher signal to noise ratio) with respect to the 0.7 T system. By use of such dedicated hardware xylem and phloem flow, and its mutual interaction, can be studied in intact trees in relation to the water balance and in response to environmental (stress) conditions (**Chapter 2**).

To further investigate the effect of susceptibility artefacts on MRI flow imaging by PFG-STE MRI on 3 T, water flow was studied in a number of model porous media with or without surface relaxation, internal magnetic field inhomogeneities (susceptibility artefacts) and exchange with stagnant water pools, mimicking the tree situation (**Chapter 3**). In such situations a clear dependence of the flow characteristics on the

observation time is demonstrated. The most reliable results are obtained at relatively short observation times. This limits the observation of low flow velocities and the discrimination between flowing and non-flowing water. It is shown that correlated displacement- T_2 measurements are available to improve the discrimination of flowing and non-flowing water and can be of help to decide about the functional activity of xylem conduits (**Chapter 4**). A method that reveals exchange between the flowing and stagnant fractions in the system is presented. Further it is demonstrated how this exchange can be quantified (**Chapter 3**).

Xylem flow, flow conducting area and water content in the storage pools of sapwood and cambial zone were investigated simultaneously and non-destructively by MRI in diffuse-porous laurel (*Laurus nobilis*) and viburnum (*Viburnum tinus*) trees during a drydown period and recovery after watering (**Chapter 4**). The development of the drought stress was detected by the decrease in average velocity, volume flow and flow conducting area as observed by MRI flow imaging. A decrease in flow conducting area was observed with a delay of one day in comparison to the observed reduction in average velocity and volume flow. The re-watering of the plants resulted in the fast restore of the flow conducting area to the value observed under well watered conditions, demonstrating that if cavitations had been induced they refilled quite fast. In addition, a significant increase in the average velocity and volume flow was observed, but still lower than the original values. Imaging water content in the cambial zone indicated a gradual decrease of the water content, which speeded up during the drought stress. The rate of decrease was dependent of day/night conditions. Watering resulted in the partial restore of water content in this zone. Water content in sapwood showed a clear diurnal variation. The water storage pool in sapwood depleted quickly upon switching on the light, gradually restoring in the afternoon. Drought stress did not change the character of diurnal variation of water content significantly, but it increased the amplitude of the diurnal variation. Re-watering of the tree resulted in a 10% water loss in sapwood. Thus, for the first time the coupling between water flow in xylem vessels and water content in storage pools was demonstrated. The oldest annual ring was rather inactive in long distance water transport. We found that the transport activity of this ring was not sensitive to any environmental change and that the variation of water content in sapwood was uniform in all annual rings.

Non-destructive measurements of cavitation were made with MRI to test whether large earlywood vessels of ring-porous xylem are as vulnerable as some standard methods have suggested (**Chapter 5**). Potted, 3-4 year old *Quercus robur* L. trees were droughted to water potentials measured with temperature-corrected stem psychrometers. Imaging of (vessel) water content indicated that earlywood cavitation in trunks was not detectable until water potentials dropped below -3 MPa. Most earlywood vessels were cavitared below -4 MPa. Dye perfusions through excised branch segments gave comparable results. Imaging of flow conducting area (FCA) indicated a gradual decline in trunk water conduction that was not solely associated with cavitation, but probably resulted from stomatal closure and too low velocities to be discriminated from non-flowing water. Dye perfusion and FCA indicated a significant portion of earlywood vessels were non-conducting even at the most favor-

able water potentials. No refilling of embolized vessels was detected in rewatering experiments. Contradictory to the MRI results, standard centrifuge and air-injection methods on *Q. robur* stem segments indicated complete cavitation at xylem pressures at or below -1 MPa. An artifact in these destructive methods was revealed by experiments on the related species *Q. gambelii* Nutt. When earlywood vessels became air-filled during collection prior to being refilled in the lab, they became much more vulnerable to cavitation. Residual bubbles left behind in the refilled vessels may be responsible. These results suggest revised protocols for measuring vulnerability curves by destructive methods.

An about linear correlation between water potential and decrease of water content in cambial zone of oak (*Quercus robur* L.) was observed (**Chapter 5**).

Chapter 7

Samenvatting

Veranderingen in klimaat zijn voor bomen van groot belang door hun lange levensduur en de gebondenheid aan hun standplaats. Klimaatveranderingen zullen een effect hebben op de waterbalans, die daardoor zelfs een limiterende factor kan worden voor fotosynthese en groei. De hoeveelheid water die in bomen wordt getransporteerd in het xyleem is direct gekoppeld aan de verdamping van water en erg gevoelig voor veranderingen in de beschikbare hoeveelheid water en de hydraulische weerstand in het continuüm bodem-plant-atmosfeer. Studie van het lange afstand xyleemtransport, de koppeling met opslagpools en het korte afstand transport levert daarom informatie op over reacties en aanpassingsmogelijkheden van een boom aan veranderende klimaatcondities. In dit proefschrift worden resultaten gepresenteerd van het dynamisch gedrag van watertransport-processen in bomen bestudeerd met behulp van de Magnetic Resonance Imaging (MRI) methode. Deze methode is niet-invasief en hiermee wordt direct aan water gemeten. MRI flow imaging is toegepast aan diffuus- en ring-poreuze bomen om droogte stress en het optreden van xyleemcavities, het breken van de waterkolom in het xyleem, te bestuderen.

Er is gebruik gemaakt van unieke MRI hardware, speciaal ontworpen voor metingen aan planten. Met behulp van deze hardware kan flow imaging in intacte bomen met een stamdiameter tot maximaal 4 cm en een hoogte van enige meters worden verricht. Deze opstelling is gebruikt om zowel stroming van water in het xyleem als floëem in een intacte boom kwantitatief te meten. De volgende stromingsparameters kunnen worden verkregen: (gemiddelde) snelheid, volume snelheid (flux) en doorstroomd oppervlak, zowel in imaging mode (per pixel) als per jaarring of voor het gehele xyleemgebied. Allereerst worden resultaten, verkregen met dezelfde boom in twee verschillende MRI systemen (0.7 en 3T) vergeleken. In hoger magneetveld (3 T) worden in het algemeen kortere T_2 waarden gemeten dan in het lagere veld (0.7 T). Hoewel in het hogere veld susceptibiliteitartefacten (locale verstoringen van het magneetveld) aanwezig kunnen zijn, zijn de resultaten nog steeds betrouwbaar en is de winst in gevoeligheid in het hogere veld zodanig dat kortere meettijden (of een hogere ruimtelijke resolutie of betere resultaten met een hogere signaal-ruis verhouding) behaald kunnen worden ten opzichte van het systeem met het lagere veld.

Gedemonstreerd wordt dat met de speciaal ontwikkelde hardware zowel xyleem als floëem stroming en hun onderlinge interactie bestudeerd kunnen worden in intacte bomen in relatie tot de waterbalans en in respons tot omgevingscondities (inclusief stress) (**Hoofdstuk 2**).

Het effect van susceptibiliteitsartefacten op MRI flow imaging gemeten met behulp van de pulsed field gradient - stimulated echo (PFG-STE) methode is onderzocht in een aantal poreuze modelsystemen met en zonder oppervlakte relaxatie, interne magnetische verstoringen en uitwisseling tussen stilstaand water in het poreuze materiaal en stromend water (**Hoofdstuk 3**). Deze systemen bootsen de situatie in een boom na. In zulke situaties is voor de stromingskarakteristieken een duidelijke afhankelijkheid van de observatietijd waargenomen. De meest betrouwbare resultaten worden gemeten met relatief korte observatietijden. Dit beperkt de betrouwbare meting van lage snelheden en het onderscheid tussen stromend en niet-stromend water. Aange-toond wordt dat gecorreleerde verplaatsings- T_2 metingen gebruikt kunnen worden om de discriminatie tussen stromend en niet-stromend water te verbeteren. Deze metingen kunnen van behulp zijn om een uitspraak te doen of xyleem elementen functioneel actief zijn (**Hoofdstuk 4**). Een methode wordt gepresenteerd waarmee uitwisseling tussen stromend en niet-stromend water zichtbaar kan worden gemaakt en kan worden gekwantificeerd (**Hoofdstuk 3**).

Xyleem stroming, doorstroomd oppervlak en watergehalte in opslagpools van het xyleem en de cambium zone, zijn met behulp van MRI gelijktijdig, niet destructief en in onderlinge samenhang bestudeerd in de diffuus poreuze bomen laurier (*Laurus nobilis*) en viburnum (*Viburnum tinus*) gedurende een uitdroogperiode en tijdens herstel na een watergift (**Hoofdstuk 4**). De ontwikkeling van droogtestress leidde tot de afname van de gemiddelde snelheid, volume snelheid en het doorstroomd oppervlak. De afname van het doorstroomd oppervlak had een vertraging van een dag in vergelijking tot de waargenomen afname in gemiddelde snelheid en volume snelheid. Na de watergift werd een snel herstel van het doorstroomd oppervlak waargenomen, tot de waarde die werd gemeten onder goed bewaterde condities. Dit demonstreert dat als er cavitaties in de waterkolom in het xyleem geïnduceerd zouden zijn er een snel herstel optreedt. Daarnaast werd een significante verhoging van de gemiddelde snelheid en van de volume snelheid waargenomen, echter tot waarden die lager waren dan de startwaarden voor de uitdroogperiode. Het watergehalte in de cambium zone vertoonde een graduele afname, met een snelheid die toenam naarmate de droogtestress erger werd. De snelheid van afname was afhankelijk van dag/nacht condities. De watergift resulteerde in een gedeeltelijk herstel van het watergehalte in de cambium zone. Het watergehalte in het xyleem vertoonde een dag/nacht cyclus. De hoeveelheid water in de opslagpool van het xyleem nam snel af na het inschakelen van licht, maar herstelde geleidelijk in de middag en avond. Droogtestress veranderde het dagelijks verloop van het watergehalte niet significant, maar het verhoogde de amplitude van de dagelijkse variaties. Het opnieuw bewateren van de boom resulteerde in een verlies van 10% van de hoeveelheid water in de opslagpool van het xyleem. De oudste jaarring was nagenoeg inactief wat lange afstand watertransport betreft. De transportactiviteit die in die ring werd waargenomen was niet gevoelig voor veranderingen in omgevingscondities. De variatie in watergehalte in het xyleem

was gelijk in alle jaarringen.

Voor het eerst is in intacte eiken (*Quercus robur* L), die een ring-poreuze xyleem structuur hebben, met redelijk grote xyleemvaten in het voorjaarshout, onderzocht bij welke waterpotentiaal cavitatie optreedt in deze vaten (**Hoofdstuk 5**). In uitdroog experimenten met 3-4 jaar oude boompjes (in 5 liter potten) werd gelijktijdig de hoeveelheid water in de vaten (via MRI) en de waterpotentiaal in de stam (met behulp van psychrometers) gemeten. Imaging van de hoeveelheid water toonde aan dat cavitatie nauwelijks optrad tot een waterpotentiaal van -3 MPa. De meeste vaten in het voorjaarshout van de laatste jaarring vertoonden cavitatie onder -4 MPa. Perfusie experimenten met kleurstoffen door stengelsegmenten van zijtakjes resulteerde in vergelijkbare resultaten. Imaging van het doorstroomd oppervlak als functie van de waterpotentiaal gaf een gradueel verloop in de stam te zien. Dit verloop van het doorstroomd oppervlak hing niet alleen samen met cavitatie, maar waarschijnlijk ook met lage stroomsnelheden in de vaten door het sluiten van de huidmondjes. Langzaam stromend water is moeilijk te onderscheiden van niet-stromend water, wat de bepaling van het doorstroomd oppervlak beïnvloedt. Perfusie experimenten met kleurstof en metingen van het doorstroomd oppervlak gaven indicaties dat een significant deel van het voorjaarshout niet-actief was in transport, zelfs niet bij de meest gunstige waterpotentialen voor transport. De watergift na het uitdroogexperiment resulteerde niet in hervullen van de gecaviteerde vaten. In tegenstelling tot de MRI resultaten, gaven standaard centrifuge en lucht-injectie experimenten aan afgesneden stengelstukjes van *Quercus robur* complete cavitatie in xyleem aan bij waterpotentialen onder de -1 MPa. Via experimenten aan de zeer verwante *Q. gambelii* Nutt kon worden aangetoond dat de oorzaak een artefact in deze experimenten was. In deze destructieve methoden wordt gewerkt met afgesneden stengelsegmenten. Als bij het oogsten en bewaren van deze stengelsegmenten de xyleemvaten eenmaal (deels) met lucht gevuld zijn geweest, voordat ze weer gevuld worden met water aan het begin van deze experimenten, worden ze veel gevoeliger voor cavitatie. Dit wordt veroorzaakt doordat zeer kleine luchtbelletjes, waarschijnlijk rond de pits, achter blijven. Daarom wordt een aangepast protocol voorgesteld voor het prepareren van de stengelsegmenten voor deze destructieve methoden.

Naast stroming kan MRI ook informatie geven over de waterpotentiaal: een nage-noeg lineair verband werd gevonden tussen de waterpotentiaal en de hoeveelheid water in de cambium zone van eik (*Quercus robur* L) (**Hoofdstuk 5**). Hierdoor kan met behulp van MRI nu het verband tussen stroming en de drijvende kracht in intacte planten niet-destructief worden bestudeerd.

Acknowledgements

This is the final chapter of my thesis. In order to start writing this thesis I had to spend a few years of my life here in the Netherlands with the people from Biophysics group of Wageningen University. Looking back I can say that I am really happy that this opportunity for doing research, developing and getting new skills, making new friends was given to me. I would like to thank all the people whom I have met here and who made my life full and comfortable in spite of my being far from home. Here are the people who were close to me over these years and to whom I would especially like to express my sincere gratitude. I feel deep gratitude to:

Professor Herbert van Amerongen, who sealed my fate, forwarding my CV to Henk. That was a good luck for me. I can now say with great confidence that I like NMR more than the optical spectroscopy.

Dr. Henk Van As, my supervisor, who gave me a chance of starting the PhD project even without interviewing me in person. Henk, you always found time for discussions, and I appreciate very much that you had an open mind for my ideas and opinions. I like your style of supervision. It happened that since the beginning of my career I have had a few scientific supervisors. So I think that I can really judge on it.

Timur Sibgatullin, for teaching me the main principles of NMR. You spent a lot of your time that saved a lot of mine.

Frank Vergeldt, for always finding time to answer my questions. All my ideas I first tested in discussions with you.

Edo Gerkema, for assistance and sharing your always good mood and positive attitude to the life. Your contribution in Chapter 3 of this thesis is undoubtedly significant. Everything you make you make with a smile and soft humor.

John Philippi, for always being very helpful in fixing hardware problems and all other things.

Carel Windt, for sharing your experience of science and routines. I have learned a lot from you.

Many thanks to Magda Witek, Bart van Oort, Sashka Krumova, Sergey Laptanok, Afonso Duarte, Lena Talmishnik, Katia Makarova, Bart Venne, Elena Golovina, Tian Lijin and Guangyuan Du for the great time and fun we had during these years. Magda, Lena, Katia, I am glad that we have our girls company. You know that sometimes it is very important to have someone with whom you can share your

secrets. Magda, I hope our collaboration in our new project will be fruitful. Bart (van Oort) you were a driving force of our Friday pub parties. Unfortunately, this tradition was gone right after you left the group. Come back, we need you! Sergey, I need you too, at least to repair my bike again! Bart (Venne) thank you for creating the special atmosphere in the office. Tian, welcome to the group.

Special thanks to Netty Hoefakker for helping with administrative issues and bureaucratic problems. Netty, your assistance in subtle nuances of Dutch life is really invaluable.

I am grateful to all colleagues from the Biophysics group of Wageningen University for a pleasant atmosphere in the group.

My warmest thanks to my family: to my husband for his patience (I still drive you to the limit of it), help and support and to my mother for believing in me.

Natalia Homan

Curriculum Vitae

NAME: Natalia M. Homan

BIRTH: May 4, 1974 in Minsk, Belarus

EDUCATION

June 1991 Secondary School No. 16, Minsk, Belarus.

- Graduated with silver medal (Educational Ministry Award).

June 1997 Belarusian State University, Minsk, Belarus.

- Diploma in Physics.
Subject: Study of fluorescent characteristics of photosynthetic apparatus of plant during its stepwise development.

EMPLOYMENT

Nov 1997 - Sep 2004 researcher in the Biophysics and Biochemistry group of the Institute of Biophysics and Cell Engineering, the National Academy of Sciences of Belarus.

Nov 2004 - Oct 2009 PhD student in the Laboratory of Biophysics of Prof. dr. H. van Amerongen, Wageningen University, the Netherlands, under the supervision of Dr. Henk Van As.

Since May 2009 researcher in the Laboratory of Biophysics, Wageningen University, the Netherlands.

Publications

Van As H., Homan N.M., Vergeldt F.J., Windt C.W. (2009) MRI of water transport in the Soil-Plant-Atmosphere continuum. In: *Magnetic Resonance Microscopy* / Codd, S.L., Seymour, J.D. - Weinheim: Wiley-VCH, (Spatially Resolved NMR Techniques and Application).

Homan N.M., Windt C.W., Vergeldt F.J., Gerkema E., Van As H. (2007) 0.7 and 3 T MRI and sap flow in intact trees: xylem and phloem in action. *Applied Magnetic Resonance*, **32** (1-2), p. 157.

Van As H., Windt C.W., Homan N.M., Gerkema E., Vergeldt F.J. (2006) Flow MRI teaches us some lessons on hydraulic conductivity in trees. Canterbury, UK: *Experimental Biology Annual Meeting*, 2006-04-03 / 2006-04-07.

Homan N.M., Venne B., Van As H. Flow characteristics and exchange in complex biological systems as observed by PFG-MRI. *To be submitted*.

Homan N.M., Gerkema E., Van As H. Dynamics of water transport and water content in storage pools in diffuse-porous tree during a dry down period and recovery after watering. *To be submitted*.

Sperry J.S., Homan N.M., Smith D.S., Christman M., Van As H. Cavitation in ring-porous xylem: magnetic resonance imaging exposes potential artifacts in vulnerable curve measurements. *To be submitted*.

Radyuk M.S., Homan N.M. (2002) Discrete character of the photosynthetic apparatus development in greening barley leaves. *Photosynthesis Research*, **72** (1), p. 117.

Homan N.M., Radyuk M.S. (2002) Influence of exogenous Mg-protoporphyrin IX and its monomethyl ester on the state and content of protochlorophyllide in greening barley leaves. *Proceedings of International Conference "Photosynthesis and Crop Production"*, Kiev, Ukraine, p. 53.

Homan N.M., Radyuk M.S. (2001) Dynamics of Mg-containing precursors of chlorophyll in greening barley leaves. *Proceedings of National Academy of Sciences of*

Belarus, **4**, p. 48.

Homan N.M., Radyuk M.S. (2001) Development of two systems of photosynthesis during the stepwise greening of etiolated leaves of barley. *Proceedings of III Congress of Photobiologists of Russia*, p. 46.

Radyuk M.S., Homan N.M. (2000) The low temperature chlorophyll fluorescence during the stepwise development of the photosynthetic apparatus in greening barley leaves. *Proceedings of National Academy of Sciences of Belarus*, **2**, p. 54.

Homan N.M., Radyuk M.S., Fradkin L.I. (2000) The regulation of the synthesis of protochlorophyllide from 5-aminolevulinic acid during greening of etiolated leaves of barley. *Doklady Akademii Nauk Belarusi*, **44** (5), p. 77.

Homan N.M. (2000) The formation of the photosystem II during the stepwise development of the photosynthetic apparatus. *Proceedings of IV Congress of Belarusian Society for Photobiologists and Biophysicists*, Minsk, p. 47.

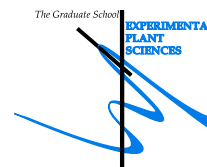
Homan N.M., Radyuk M.S., Fradkin L.I. (2000) The oscillation character of the effectiveness of the energy transfer from protochlorophyllide to chlorophyll during greening of etiolated leaves of barley. *Proceedings of IV Congress of Belarusian Society for Photobiologists and Biophysicists*, Minsk, p. 48.

Radyuk M.S., Homan N.M. (2000) Protochlorophyllide dynamics in etiolated leaves of barley. *Proceedings of IV Congress of Belarusian Society for Photobiologists and Biophysicists*, Minsk, p. 72.

Homan N.M., Radyuk M.S., Fradkin L.I. (1999) The regulation of the synthesis of chlorophyll during greening of etiolated leaves of barley. *Proceedings of International Conference "Photosynthesis and Crop Production"*, Minsk, p. 37.

Homan N.M., Radyuk M.S. (1998) The kinetics of the low temperature chlorophyll fluorescence during the stepwise development of the photosynthetic apparatus. *Proceedings of III Congress of Belarusian Society for Photobiologists and Biophysicists*. Minsk, p. 46.

**Education Statement of the Graduate School
Experimental Plant Sciences**



Issued to: Natalia Homan
Date: 04 November 2009
Group: Laboratory of Biophysics, Wageningen University

1) Start-up phase ▶ First presentation of your project T2 and flow measurement in cherry tree ▶ Writing or rewriting a project proposal Transport in unsaturated porous system: xylem-phloem interaction in plants and trees ▶ Writing a review or book chapter ▶ MSc courses Biophysical imaging ▶ Laboratory use of isotopes	<u>date</u> Jun 16, 2005 May 2005 2007
<i>Subtotal Start-up Phase</i>	<i>10.5 credits*</i>
2) Scientific Exposure ▶ EPS PhD student days Wageningen University Wageningen University ▶ EPS theme symposia EPS theme 3 symposia 'Metabolism and Adaptation, University of Amsterdam ▶ NWO Lunteren days and other National Platforms ALW_EPS 2007 ▶ Seminars (series), workshops and symposia Biophysical days Biophysica seminar series, WUR, Lab. of Biophysics Caput Series: Structure and dynamics of biomolecules in vitro and in vivo Biophysica seminar series, WUR, Lab. of Biophysics User meeting NMR Center, WUR Biophysica seminar series, WUR, Lab. of Biophysics User meeting NMR Center, WUR ▶ Seminar plus ▶ International symposia and congresses Biophysical and molecular mechanisms for water transport, Turin, Italy International conference on Magnetic Resonance in Porous Media, Aachen, Germany ▶ Presentations poster: Characteristics of water transport in diffuse-porous trees poster: MRI of axial and radial water transport in tree Oral presentation at ICMRPM Oral presentation at User meeting NMR Center ▶ IAB interview ▶ Excursions	<u>date</u> Sep 19, 2006 Sep 13, 2007 Nov 10, 2006 Apr 02-03, 2007 Dec 20, 2005 2006 Oct-Dec, 2006 2007 Nov 29-30, 2007 2008 Jun 18-19, 2009 Feb 28-Mar 01, 2005 Sep 03-07, 2007 Sep 11, 2006 2008 Sep 03-07, 2007 Jun 18-19, 2009 Sep 14, 2007
<i>Subtotal Scientific Exposure</i>	<i>11.1 credits*</i>
3) In-Depth Studies ▶ EPS courses or other PhD courses PhD course 'in vivo NMR' Socrates Intensive Programme "Mathematics and Biology" ▶ Journal club Study group Biophysics ▶ Individual research training	<u>date</u> Oct 31-Nov 18, 2005 Jul 02-Jul 13, 2007 2005-2008
<i>Subtotal In-Depth Studies</i>	<i>12.7 credits*</i>
4) Personal development ▶ Skill training courses English language Dutch language ▶ Organisation of PhD students day, course or conference ▶ Membership of Board, Committee or PhD council	<u>date</u> 2004 2005
<i>Subtotal Personal Development</i>	<i>3.0 credits*</i>
TOTAL NUMBER OF CREDIT POINTS*	37,3

Herewith the Graduate School declares that the PhD candidate has complied with the educational requirements set by the Educational Committee of EPS which comprises of a minimum total of 30 credits

* A credit represents a normative study load of 28 hours of study